TAMPERE UNIVERSITY OF TECHNOLOGY
Degree Programme in Automation

JUHA HIRVONEN

ESTIMATION OF INJECTION VOLUME IN CAPILLARY MICROINJECTION USING ELECTRICAL IMPEDANCE MEASUREMENT

Master of Science Thesis

Examiners:
Prof. Pasi Kallio, PhD Matti Vilkko

The topic and the examiners have been approved by the Faculty of Automation, Mechanical and Materials Engineering Council meeting on 19.08.2009

ABSTRACT

TAMPERE UNIVERSITY OF TECHNOLOGY
Master's Degree Programme in Automation Technology
HIRVONEN, JUHA: Estimation of Injection Volume in Capillary Microinjection Using Electrical Impedance Measurement
Master of Science Thesis, 90 pages, 2 appendix pages
January 2010
Major: Microsystem Technology
Examiners: Professor Pasi Kallio and PhD Matti Vilkko
Keywords: Capillary pressure microinjection, CPM, injection volume, impedance measurements, modelling

Capillary pressure microinjection (CPM) is a tool for transporting small sample volumes into living cells utilizing a sharp glass pipette and pressure pulses. The automation level of the current state-of-the-art microinjection devices is low and this makes the technique slow, imprecise and inefficient. The objective of this thesis work is to develop a method to estimate the injection volume in the capillary pressure microinjection technique of living adherent cells. This method would improve the reliability and repeatability of CPM and facilitate automating the injection procedure.

Due to the extremely small dimensions involved in the process, a straight measurement of the injection volume is not possible. The strategy used in this work is to generate a mathematical model for the injection volume as a function of the injection pressure and the pipette electrical resistance. A measurement setup is built around a microinjection system to gather data for constructing the model. The injection pressure is measured with a pressure sensor, the pipette electrical resistance is determined using a custom-made impedance measurement circuitry and the injection volume is estimated by using a fluorescent dye as the injection liquid and recording image data from the injections. Several injection pressures and micropipette sizes are used to achieve data extensively enough. A MATLAB based automated algorithm is generated to handle the measurement data and organize the results efficiently.

The measurement results give a rough estimate of the relationship between the injection volume, the injection pressure and the pipette electrical resistance. However, a reliable model cannot be built based on the data. The reason is the rather limited amount of suitable measurement data for modelling it was possible to collect due to the numerous error situations. Nevertheless, new important information of the nature of the microinjection procedure is obtained and valuable observations on measurements connected to microinjection are made. Further studies must be done to solve the problems in the tests to be able to gather the data more efficiently and construct the actual model.

SUOMENKIELINEN TIIVISTELMÄ

TAMPEREEN TEKNILLINEN YLIOPISTO
Automaatiotekniikan koulutusohjelma
HIRVONEN, JUHA: Kapillaarimikroinjektion injektiotilavuuden arviointi sähköisellä impedanssimittauksella
Diplomityö, 90 sivua, 2 liitesivua
Tammikuu 2010
Pääaine: Mikrosysteemitekniikka
Tarkastajat: Professori Pasi Kallio ja TkT Matti Vilkko
Avainsanat: Kapillaarimikroinjektio, injektiotilavuus, impedanssimittaus, mallintaminen

Kapillaarimikroinjektio on menetelmä, jossa elävän solun kalvo läpäistään ohuella lasisella mikropipetillä ja pieni määrä näyteainetta saatetaan solun sisälle painepulssilla. Menetelmän sovelluksia on muun muassa lääketeollisessa tutkimuksessa, syöpä- ja AIDS-tutkimuksessa, solututkimuksessa sekä toksikologiassa. Yleistettynä tekniikan avulla saadaan tietoa siitä, miten solu reagoi eri aineisiin ja miten solu toimii eri olosuhteissa. Mikroinjektioiden kohdesolut voidaan jakaa kahteen pääryhmään: suspensiosoluihin ja adherenttisoluihin. Maljalla kasvatettaessa suspensiosolut kelluvat kasvatusliuoksessa, mutta adherenttisolut kiinnittyvät maljan pohjaan. Tämän työn painopiste on adherenttisolujen mikroinjektiossa, joka on vähemmän tutkittu ala kuin suspensiosolujen mikroinjektio.

Adherenttisolujen injektioon suunnattujen mikroinjektiolaitteistojen automaatioaste on matala, ja siksi tekniikka on hidas, epätarkka ja tehoton ja vaatii taitavan käyttäjän. Käyttäjän täytyy ensin kalibroida laitteisto, sitten etsiä kohdesolut maljalta, liikuttaa mikropipetti kontaktiin solun kanssa, läpäistä solukalvo, laukaista painepulssi ja toistaa viimeiset kolme vaihetta jokaiselle solulle, johon tahdotaan injektoida näytettä. Automatisoinnin pääasiallisena esteenä ovat puutteet keinoissa mitata kapillaarimikroinjektion eri vaiheita ja niihin liittyviä muuttujia, joita voisi hyödyntää laitteiston säädössä. Olennaisimmat mitattavat parametrit ovat mikropipetin sijainti suhteessa kohdesoluihin, mikropipetin ja solukalvon välisen kontaktin tunnistaminen ja soluun injektoitava näytemäärä eli injektiotilavuus. Tämän diplomityön tavoite on kehittää menetelmä injektiotilavuuden arviointiin. Menetelmä sekä parantaisi kapillaarimikroinjektioiden luotettavuutta ja toistettavuutta että helpottaisi laitteiston automatisointia.

Injektiotilavuus on tärkeä parametri, koska elävät solut vaurioituvat herkästi, jos niiden tilavuus kasvaa äkillisesti liikaa. Nyrkkisääntönä voidaan sanoa, että injektiotilavuuden ei tulisi ylittää 5% solun alkuperäisestä tilavuudesta. Nisäkkään adherenttisolujen tapauksessa tämä tarkoittaa sitä, että injektiotilavuuden tulisi olla kymmenistä satoihin femtolitroihin. Koska useat kosketukset solukalvon kanssa muuttavat helposti mikropipetin ominaisuuksia, ennen testejä tehtävä kalibrointi on tehoton keino injektiotilavuuden vakioimiseksi. Nämä seikat asettavat mittausjärjestelmälle korkeat vaatimukset.

Suora injektiotilavuuden mittaus mikroinjektioiden aikana ei ole mahdollista prosessin vaatiman erittäin pienen mittakaavan takia. Tilavuusvirran mittaukseen käytettävät mikroanturitkaan eivät sovellu injektiotilavuuden mittaamiseen tilanpuutteen vuoksi tai kustannussyistä. Tässä työssä ehdotettu strategia on kehittää matemaattinen malli, jossa injektiotilavuus määritellään injektiopaineen ja mikropipetin sähköisen resistanssin funktiona. Mallinnuksessa tarvittavan datan keräämistä varten mikroinjektiojärjestelmän ympärille rakennetaan mittauslaitteisto. Injektiokokeita tehdään solujen kasvatusliuokseen ja samalla mittausdataa kerätään laitteistolla. Injektiopaine mitataan paineanturilla, pipetin sähköinen resistanssi määritetään käyttämällä impedanssinmittauspiiriä ja injektiotilavuus arvioidaan injektoimalla nesteeseen fluoresoivaa väriainetta, kuvaamalla injektiot mikroskooppikameralla ja analysoimalla kuvat kuvankäsittelyohjelmalla. Useita injektiopaineita ja mikropipettikokoja käytetään, jotta dataa saadaan tarpeeksi kattavasti. Paineanturin ja impedanssinmittauspiirin mittausdata kerätään käyttämällä Matlabin xPC Target -lisäosaa ja kuvadata taltioidaan Genomanda-nimisellä ohjelmistolla. Datan automaattista käsittelyä ja tulosten tehokasta järjestelemistä varten työssä kehitetään Matlab-pohjainen algoritmi, johon toteutetaan yksinkertainen käyttöliittymä. Mittaustulosten johdonmukaiseen arkistointiin suunnitellaan tietorakenne, johon algoritmi tulokset tallentaa.

Mittaustulokset antavat karkean kuvan injektiotilavuuden, injektiopaineen ja mikropipetin sähköisen resistanssin välisestä yhteydestä. Injektiopaineen merkitys injektiotilavuudelle samoin kuin pipetin resistanssin merkitys injektiotilavuudelle pystytään arvioimaan. Kuitenkaan luotettavaa mallia kaikkien kolmen parametrin välillä ei saada rakennettua tulosten perusteella, sillä lukuisien virhetilanteiden takia mallinnukseen sopivan datan määrä jää alhaiseksi. Siitä huolimatta tulokset tarjoavat uutta tärkeää tietoa mikroinjektion luonteesta, ja niiden pohjalta voi tehdä arvokkaita havaintoja mikroinjektioon kohdistuvista mittauksista. Tulokset osoittavat, että pienetkin mikropipettien kärkien kokojen vaihtelut saavat aikaan suuria eroja injektiotilavuudessa, sekä paljastavat kapillaarimikroinjektion virheherkkyyden. Nämä löydökset korostavat mittausinformaation merkitystä mikroinjektioissa ja kertovat työssä tavoitellun mallin hyödyllisyydestä.

Työssä toteutetuissa ylimääräisissä testeissä tutkitaan myös pipetin liikuttelun sekä elektrodimateriaalin vaikutusta pipetin resistanssin mittaukseen. Saadut tulokset tähdentävät materiaalivalintojen ja elektrodin kulumisen merkitystä mittaustuloksiin sekä kannustavat jatkotutkimukseen aiheen saralla.

Jatkossa lisäkokeita tulee tehdä testeissä esiintyneiden ongelmien kuten mikropipetin tukkeutumisen ja elektroniikkaongelmien ratkaisemiseksi, jotta kunnollista mittausdataa saataisiin kerättyä enemmän ja toimiva malli pystyttäisiin rakentamaan. Myös resistanssin mittaamisessa käytettävien elektrodien valintaan, valmistukseen, ominaisuuksiin ja kunnonvalvontaan täytyy panostaa enemmän.

FOREWORD

This thesis has been made in the Department of Automation Science and Engineering at Tampere University of Technology. The examiners have been Prof. Pasi Kallio and PhD Matti Vilkko and I would like to acknowledge them for their valuable instructions during this demanding work. Without good guides one can easily get lost in the multidisciplinary jungle of microsystem technology.

My deepest gratitude goes also to the whole MST-group (Micro- and Nanosystems Research Group), which has been an encouraging, inspiring and pleasant work community. It is hard to imagine Friday afternoons without doughnuts and the weekend song by Martti Servo.

I would like to express my sincerest appreciation to my parents Tuomo and Anja and my brother Vesa for supporting me in the never-ending struggles with my studies. My friends have also been an important stone base preventing me from sinking into the dark abyss of scientific problems. Finally, I would like to thank my bands and the people I have been playing with for rocking out my consciousness. Get on!

Tampere, January 2010

Juha Hirvonen
Tumppi 3 B 63
FIN-33720 Tampere
Tel.: +358 50 339 4745

TABLE OF CONTENTS

TERMS AND ABBREVIATIONS

Terms

A	[m^2]	Cross-sectional area of a channel
a		Constant used in calculating the pressure from the pressure sensor output signal
a_{exc}	[V]	Amplitude of the excitation signal going to the pipette
$a_{meas}(q)$	[V]	Amplitudes of the measurement signal pulses coming from the pipette
b		Constant used in calculating the pressure from the pressure sensor output signal
$C_{lb1...lb3}$	[F]	Lipid bilayer capacitance
C_m	[F]	Membrane capacitance
C_{pip}	[F]	Pipette capacitance
d_{pip}	[m]	Pipette tip diameter
$e(k)$		Sample indexes of the ends of the injections in an experiment
F_s	[Hz]	Sampling frequency
$f(u,w)$		Digital image matrix
f_{exc}	[Hz]	Excitation signal frequency
G_{ic1}	[S]	Ion channel conductance
$g(u,w)$		Mask image
h	[m^2kg/s]	Planck's constant (6.62×10^{-34} m^2kg/s)
$h(u,w)$		Masked image
$I(t,V)$		Intensity function
I_{im}		Image intensity
k		Injection index
l_{pip}	[m]	Length of the narrow pipette section
l_{tip}	[m]	Length of the pipette part under medium
n		Sample index
$o_{meas}(q)$	[ms]	Offsets of the measurement signal pulses of the CDD
p	[Pa]	Pressure

p_{meas}	[Pa]	Pressure measured with the pressure sensor
p_{inj}	[Pa]	Injection pressure
Q	[m^3/s]	Volume flow
q		Pulse index
R_{hyd}	[Ω]	Hydraulic resistance
R_{i2v}	[Ω]	Current-to-voltage converter resistor value
$R_{ic1…ic2}$	[Ω]	Ion channel resistance
R_{leak}	[Ω]	Leakage resistance
R_m	[Ω]	Membrane resistance
R_{patch}	[Ω]	Patch resistance
R_{pip}	[Ω]	Pipette resistance
r		Image index
S_0		Initial energy state of a fluorophore
S_1		Relaxed energy state of a fluorophore following S_1'
S_1'		Energy state of a fluorophore after excitation
$s(k)$		Sample indexes of the starts of the injections in an experiment
$t_{1,2}$	[s]	Time instant
$t_{end}(k)$	[ms]	Ending times of the injections in an experiment
$t_{im}(r)$	[ms]	Timestamps of the images taken in an experiment
$t_{start}(k)$	[ms]	Starting times of the injections in an experiment
U	[V]	Output voltage of the pressure sensor
U_{in}	[V]	Input voltage of the CDD
U_{out}	[V]	Output voltage of the CDD
u		Digital image coordinate, horizontal
V_{inj}	[m^3]	Injection volume
v	[m/s]	Liquid velocity
w		Digital image coordinate, vertical
X		Length of the data array given by the xPC Target computer
$x(n)$	[V]	CDD excitation signal measured from the CDD
$x_{prec}(n)$	[V]	Preconditioned measured CDD excitation signal

$y(n)$	[V]	CDD measurement signal
$y_{prec}(n)$	[V]	Preconditioned CDD measurement signal
Z_{clog}	[Ω]	Impedance of a clogging particle
Z_{con}	[Ω]	Impedance of a pipette in contact with a cell
Z_{pip}	[Ω]	Pipette impedance
α_{ampl}		Output amplification of the CDD
α_{scale}		Input scaling of the CDD
$\Delta t_{im}(r)$	[ms]	Time values of the images taken in an experiment relative to the beginning of the first injection
ε_0	[F/m]	Vacuum permittivity
ε_g	[F/m]	Permittivity of the pipette glass
ν_{EM}	[Hz]	Frequency of a photon emitted by a fluorophore
ν_{EX}	[Hz]	Frequency of a photon exciting a fluorophore
ρ_{liq}	[Ωm]	Resistivity of the injection liquid
T_{exc}		Period of the excitation signal
$T_{transient}$		Length of the transient estimate
τ_g	[m]	Thickness of the pipette glass
σ		Threshold level

Abbreviations

A/D	Analog-to-digital converter
Ag/AgCl	Silver – silver chloride
CCD	Charged coupled device
CDD	Contact detection device
CPM	Capillary pressure microinjection
D/A	Digital-to-analog converter
DI	Digital input
DNA	Deoxyribonucleic acid
FITC	Fluorescein isothiocyanate
GFP	Green fluorescent protein
GENOMANDA	The machine vision program used in the work
in vitro	Cells cultivated outside body, e.g. in a Petri-dish

KCl	Potassium chloride
MANiPEN	The name of the micromanipulator
MATLAB	The program used in measurements and handling of the measurement results
MART	The controlling program of MANiPEN
mRNA	Messenger RNA
MST-group	Micro- and Nanosystems Research Group of Tampere University of Technology
RC circuit	An electrical circuit consisting of resistors and capacitors
RNA	Ribonucleic acid
SEM	Scanning electron microscopy
siRNA	Small inhibitory RNA
SNR	Signal-to-noise ratio
TUT	Tampere University of Technology
VTT	Technical Research Centre of Finland
xPC Target	The trademark of the MATLAB real-time measuring and control toolbox

1. INTRODUCTION

Microinjection is a technique for delivering small volumes of samples into living cells. It is a tool to study diverse cell responses to different substances in a variety of systems and it has lots of applications in the fields of cell biology, medicine, *in vitro* toxicology and drug development [10], [18], [57]. Several methods to transport sample substance in the cell exist in mechanical, optical, electrical and chemical energy domains. In capillary pressure microinjection, a cell membrane is penetrated using a thin glass pipette and a small amount of liquid is injected into the cell by applying a pressure pulse. Due to the popularity of the technique and the number of research applications, there are several commercial capillary pressure microinjection systems available from various manufacturers. However, some fundamental problems still remain unsolved in the technique.

Cells can be divided to two groups depending on their behavior when they are grown in culturing medium in a Petri-dish: suspension cells and adherent cells. Suspension cells float in medium whereas adherent cells grow attached on the bottom of the dish. Oocytes and blood cells are examples of suspension cells while most cells derived from solid tissues are adherent. In this work, we focus on microinjection of living adherent cells.

Microinjection of especially adherent cells is currently done either manually or using a semi-automatic joystick-controlled system with a human operator. The operator moves the pipette to a contact with a target cell, injects the liquid, moves the pipette to a contact with another cell and so on. This makes the manipulation slow and inefficient. Furthermore, a skillful operator is required since living cells – especially primary cells – are extremely sensitive. Also, it is not possible to treat cells manually in such great quantities that are sufficient for molecular biology analysis. Therefore, automation of the injection system is essential for making the research method faster, more robust, more reliable, more repeatable and more efficient.

Automating the microinjection system needs different sensors to give the system feedback of the status of the process. Firstly, feedback of the position of the pipette with respect to the target cells has to be given to the system. This is possible to realize by using machine vision and such systems have been reported with suspension cells [59] as well as with adherent cells [62]. Secondly, the automated microinjection system must detect the contact between the pipette and the target cell in order not to go through the cell and hit the bottom of the dish but to start the injection in a correct point. This is a somewhat more demanding requirement. Again, machine vision has been applied in solving the problem with suspension cells and indirect method utilizing machine vision

and height measurement has been used to approximate when the pipette tip penetrates the cell membrane [59]. Also, machine vision based height estimation has been utilized in microinjection of adherent cells [62] but the small size of the target cells may make the method imprecise. Other means utilized in the contact and penetration detection with suspension cells include force sensors [6], [31], [48] and vision-based force estimation [1], [36]. However, these methods are not applicable to adherent cells. Currently, the only reported system for contact detection with adherent cells is based on electrical impedance measurement [20], [33]. Thirdly, the system should be able to inject a repeatable and known amount of studied substance to the cells in order to perform repeatable injections and thus yield quantitative results. This has been found to be really challenging.

The average volume of adherent mammalian cells is in the scale of picoliters and the microinjected sample volume must not exceed 5% of the cell volume in order not to cause too big a stress onto the cell [25]. This means that the injection volume should be in the order of femtoliters. Also, as mentioned above, the volume should stay constant over injections. The injection time and the injection pressure can be adjusted in most of the devices but there are no reliable methods for estimation of the injection volume during the experiments. Traditionally, the injection devices are calibrated before tests using a microscopic scale or machine vision or using markers such as fluorescence. This kind of feed-forward control works well if the pipette properties remain constant during the experiments. However, consecutive contacts with cell membranes break easily the tip of the fragile instrument and thus change its geometry. Furthermore, some parts of cell organelles can get stuck into the pipette tip and clog the pipette partly or totally. Both breakage and clogging cause the injection volume to change while the pressure remains constant. In order to keep the injection volume constant, there should be a method to measure the changes and control the injection pressure to balance them during injections. This work aims at developing a real-time applicable technique to estimate the injection volume based on measuring the pipette impedance.

A procedure utilizing the measurement of the electrical impedance of the pipette and the cell in microinjection has been used to detect pipette breakage, clogging and the contact between the pipette and a cell [33]. The detection is based on estimating the impedance of the pipette and the cell and observing its changes during the injections. Since the impedance of the pipette is highly dependent on its geometry, the method is potential also in estimation of the tip diameter. The tip diameter affects the volume flow out of the pipette tip and thus the injection volume estimation could be done using the pipette impedance measurement as one feedback.

In this thesis work, the goal is to build a model for the injection volume using the injection pressure and the electrical impedance of the pipette as the input parameters. Pressure is measured by a pressure sensor and the pipette impedance is estimated using a custom made circuitry. By applying the model, the pressure can be controlled during injections to yield a desired injection volume despite of changes in the pipette tip geometry. For the generation of the model, experiments are performed.

This thesis work has been done in Micro and Nanosystems Research Group (MST-group) of Tampere University of Technology (TUT). The group has been working with the capillary pressure microinjection and its automation almost 10 years and cooperates with the cell and stem cell researchers of the Tampere region.

Chapter 2 introduces the capillary pressure microinjection technique and the equipment needed for that. The main application areas are described briefly in the beginning and some examples of the research done in those areas are given. In addition, the challenges of the method and especially the challenges in automation of the method are discussed. In the end of the chapter, an introductory to fluorescence measurements and their connection to microinjection is given.

Chapter 3 discusses impedance measurements of living cells. First, the background and the objectives of the technique is presented; secondly, the electrical models essential to understand the basis of the technique are described; then, the measurement device for the impedance measurements in microinjections developed in our research group is introduced and finally, the potential of the method for this thesis work is discussed.

In Chapter 4, the measurement setup built for performing the experiments in this work is presented. The architecture and the components are described and then the possible errors in the measurements are discussed.

Chapter 5 concentrates on the measurement data and data handling. The structure of the measurement data gained is described and the computer algorithm to automatically handle the data to this form is presented. Also, the data visualization for observing the progression of the experiments afterwards, clarifying the connection between the injection moments and the changes in data, and detecting the results of tests is presented.

Chapter 6 presents the experiments made and the results gained. The experimental procedure is illustrated and different relationships of the measured parameters are defined. Also, the observations made during the tests and data handling are discussed. In the end, the results, their usability and the success of the work are assessed.

Finally, Chapter 7 draws a conclusion of this all.

2. CAPILLARY PRESSURE MICROINJECTION

Capillary pressure microinjection (CPM) is a mechanical microinjection method and it utilizes an extremely sharp microcapillary or micropipette made of glass, having an opening with a diameter of less than a micrometer and filled with the substance of interest. The pipette is positioned accurately to a close proximity of the cell utilizing a micromanipulator, the pipette tip is penetrated through the cell membrane and a small amount of the substance is delivered from the pipette to the cell upon a pressure pulse. The advantages of this method compared with the other techniques to transport material to living cells are high selectivity of the cells injected, less material needed due to direct delivery to the cells, less damage caused to the cell, fewer limitations in the material injected and known timing, which allows temporal experiments [35], [47], [59], [63]. Disadvantages of CPM include the low amount of cells possible to inject in a certain time and the need of high-level skill from the operator [35], [47], [59], [63]. Figure 2.1 shows a cell being injected with CPM.

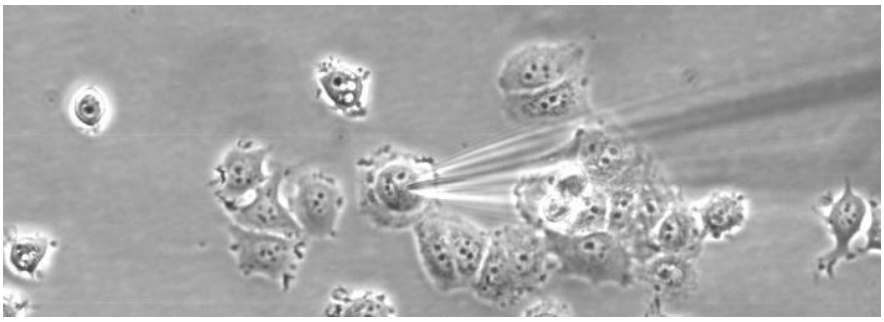

Figure 2.1: A cell being injected with a pipette approaching from above.

This chapter discusses the CPM technique. Section 2.1 presents briefly the applications of CPM, Section 2.2 describes the equipment needed for CPM experiments, and Section 2.3 discusses the challenges in the CPM technique. The currently used calibration procedures for the injection volume are depicted in Section 2.4 and Section 2.5 discusses fluorescence measurements and their connection to capillary pressure microinjection. A conclusion of this chapter is drawn in Section 2.6.

2.1. Applications

This section presents the applications of CPM. First, the applications with suspension cells are presented and then the applications with adherent cells are introduced.

2.1.1. Suspension Cells

The most common medical application of capillary pressure microinjection must be *in vitro* fertilization used as a major treatment in infertility in clinics [63]. In this approach, sperm is injected to oocytes cultured in a Petri-dish. The fertilized egg is then transferred to the patient's uterus in order to start a successful pregnancy. Other applications of cell capillary microinjection of suspension cells in the field of medical research include studies on cryopreservation of oocytes and fertilized eggs [9] and surveys on oocyte maturation [10].

One application outside the medical field is the production of transgenic animals [10], [64]. In this application, modified genes or genes of different species are injected to animal embryos. The purpose is to make the animals more efficient in production of meat, wool or milk or otherwise more beneficial (for example, to generate cows that have insulin in their milk) for agriculture or industry.

2.1.2. Adherent Cells

The applications of capillary pressure microinjection of living adherent cells divide to three categories: basic cell biological research, drug development and toxicology, and medical research.

The cell biological research applications include observing the regulatory mechanisms of different cell functions, examining gene expression, studying metabolic pathways and signal transduction, and manipulating cells to work in a desired way [10], [18]. For example, enzymes, proteins, genes, antibodies, DNA and RNA can be injected to target cells [10], [57], [63]. In genetic research, silencing genes by injecting small inhibitory RNA (siRNA) and activating them by injecting messenger RNA (mRNA) constructs is a valuable research tool [18]. Among others, microinjection has been used in studies on antiviral activity of cells [7], gravity response of plant cells [52], ion channels and receptors for cloned genes, growth control of mammalian cells and heat shock proteins [10]. Also, step-by-step protocols for successful injection tests with antibodies, nucleic acids and peptides have been proposed by researchers [28].

In drug development and toxicology, the idea is to use cell cultivations for testing of drugs and determining the toxicity of certain compounds instead of laboratory animals [18], [57]. Effect of drug candidates on the infected cells is observed instead of infecting and performing treatments on animals. This strategy is more ethical and economical and it might be even more reliable since human cells describe functioning of the human body more than the animal cells [18]. Also, European Union aims at forbidding the use of test animals in cosmetic industry as soon as alternative methods become available [18].

The medical applications of CPM of living adherent cells include studies on Alzheimer disease [64] and stem cell research [21]. Stem cell research is a growing and promising research field, which has need for efficient research instruments to reduce the amount of manual work.

2.2. Structure of a Capillary Pressure Microinjection System

A CPM system consists of a micromanipulator, a pressure system and a vision system. The micromanipulator provides the motion, the pressure system the pressure signals and the vision system the visual feedback. [25]

The task of the micromanipulator is to move the micropipette to contact with the target cells for injections. Since the diameter of the adherent mammalian cells is in scale of tens of micrometers, the resolution of the manipulator should be in micrometers, thus high amount of precision is needed in its motion. Its movement should also be stable to avoid harming the cells when making a contact with them.

The pressure system generates the pressures needed for microinjections. Precise and short pressure pulses are used to inject the liquid into the cells and stable and accurate back pressure is maintained between the injections to hold the boundary surface of the injection liquid in the very tip of the pipette and thus prevent the cell growth medium from flowing into the pipette from the tip.

The vision system gives the operator visual feedback of the experiments. An inverted microscope is used as a base of the system. The cells are growing on the bottom of a Petri-dish and the micromanipulator brings the pipette to the dish from above. Because of the limited space and the short focus distance, the microscope has to be inverted and image the cells from below the dish.

Figure 2.2 illustrates the structure of a microinjection system. The parts described above are marked to the schematics with alphabets.

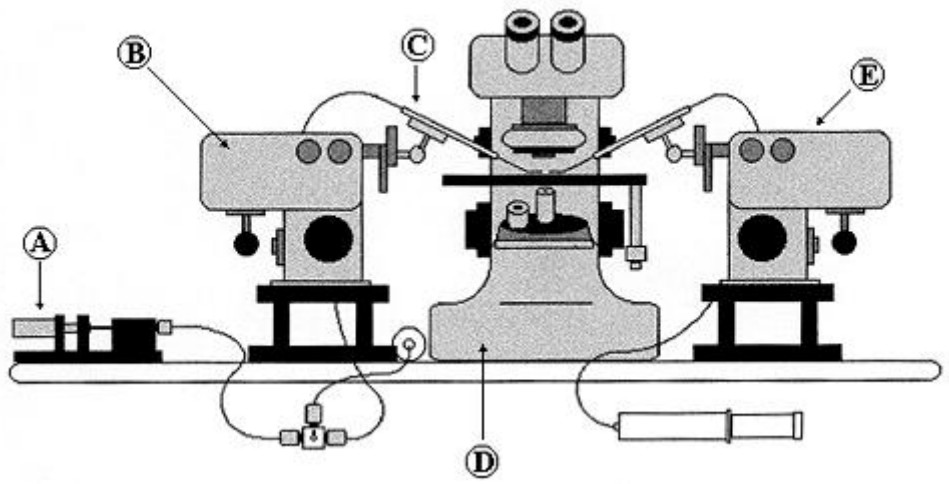

Figure 2.2: Schematics of a microinjection system: a pressure source (A), a micromanipulator (B) with a pipette holder (C), a vision system (D) and a second micromanipulator for holding the cell to be injected (optional) (E) [4].

The manufacturers of commercial microinjection equipment include Eppendorf [8], WPI [60], Narishige [41], Harvard Apparatus [14] and Luigs & Neumann [32]. The

companies offer either whole microinjection systems or parts of them such as manipulators and pressure systems.

2.3. Challenges in Capillary Pressure Microinjection

As mentioned in the beginning of this section, one disadvantage of the CPM technique is the requirement of a skilled person to perform the experiments. Thus, an automatic microinjection system is needed to make the method more efficient, reliable and repeatable and several groups have been working to automate the process [17], [35], [57], [59], [62]. One of the bottlenecks of automation was to detect the contact between the pipette tip and the target cell [20], [33]. The glass pipette is almost transparent and it is approaching the cell from above while the objective is viewing the situation from below. Therefore, detecting the contact from the microscope image is really demanding. Embryos and oocytes are relatively large and contact detection is easier with them than with adherent cells. In [59] the problem has been solved using indirect image processing methods based on the deformation of the pipette and the authors of [1] and [36] utilize machine vision based force estimation where a mechanical model for cell deformation presented in [54] is applied. In [6], [17], [31] and [48] force measurement from the pipette is used to sense the contact. However, these methods are not applicable to microinjection of adherent cells since the forces are much smaller, the deformation of a cell much less visible and the tools more fragile. In [62] a machine vision based estimation of the vertical distance between the pipette tip and the bottom of the Petri-dish is utilized in approximating the moment the pipette tip hits the cell culture, which grows on the bottom. However, as the height of the cell cultivation differs in the dish and in addition the dish might be bit tilted, the method is not exactly reliable with adherent cells, which are much smaller than oocytes. Our group uses electrical measurements for the contact detection and it is the only reported method for detecting the actual contact between a pipette and an adherent cell today [33]. The basis of the technique is the change of the pipette resistance in a contact moment. Chapter 3 discusses this more.

Another problematic variable to measure and yet hindering the automation is the injection volume. In order to perform repeatable and quantitative tests, the injection volume should remain constant during the tests. However, currently there is no method whatsoever to measure the injection volume in real-time while performing the experiments. Only the injection pressure and the injection time are adjustable in the pressure systems of the microinjection stations. In the existing state-of-the-art systems, the injection volume is calibrated before the tests using drop measuring methods [9], [25], [59] or fluorescence dyes [25], [37], [45], which are presented in more detail in the next section. This, so-called feed-forward control would be adequate if the pipette remained unchanged during the tests. However, the thin pipette tip is extremely fragile and it can break down when in contact with a target cell. This enlarges the tip opening and causes the volume flow out from the tip with a certain pressure to increase. Also,

reverse changes may occur since a part of the cell membrane can get stuck into the pipette tip during a contact and clog the tip. This decreases the injection volume or cuts it entirely. For these reasons, a feedback system is needed in control of injection volume instead of simple feed-forward control.

The difficulty in measuring the volume injected is on one hand the tininess of the volume and on the other hand the lack of space in the injection equipment. As mentioned earlier in Introduction, the volume of the adherent mammalian cells is a couple of picoliters and thus the injected volume should be in tens of femtoliters in order not to harm the cell [25]. This lays highly demanding requirements for the volume flow measurement. The conventional volume flow measurement methods are based on orifice plates, pistons, measurement nozzles, flow elbows, blade wheels and turbines [12]. Needless to say, these methods are not sufficient for the microworld. The microsensors for measuring liquid flow have been realized using tiny heater elements and temperature sensors, heat loss in a thin wire, resonating microstructures and bending of thin cantilevers and orifice structures [19], [29]. Even these structures are too cumbersome to be positioned into the small micropipette and even if it was possible, the costs of one pipette would raise too high. Thus, novel methods for measurement or estimation of the volume flow are needed to approximate the injection volume in microinjections.

This thesis work aims at producing a method to estimate the injection volume. This method could be used in controlling the injection pressure later on. The strategy is to measure certain parameters affecting injection volume and estimate the volume based on those measurements.

2.4. Methods for Calibrating Injection Volume

Since the calibration methods of the injection volume are important background knowledge for this work, they are presented briefly in this section. The details are left out and only the basic idea of the most common methods is given to the reader.

The general calibration sequence is the following: first, injections are made to a test dish; secondly, the volume injected is approximated using some indirect method; thirdly, injection pressure or/and injection time is/are adjusted and the first two steps are repeated if the volume gained is not satisfactory. When the injection volume is as desired, the tests are started. The indirect methods used for volume measurement in the calibration process are – as mentioned in the previous section – drop measuring methods and fluorescence dyes. Both methods are next discussed briefly.

2.4.1. Drop Measuring Methods

In drop measuring methods, the strategy is to inject a drop of liquid out of the pipette, measure the size of the drop and estimate the volume from the size. The simplest method for this is the use of microscopic scales. The drop is injected on the scale and then the diameter of the drop is read from the scale. More advanced technique is to use

machine vision and image processing methods. Here, the drop is imaged and the diameter is then measured using an image processing program. Also, more sophisticated image processing methods such as circular and ellipsoidal fitting can be applied to the image if diameter measurement appears insufficient or unsuitable.

There are a couple of different practical approaches in drop measuring. One practice is to inject liquid into oil and estimate the volume of the drop from its dimensions [25]. Another approach is to inject liquid inside a droplet of medium several times, image the droplet before and after the injections, estimate the volume change using image processing methods and divide it with the number of injections [9]. The advantage of oil is that the injected liquid is not mixed with the oil and therefore the injected liquid remains in a form of a drop or a spherical object inside it. However, the disadvantage is that oil is too dense compared with the properties of a cell [9]. Some researchers claim that a medium drop resembles more a cell [9] but then the injection liquid mixes to the medium and the size of the medium drop itself has to be used in measurement.

The disadvantage of the methods presented in this section is that they both assume the droplet measured to be a sphere or otherwise regular object. If the form differs much from the assumption, the difference between the volume calculated and the true volume is remarkable and the calibration fails.

2.4.2. Fluorescent Dyes

In calibration of the injection volume, the fluorescent dye is injected from the micropipette, the injected dye is excited and the intensity of the emission is measured. The intensity is the higher the greater the volume is. Thus, the injection volume is estimated using the intensity and the concentration of the fluorescent dye. Disadvantage of this method is that the result is highly dependent on the equipment such as the microscope, the CCD camera and the fluorescent dye [25]. The next section discusses more fluorescence measurements and fluorescent dyes.

2.5. Fluorescence Measurements

Since fluorescent dyes are often used in calibration of the injection volume and are used also in this work, it is reasonable to describe them more in detail. This section will introduce the basic principle of fluorescence as well as the structure of a measurement system used in fluorescence measurements. The connection to microinjection is also presented more widely and an overview to some problems related to fluorescence measurements is given in the end of the section.

2.5.1. Basic Principle

Fluorescence is a phenomenon, in which a substance absorbs light with a certain wavelength and emits light with a longer wavelength almost immediately after that.

Some fluorescence is found in many substances but this so-called autofluorescence is usually rather weak and therefore special fluorescent dyes or fluorophores with really strong fluorescence have been developed for actual fluorescence experiments. The wavelength a fluorescent dye absorbs is called *the excitation wavelength* and the wavelength a fluorescent dye emits is called *the emission wavelength*. For example, a fluorescent dye called as fluorescein has an excitation wavelength of 450–490nm and an emission wavelength of 514–568nm, which means that it is excited with blue light and it emits green light. The processes involved in fluorescent activity are traditionally illustrated with a Jablonski diagram shown in Figure 2.3. [13].

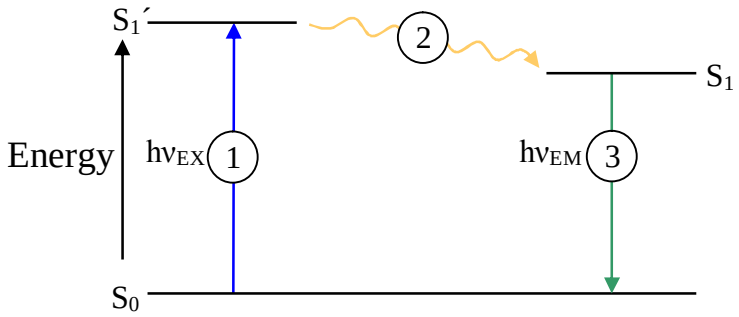

Figure 2.3: The Jablonski diagram describing the processes involved in optical absorption and emission of fluorescence. The numbers and symbols in the figure are explained in the text below.

The interpretation of Figure 2.3 is as follows: (1) An external source such as an incandescent lamp or a laser supplies a photon of energy hv_{EX}, where h is Planck's constant (6.62×10^{-34}m^{2}kg/s) and v_{EX} is the frequency of the photon. A fluorophore particle, which has an initial energy state S_0, absorbs the photon and moves to a higher energy state S_1'. This state lasts only 1–10ns. (2) The energy of S_1' is partially dissipated and a relaxed state S_1 is created. This state is the origin of the fluorescence emission. (3) A photon of energy hv_{EM}, where v_{EM} is the frequency of the photon, is emitted and the fluorophore returns to its initial energy state S_0. Since some energy is dissipated in the step 2, the energy of the emission photon hv_{EM} is lower than the energy of the excitation photon hv_{EX} and thus the frequency v_{EM} is lower than v_{EX}. In other words, the emitted light has a longer wavelength. [13].

Fluorescent dyes are widely used in labelling of biological units and molecules such as cells, parts of the cells and DNA. The common strategy is to combine fluorescent molecules with, for example, antibodies and DNA counterparts to make them attach selectively to a specific region of a biological specimen or respond to a specific stimulus [13]. These kinds of fluorophores are known as fluorescent probes. Figure 2.4 shows fluorescent probes attached to cell nuclei.

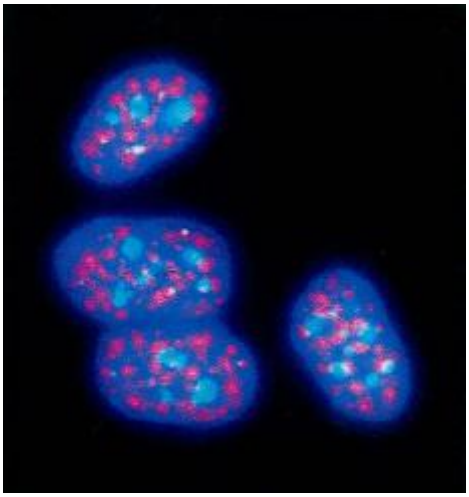

Figure 2.4: HeLa cell nuclei incubated with blue and red fluorescent probes targeted to different nuclear-localized antigens [13].

As it can be seen in Figure 2.4, the different parts of the cell, which are not normally distinguishable, can be made clearly differentiable with fluorescence.

2.5.2. Structure of a Fluorescence Measurement System

The system for fluorescent measurements consists of an effective light source for excitation, a wavelength filter for the excitation light, a wavelength filter for the emission light and a detector [25]. The first filter is used to filter all other wavelengths except the excitation wavelength out from the light coming from the light source to the specimen. The second filter filters all other wavelengths but the emission wavelength out from the light going to the detector from the specimen. Thus, the second filter removes the reflections of the excitation light and the possible disturbances from the environment from the light going to the detector. The detector such as a CCD cell detects the number of photons it receives from the specimen and thus detects the number of the fluorophores in the specimen. This way, for example, the number of specific DNA sections, to which the fluorescent probes attach, in the specimen can be counted. If the mission is only to see some particular divisions of the sample, a microscope ocular is used instead of an actual detector. Figure 2.5 illustrates the structure of the fluorescence measurement system.

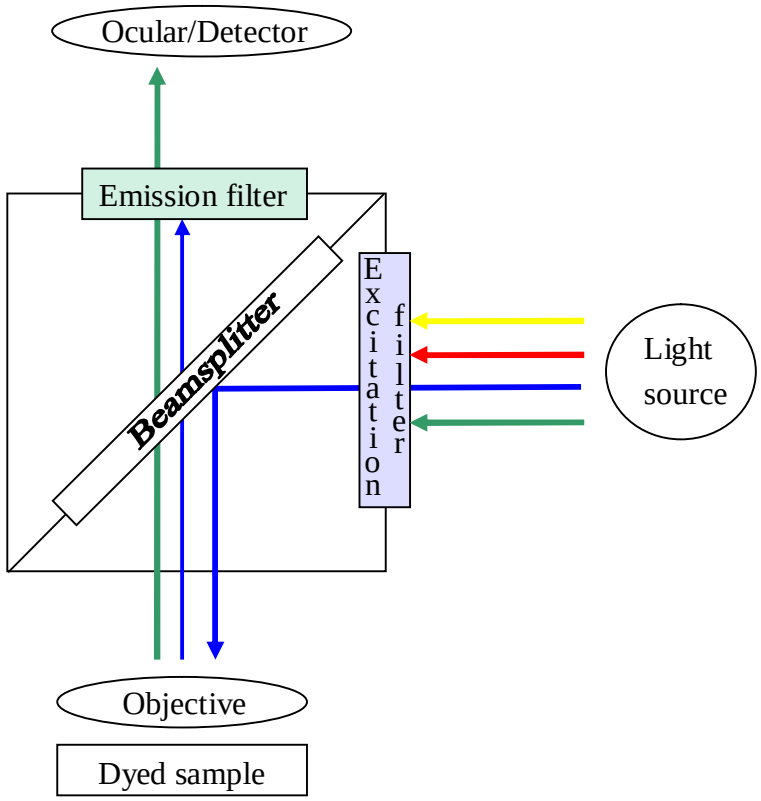

Figure 2.5: Schema of the filters in the fluorescence measurement system.

The excitation filter, the emission filter and the beam splitter are all integrated to a component called the filter cube. Different filter cubes are available for different fluorescent dyes and they can be changed easily to the measurement system.

2.5.3. Connection to Microinjection

Microinjection is one way to transfer the fluorescent probes into the target cells. Also, as mentioned in Section 2.4.2, fluorescent dyes are commonly used in calibration of microinjection systems. In addition, fluorescence is used in testing the performance of microinjection systems. By injecting a fluorescent dye into cells one can easily see the number of successful injections as a number of cells that exhibit fluorescence. Fluorescein isothiocyanate (FITC) is a derivative of fluorescein, which is often used in cell research and also for this purpose. On the other hand, injections with some gene, which induces production of fluorescent protein in the cell after some hours or a day, provide information on the survival rate of the injected cells. One dye used in such tests is green fluorescent protein (GFP). Figure 2.6 presents microinjections with fluorescent dye as the injection liquid.

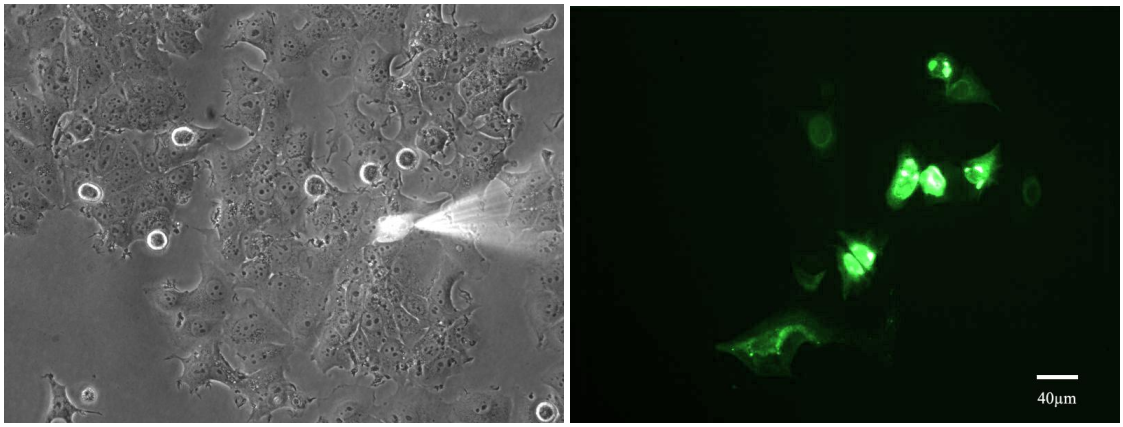

Figure 2.6: MCF-7 cancer cells injected with FITC (in the left, the pipette seen in the middle of the picture in the right) and cells exhibiting fluorescence after injections (in the right) [24].

2.5.4. Challenges in Fluorescence Measurement

The common problem in fluorescence measurements is photobleaching, which means destruction of excited fluorophores (in state S_1 in Figure 2.3). This phenomenon lowers detectability of fluorescence. There are numerous photochemical reaction pathways, which cause photobleaching, but they are not in the scope of this thesis and thus are not covered in this section. [13].

As discussed earlier in this section, many substances exhibit fluorescence. Therefore, the plastic wells, in which the specimen lays, or the liquid media it is immersed in, may exhibit some fluorescence and this background fluorescence disturbs the actual measurements. It is important to use material with as low fluorescence as possible and measure the background fluorescence before actual measurements. This way, the background fluorescence can be subtracted from the measurement results afterwards.

2.6. Conclusion

This chapter presented the capillary pressure microinjection technique and its applications with suspension cells and adherent cells as well as gave an overview of the system needed in CPM. It revealed that the most crucial problems are faced in the CPM of living adherent cells. Therefore, the scope of this thesis work is in the field of adherent cells and this work aims at developing a method for estimation of the injection volume to enable automating of the CPM technique for adherent cells.

3. IMPEDANCE MEASUREMENTS OF LIVING CELLS

The previous chapter introduced the capillary pressure microinjection technique with its applications and gave insight into the CPM equipment. It also indicated on one hand the need and on the other hand the lack of the measurement devices gathering data and giving feedback during microinjection experiments. This chapter will discuss the impedance measurement of living cells, a measurement technique used in the field of cell research, and its potential for a measurement method in microinjection.

Section 3.1 introduces the background of the measurement technique and Section 3.2 describes the mathematical models the method is based on. Section 3.3 presents the contact detection device, a custom made measurement device for microinjections produced in the MST-group and Section 3.4 discusses the use of the device and the impedance measurement technique presented in this chapter for the measurements needed in this thesis work.

3.1. Background

Since cells are electrochemical systems, electrical measurements provide useful information of their properties and functioning. A method called patch clamp technique has been used for measuring electrical activity of the ion channels of a single cell for over thirty years. Recordings from an individual channel as well as from all channels in one cell are possible. The method utilizes micropipettes in similar size as in microinjections with chloridized silver electrodes inside. The pipettes are filled with a solution matching the ionic composition of the cell medium or the cytoplasm, depending on the measurement type. The tip of the pipette is brought to a close proximity of a cell to form a tight seal. The seal is still improved by applying a small suction in the pipette. When the contact between the pipette and the cell membrane is tight enough to correspond to a resistance of several gigaohms, the extracellular electrical activity no longer masks the desired ionic currents, which are in the scale from picoamperes to nanoamperes, and they can be measured using a special patch clamp amplifier. [22], [34].

In addition to measuring the ionic currents, a patch clamp system can be used to measure the impedance of the cell, which is another parameter giving lots of valuable information of the cell and its functioning. With single cells, the impedance measurement has been used in measuring endo- and exocytosis of the cell [27], [55], as well as in measuring the size, the shape, abnormalities and aging of the cells [11,] [30],

[50], [51], [56]. In addition to using a patch clamp device, the impedance measurements can be done using planar film electrodes, on which the cells are growing, [56] or microfluidic channels, through which the cells are flowing [11], [40]. However, the patch clamp configuration is the most interesting for this work since it resembles the microinjection setup.

3.2. Electrical Circuit Models of Pipette and Cell

The impedance measurement of the cells is based on the fact that living cells can be described as passive electrical circuits, whose component values are proportional to the geometry, morphology and electrical properties of the different parts of the cell. Functioning of the cell changes some of these parameters – for example, endo- and exocytosis change temporarily the surface area of the cell – and these changes cause also the impedance of the cell to change. Impedance changes can be linked to the specific parts and actions of the cell by comparing the actual measurements to calculations and simulations with the electrical circuit models. Hence, the electrical circuit models help in interpreting the measurement results. Since the patch clamp configuration for impedance measurement is the most relevant setup for this work, this section concentrates on the models related to it and introduces the electrical circuit models for a cell, a pipette and a system consisting of a cell and a pipette.

3.2.1. Cell

When thinking a flow of current to or from a cell, the most important part of the cell is the cell membrane. Inside the cell is the cytoplasm, which consists of the intracellular fluid cytosol and the cell organelles, and since cytosol is mostly water it does not affect much the flow of current. Therefore, the component having most influence on the current is the cell membrane. The cell membrane comprises a lipid bilayer and ion channels, which go through the bilayer. The structure of the cell membrane is shown in Figure 3.1.

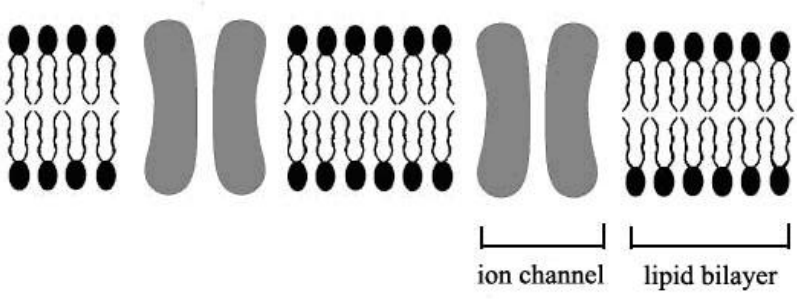

Figure 3.1: The schematic structure of the cell membrane [2].

The ion channels transport ions to and from the cell and therefore the channels have a certain conductance while they are open. Thus, the ion channels can be described by resistors with resistance equal to the inverse of the conductance of the channels [2].

Since the lipid bilayer consists of two layers near each other and charged particles cannot penetrate it, the lipid bilayer can be presented as a capacitor [2], [30]. Therefore, the cell membrane can be modelled as a parallel connection of resistances and capacitors and further simplified as a parallel connection of a single resistor and a single capacitor [2], [39]. This model is presented in Figure 3.2.

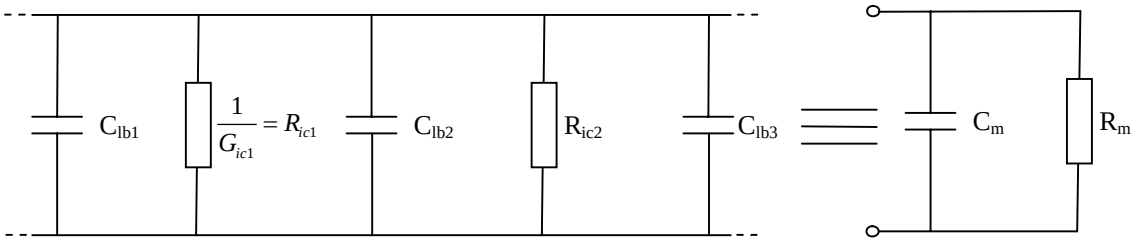

Figure 3.2: The RC circuit model of the cell membrane. G_{ic1} is the conductance of an ion channel, R_{ic1} and R_{ic2} are the resistances of the ion channels and C_{lb1}, C_{lb2} and C_{lb3} are the capacitances of the lipid bilayer sections between the channels. C_m is the membrane capacitance that consists of all the bilayer section capacitances and R_m is the membrane resistance consisting of all the ion channel resistances.

As mentioned above, the intracellular fluid is mostly conductive and hence we can model the whole cell with the RC model presented in Figure 3.2. This simplified model is very popular and commonly applied and it has been used, for example, in [2], [3], [38], [39], [40], [44], [46], [51], [55] and [61].

3.2.2. Pipette

Since a micropipette with electrode inside is used in measuring the cell impedance, its impedance is visible as well in the measurement result. Therefore, the electrical properties of the pipette should be known. The silver wire electrode connected to the measurement circuitry is inside the pipette in the pipette solution and the pipette is pushed into the cell growth medium, which is grounded with the ground electrode. When a stimulus signal is fed to the pipette electrode, the current can flow to the ground electrode using two routes. The first is through the pipette tip. Since the pipette solution forms a very narrow column of conductive liquid in the tip, the tip could be modelled as a resistor with the formula [16]:

$$R_{pip} = \rho_{liq} \frac{4l_{pip}}{\pi d_{pip}^2} \qquad (3.1)$$

where ρ_{liq} is the resistivity of the liquid, l_{pip} is the length of the narrow tip section and d_{pip} is the tip diameter of the pipette. The second route is through the wall of the pipette.

The immersed part of the pipette is an insulating pipe full of and surrounded with conductive media with a potential difference. Hence, the pipette and the liquids can be thought to form a capacitor whose capacitance may be approximated with the capacitance of a cylindrical capacitor [16]:

$$C_{pip} = \frac{2\pi\varepsilon_g\varepsilon_0 l_{tip}}{\ln\left(\frac{2\tau_g + d_{pip}}{d_{pip}}\right)} \qquad (3.2)$$

where ε_0 is vacuum permittivity, ε_g is the permittivity of the pipette glass, l_{tip} is the length of the pipette part in the medium and τ_g is the thickness of the glass. The current can flow from a capacitor plate to another that is from the pipette solution to the cell growth medium using the capacitance. Thus, also the electrical circuit model of the pipette is a parallel connection of a resistor and a capacitor [39], [55]. Figure 3.3 illustrates the pipette tip in the medium as well as its passive circuit component model.

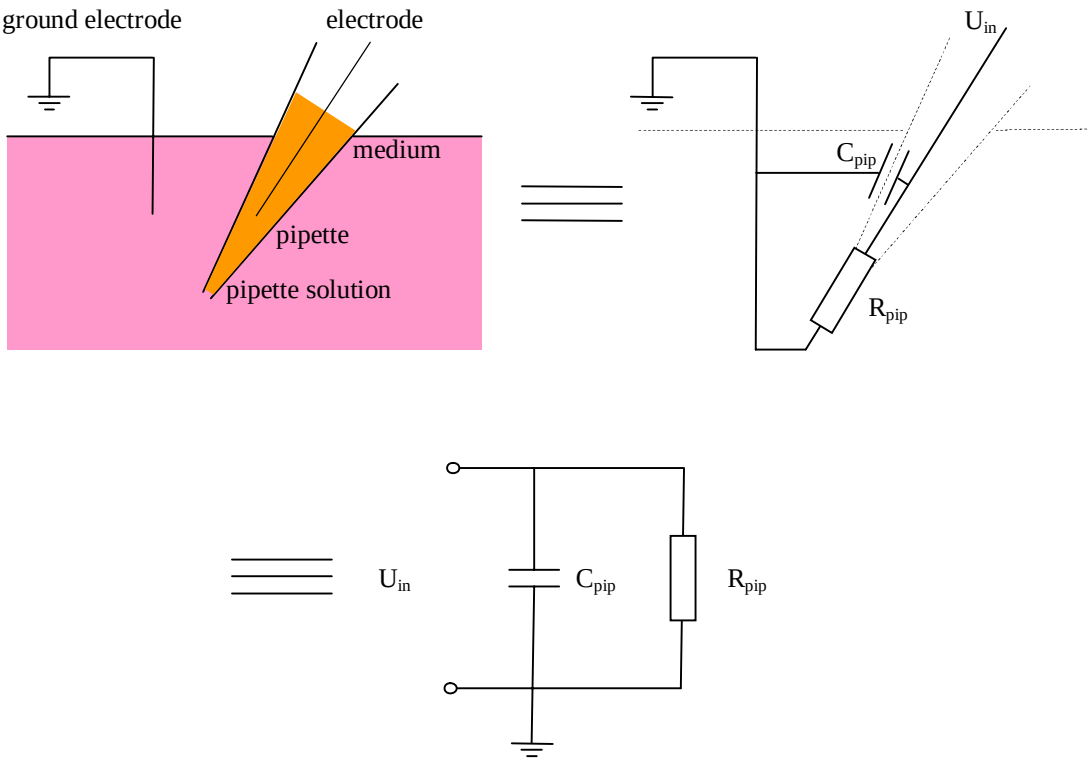

Figure 3.3: A sketch of the pipette tip immersed into cell growth medium (up, left), electrical circuit model components added to the sketch (up, right) and the redrawn circuit mode (down).

3.2.3. Pipette – Cell System

When the pipette is not in contact with the cell, only the circuit in Figure 3.3 can be thought to be connected to the electrodes of the measurement device. However, during a contact, the circuits in Figure 3.2 and Figure 3.3 are connected to each other and the system is described with a circuit model shown in Figure 3.4 [39]. Slightly more simplified versions of the model in Figure 3.4 are seen in [44] and [55].

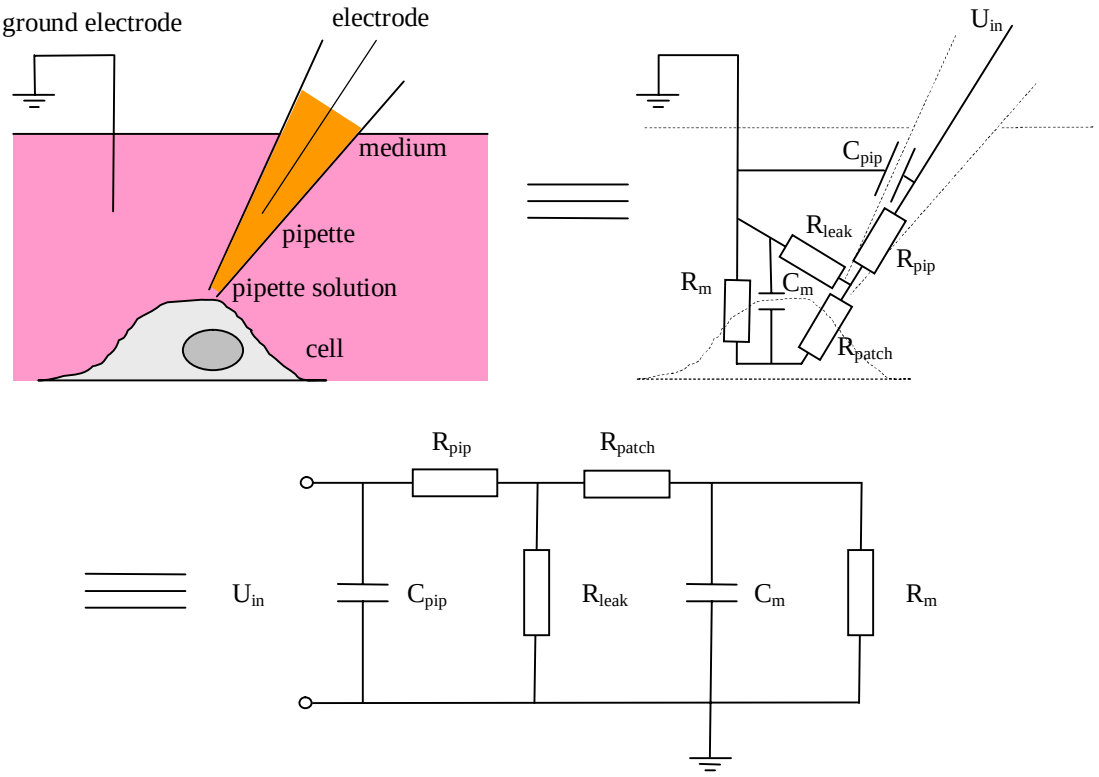

Figure 3.4: The electrical circuit model of the contact between the pipette and the cell.

The parameter R_{patch} means the resistance of the area of the cell membrane just under the pipette tip [39] and it becomes negligible after penetration. The value of the parameter R_{leak} is directly proportional to the tightness of the contact between the pipette and the cell [39]. If the contact is not tight, a great portion of current flows from the capillary to the medium through the gap between them. Thus, the value of R_{leak} is low and the flow of current to the circuit describing the cell is low as well. If the contact is tight, the gap is very small and the amount of the leaking current is significantly lower. [16]

Use of the electrical measurements and the model in Figure 3.4 for the interpretation of the results of the electrical measurement can provide useful information of the injection procedure. The difference between the circuits in Figure 3.3 and Figure 3.4 indicates that the contact between a pipette and a cell can be detected by electrical measurement. The impedance of the model in Figure 3.3 can be expressed in *s*-form as

$$Z_{pip}(s) = \frac{1}{C_{pip}s + \frac{1}{R_{pip}}} \tag{3.3}$$

whereas the impedance of the model in Figure 3.4 is the form

$$Z_{can}(s) = \frac{R_m C_m (R_{leak}R_{patch} + R_{leak}R_{pip} + R_{patch}R_{pip})s + R_{leak}(R_{patch} + R_m + R_{pip}) + R_{pip}(R_{patch} + R_m)}{R_m C_m C_{pip}(R_{leak}R_{pip} + R_{leak}R_{patch} + R_{patch}R_{pip})s^2 + \left[R_m C_m (R_{leak} + R_{patch}) + R_{pip}C_{pip}(R_{leak} + R_{patch} + R_m) + R_{leak}C_{pip}(R_{patch} + R_m)\right]s + R_{leak} + R_{patch} + R_m} \tag{3.4}$$

Therefore, the contact can be detected as a change of impedance. Since the capillary parameters R_{pip} and C_{pip} depend on the geometry of the capillary, the size of the capillary or the changes in the geometry affect these parameters. Thus, changes in R_{pip} and C_{pip} are assumed to indicate the condition of the pipette. In addition to the capillary diagnostics, it is supposed that the model offers information of the target cell. Tumorous tissue has been found to have a lower capacitance than healthy tissue [30]. Therefore, changes in the cell membrane capacitance, C_m, could indicate the condition of the cell. Furthermore, cell division and growth result in changes in the membrane area and therefore affect its capacitance [30]. The state of the cell could hence be detected from the value of C_m. [16]. To be able to estimate R_m and C_m precisely, R_{leak} should be as high as possible and R_{leak} negligible. Penetration with very sharp tips could enable this.

3.3. Contact Detection Device (CDD)

Since the pipettes used in the patch clamp technique are in the same scale as in the capillary pressure microinjections, it is possible to perform the impedance measurements during microinjection tests using similar arrangements. The contact between the cell and the pipette is not as tight as it should be to measure endo- and exocytosis and fine cell morphology but it is still sufficient to sense the difference between the impedances described in Equation (3.3) and (3.4), that is, to detect the contact between the pipette and the cell. Also, when the pipette is not in a contact with the cell, the impedance of the bare pipette can be measured. As mentioned in the previous section, breaking and clogging of the pipette change the geometry of the pipette and thus they also change its impedance as it can be seen from the Equation (3.1) and (3.2). Hence, breaking and clogging can be detected using the impedance measurement.

A separate device for performing impedance-based measurements of the micropipette in microinjection has been developed in MST-group [33]. An injection guidance system based on the device has been created [20] and it has been successfully used in single cell microinjections [20] and micropipette aspirations [23]. The device is called the contact detection device (CDD) and it is an electronic circuitry made for sensing the contact between the pipette and cell, pipette clogging and pipette breakage. It consists of two electronic circuit boards: the main board and the head stage. The main

board contains the electronics for signal preconditioning, filtering and amplification and it is placed further away from the pipette. The head stage comprises the actual sensitive measurement circuitry and it is connected to the pipette using two Ag/AgCl electrodes: the pipette electrode and the ground electrode. The pipette electrode is put inside the pipette to touch the injection liquid and the ground electrode is put into the cell growth medium in the well-plate. To minimize the disturbances and parasitic capacitances, the head stage is placed as close to the capillary as possible. The main board is connected to the head stage with six wires, which feed the head stage the operation voltages and transfer the measurement signals between the head stage and the main board. The operation principle of the CDD is the following: a square form voltage signal is fed to the pipette electrode, the current flowing between the electrodes is measured and converted to a voltage signal, and the different injection moments are detected from the changes in the pulse level of the signal. In other words, the impedance changes of the pipette as presented in Section 3.2.2 and 3.2.3 are used as the markers for the injection moments. Since time domain analysis is used, only resistance is visible in the impedance. Figure 3.5 illustrates the contact detection device connected to a pipette and the main board of the device is shown in Figure 3.6.

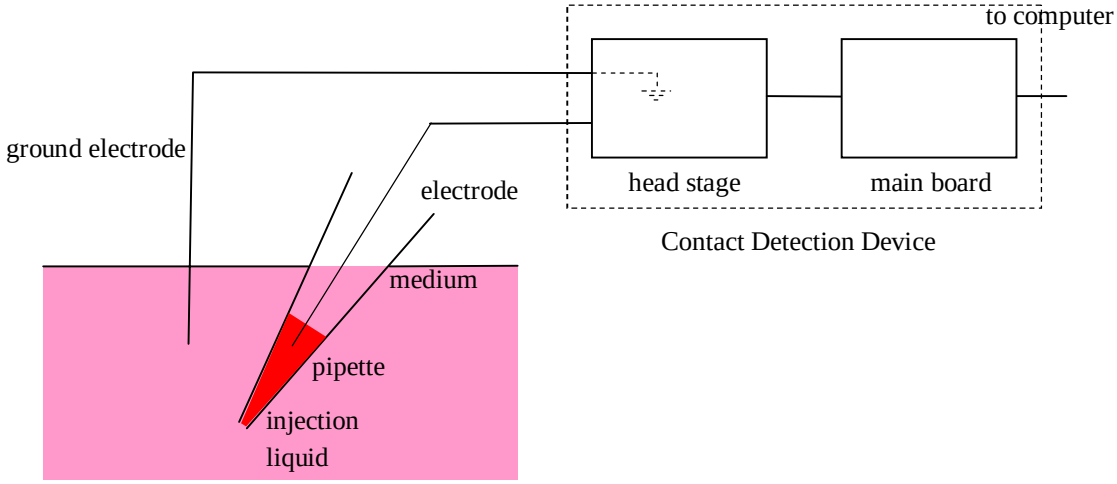

Figure 3.5: Schematic drawing of the contact detection device connected to a pipette.

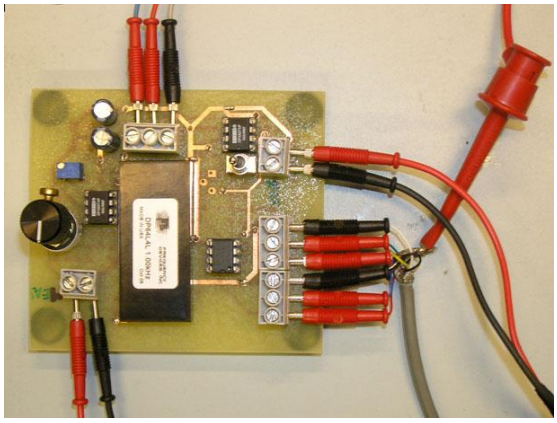

Figure 3.6: The main circuit board of the contact detection device.

The simplified circuit drawing of the device is presented in Figure 3.7. The incoming stimulus signal is first impedance matched with a buffer amplifier and scaled down in the main board. It is then fed to the pipette from the head stage by using a current-to-voltage converter and the Ag/AgCl electrodes. The current induced in the pipette is converted to voltage by the converter in the head stage and this voltage signal is then filtered and amplified in the main board and fed out from the CDD to the measurement board connected to it.

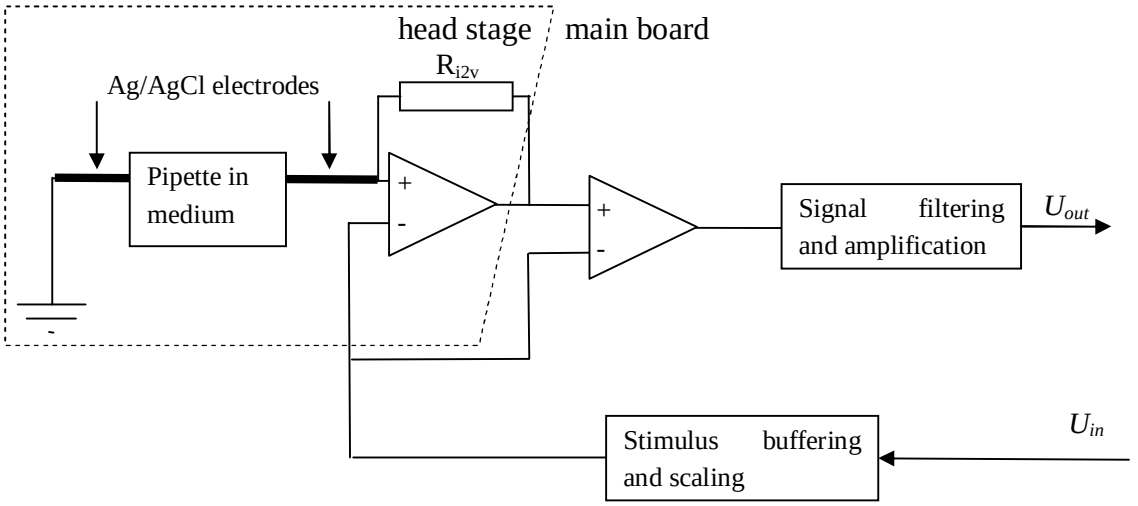

Figure 3.7: Simplified circuit drawing of the contact detection device.

The resistance of the pipette can be calculated using the input and output signals of the CDD. It can be seen from Figure 3.7 that the pipette resistance can be expressed with U_{in} and U_{out} as follows:

$$R_{pip} = \frac{\alpha_{scale}}{\alpha_{ampl}} R_{i2v} \frac{U_{in}}{U_{out}} \qquad (3.5)$$

where α_{scale} is the attenuation in the stimulus scaling block, α_{ampl} is the amplification in the signal amplification block and R_{i2v} is the resistor value in the current-to-voltage converter.

3.4. Pipette Size Measurement Using Impedance Measurement

If the contact detection device is used to measure the pipette resistance by applying Equation (3.5), the result can be used to estimate the size of the pipette tip as pointed out in Section 3.2.3. As shown in Equation (3.1), the resistance is inversely proportional to the pipette tip diameter. The exact diameter is difficult to solve using the resistance value gained since the other parameters, the length of the narrow section of the tip and

the resistivity of the injection liquid, are hard to determine. However, by measuring pipettes of known diameters or combining the CDD measurements with microscopy, some particular resistances and diameters can be linked together. Using these results and intra- and extrapolation, theoretically a diameter corresponding to whatever resistance can be estimated. Also, size monitoring can be continuous in microinjection and therefore the size changes caused by breaking and clogging can be observed. Therefore, this resistance measurement is a potential feedback for a system controlling the injection pressure to maintain a constant injection volume.

3.5. Conclusion

This chapter presented the electrical measurements of the living cells. The background and basics were introduced and an insight to the electrical models behind the technique was given. Also, the custom-made measurement circuitry for impedance measurements in microinjections was depicted. This so-called contact detection device could be used in measuring the resistance of the pipette, which should give information of the geometrical properties of the pipette. This information should be useful in determining the injection volume.

4. MEASUREMENT SETUP

The aim of the thesis work is to develop a method to estimate the injection volume in microinjection in real-time. Since the direct measurement of the flow is extremely challenging as discussed in Section 2.3, the goal is to produce a method, which uses indirect measurement. Here, the actual volume flow is not measured but the key parameters affecting it are measured and the flow is then approximated using these measurements. In other words, the objective is to generate a model for injection volume as a function of the key parameters.

The key parameters were chosen based on the basic equations of the volume flow: the continuum equation

$$Q = vA \tag{4.1}$$

where Q is the volume flow, v is the liquid velocity and A is the cross-sectional area of the channel the liquid is flowing in, and the so-called Ohm's law for fluids

$$Q = \frac{p}{R_{hyd}} \tag{4.2}$$

where p is the pressure and R_{hyd} is the hydraulic resistance. In capillary pressure microinjection, the velocity in Equation (4.1) is caused by the injection pressure. Hence, the injection pressure is the first key parameter. Since the hydraulic resistance depends on the geometry of the channel and the properties of the fluid [5], it can be seen from both equations that the injection volume is proportional to the geometry of the pipette. Thus, the pipette geometrical properties are chosen to be the second key parameter. The properties are measured using the electrical impedance measurement as described in Section 3.4. Therefore, the actual model to be generated is a model of the injection volume as a function of the injection pressure and the pipette electrical resistance. Figure 4.1 depicts the operation principle of the model.

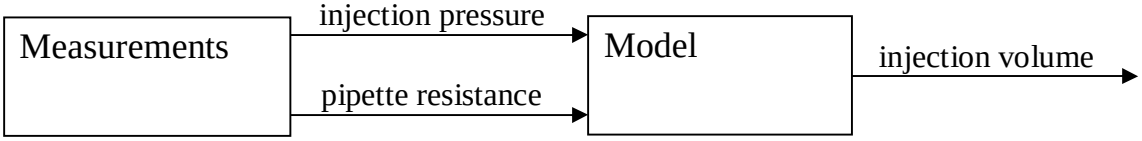

Figure 4.1: Schematic drawing of the operation principle of the model.

The objectives of the measurements are to generate data to compose the model for the injection volume described above. The requirements for the test bench the measurement are performed in are the following: (1) The test bench has to be build around a microinjection system in order to perform measurements during a microinjection process; (2) The test bench has to be able to measure injection pressure and the pipette resistance during a microinjection process; (3) There must be a mean to estimate also the injection volume to link the injection pressure and the pipette resistance to certain volumes; (4) The measurement software should support at least a kilohertz sampling frequency to obtain enough data points from the short injection moments; (5) The measurement software should also be capable of running continuous measurements with the frequency mentioned for 10–15 minutes to record a full injection test.

This chapter discusses the measurement setup used in this work. Section 4.1 presents the test bench architecture. All parts of the test bench are introduced and their main properties and parameters are given. Section 4.2 briefly describes the possible measurement errors of the setup and Section 4.3 introduces the measurement algorithm.

4.1. Test Bench Architecture

The test bench used in the measurements of this work consists of a microinjection system, around which different sensor systems are attached to acquire data of the three variables of interest: the injection pressure, the pipette electrical resistance and the injection volume. The microinjection system the test bench is based on is the microinjection workstation of MST-group and it is presented in more details in Section 4.1.1. Sections 4.1.2–4.1.5 describe the materials and instruments used in the experiments. Section 4.1.2 discusses the pipettes used in the tests, Section 4.1.3 presents the pipette puller used in fabricating some of the pipettes, Section 4.1.4 describes the electrodes used for electrical measurements and Section 4.1.5 introduces the fluorescence dye and the cell growth medium used in the experiments.

The injection pressure is the most straightforward of the measurements. It is measured with a pressure sensor connected to the pressure system of the microinjection workstation. The output of the pressure sensor is connected to a measurement computer to gather the measurement data for the later analysis. The pressure sensor is presented in more details in Section 4.1.6. The computer and software system used is presented in Section 4.1.7.

Pipette resistance is measured using the contact detection device introduced in Section 3.3. In standard microinjection applications, the CDD is connected to the computer controlling the microinjection system and the same user interface, which is used to control the microinjection system, feeds the stimulus signal to the CDD and analyzes the pulse levels of the measurement signal to detect the contacts, the breakages and clogging as discussed in Section 3.3. However, in this application both the input and the output of the CDD are connected to the same measurement computer as the

pressure sensor. The measurement program used feeds the stimulus signal and saves both the stimulus signal and the measurement signal for the later analysis.

The hardest parameter to measure is the injection volume as discussed in Section 2.3. Information of the injection volume is obtained by using a fluorescent dye as the injection liquid and measuring the intensity of the outcome of a single injection using fluorescence microscope imaging and image processing. Thus, the procedure is similar to the one described in Section 2.4.2. Fluorescence was selected for the method for the volume estimation in this work since it there is experience on its use in the MST-group, the devices and software for fluorescence measurements exist and the technique and the analysis of the measurement results are rather simple. The fluorescence dye is injected in a well-plate well filled with cell culturing medium, the injection process is imaged and the images are processed afterwards with a data handling algorithm realized in a computer program. The micropipette is immersed into the medium and driven near to the bottom of the well-plate to get the tip and the fluorescent dye coming out from the tip in injections in focus.

For finding easily the injection moments from the measurement data, the control signal of the solenoid valve used for pulse generation in the pressure system is also recorded. The control signal is a digital signal and thus the opening and closing moments of the valve are simple to find from the data. By using the injection moments, parameters such as the pipette resistance just before the injection, actual injection pressures and images taken before and after an injection are detected for modelling. Figure 4.2 illustrates the simplified test bench architecture.

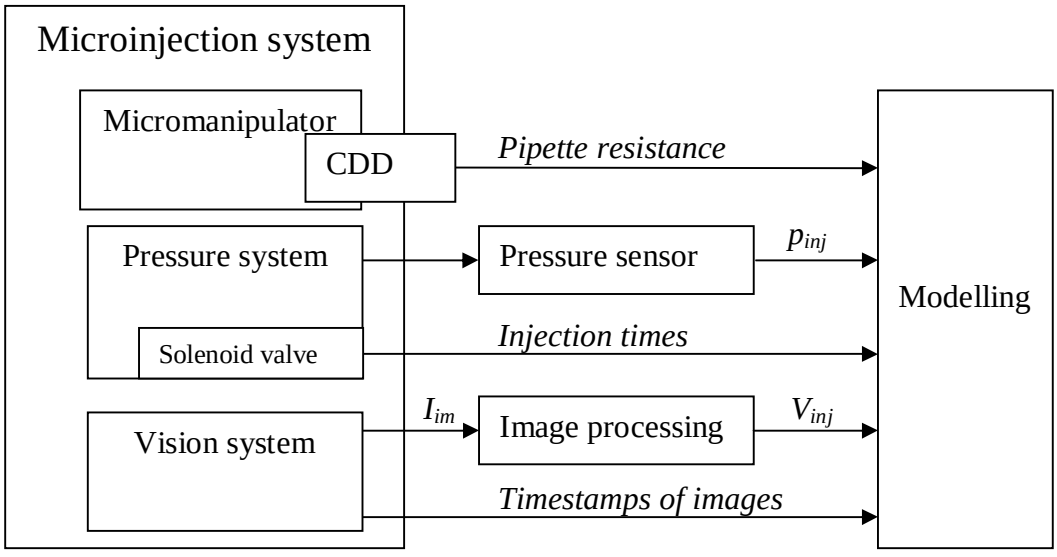

Figure 4.2: Simplified test bench architecture with the information flows, where p_{inj} is the injection pressure, I_{im} is the image intensity and V_{inj} is the injection volume.

4.1.1. Microinjection System

MST-group has developed a semi-automatic microinjection system [26], which has been successfully used in performing single cell microinjections [57], [58] as well as micropipette aspirations (picking up cells) [23]. The microinjection system consists of the MANiPEN 4 micromanipulator, the pressure system and the vision system. The microinjection system is controlled with two computers, both of which have a separate controlling program. The parts of the microinjection system as well as the software used to control it are all presented in more details below.

MANiPEN 4 Micromanipulator

The micromanipulator used in the system is a custom made manipulator with three degrees of freedom and it is called MANiPEN 4. It comprises a linear stepper motor, which provides the vertical motion, and two piezoelectric bender actuators, which are responsible of the horizontal movement. Also, there is a piezoelectric stack actuator for really fine, short and rapid vertical movements. The actuators are connected in series and the micropipette is attached to the end of the lowermost bender as illustrated in Figure 4.3.

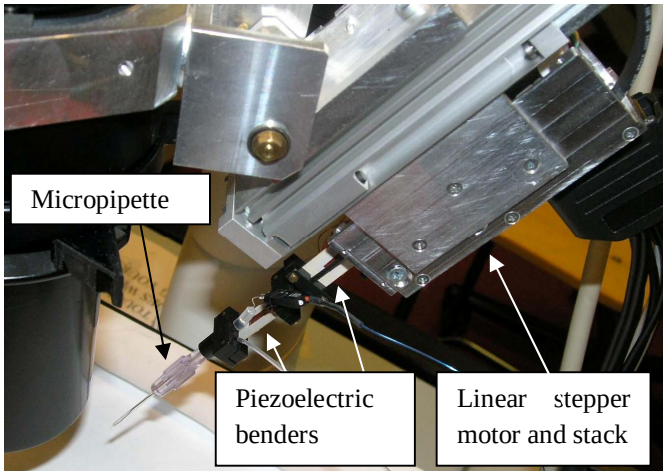

Figure 4.3: The MANiPEN 4 micromanipulator.

The range of the linear motor is +10mm while the range of the piezoelectric benders is ±1mm. The resolution is about 1µm. As seen in the figure, the manipulator is fixed on an inverting microscope in an angle of 45º. The micromanipulator is controlled by a tailor-made computer program MART, of which there is more information in the end of this section.

SmarAct Micromanipulator

Due to some technical problems encountered with the MANiPEN 4 micromanipulator, also a new manipulator using commercial SmarAct SC-1760 linear positioners was implemented. The positioners have one degree of freedom, a moving range of ±20.5mm

and a sub-nanometer resolution [53]. The operation principle of the positioners is oscillating piezoelectric actuators. The manipulator consists of an aluminium stand, three SmarAct positioners fixed to the Cartesian coordinate system and a pipette holder. The stand is fixed on the inverting microscope as MANiPEN 4. Figure 4.4 represents the SmarAct micromanipulator.

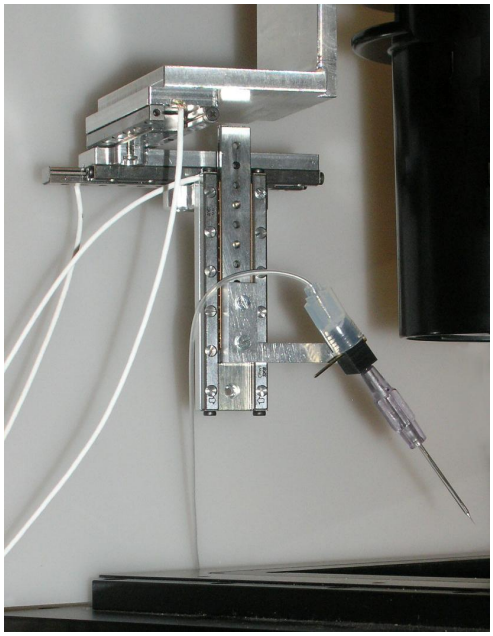

Figure 4.4: The SmarAct micromanipulator.

As seen in Figure 4.4, the pipette is fixed to a bit steeper angle than in MANiPEN 4. The SmarAct manipulator is controlled with a separate SmarAct HCU-3D control unit. The operator moves the positioners and changes the step size by turning the knobs in the control unit.

Pressure System

The pressure system of the microinjection station is also custom-made and controlled with the same computer program as the manipulator. The system obtains its input pressure from a 700kPa pressure line and lowers and adjusts the pressure for microinjections and aspirations with an electro-pneumatic transducer. With injections, the pressure range is from 0 to 35kPa. The adjusted pressure flows to the micropipette through a solenoid valve, which generates the fast and precise pressure pulses needed in injections and aspirations. The output of the solenoid valve is connected to the pipette connector of the micromanipulator in use by using a thin silicone hose. [15].

Vision System

The core of the vision system is a Nikon Eclipse TS100F inverted microscope with a Nikon TI-FM epi-fluorescence attachment and a Nikon C-SHG mercury lamp illuminator for fluorescence experiments. The microscope has objectives with magnifications of 4x, 20x and 40x and an eyepiece with magnification of 10x. The total

magnifications gained are then 40x, 200x and 400x. The dish containing the cells to be injected is fixed on the Märzhäuser SCAN IM 120 x 100 xy-table of the microscope below the MANiPEN micromanipulator. To free the operator from looking through the microscope eyepieces during experiments and to enable recording of visual data from tests there is a Diagnostic Instruments SPOT RT Monochrome CCD camera connected to the microscope. The camera sends the video signal to the computer and the entire process is seen in the monitor. A custom-made machine vision program Genomanda is used in gathering the image data. The program itself is presented in the end of this section.

Software

MART

MART is the program used to control MANiPEN and the pressure system in real-time. Operator moves the manipulator and performs the injections and aspirations by using a keyboard or a joystick and the program gives the feedback by showing the relative position of the needle tip and graphs describing the actuator limits. The operator can change the manipulator speed and the injection parameters such as the injection time, the injection pressure and the back pressure from the program menus. [49]. Figure 4.5 shows the MART main window and the control output and measurement signal graphs, which are the most important graphs for operating MANiPEN.

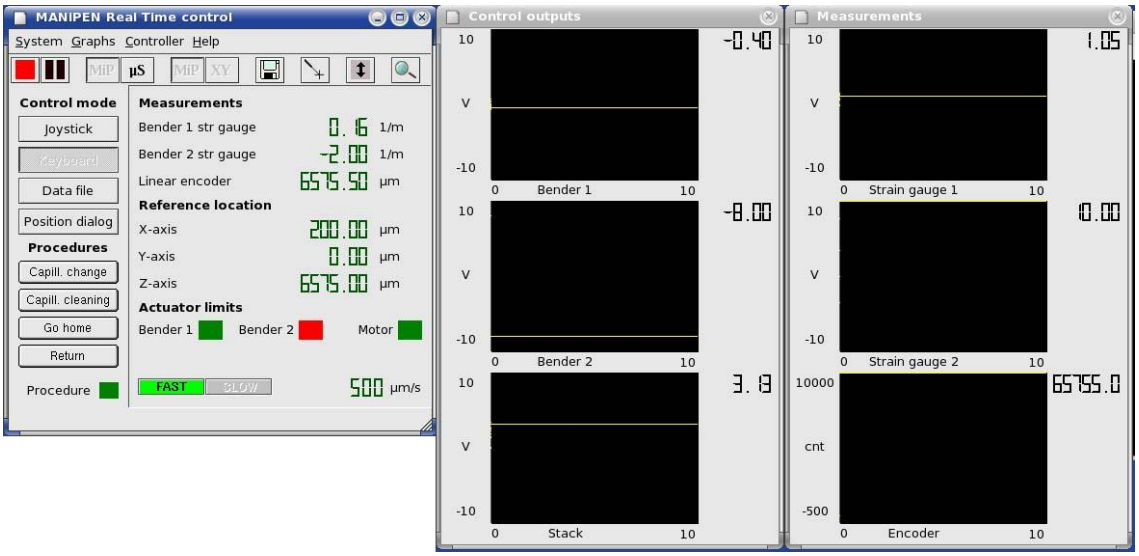

Figure 4.5: MART main window and two most important graph windows.

The main window is used for controlling the manipulator. The control signals going to the actuators of MANiPEN can be monitored in the control outputs window and the measurement signals coming from the sensors measuring the actual motion of the actuators are seen in the measurements window.

Genomanda

The program, which reads the image data from the camera of the microscope, is called Genomanda. It was originally developed by VTT (Technical Research Centre of Finland) for a project for manipulation, detection and analysis of genes. The program shows the microscope view in a computer monitor in real-time and the user can save the image data of interest to the hard drive in jpeg-form. Saving can be done either manually by saving the view currently displayed in the program window or in a certain interval. The saving interval as well as the saving directory can be chosen in the program menu. The program puts a timestamp describing the time the image has been taken in precision of one hundredth of a second to the image names. The user can also define the exposure time, which means how long the camera is allowed to gather light for one image and thus what is the interval between the microscope views shown in the program window. Therefore, the exposure time is also the limit for the saving interval. The exposure time is in tens of milliseconds in normal light microscopy with a sufficient light source while it must be in hundreds of milliseconds in fluorescence microscopy where the amount of light is significantly lower. In addition to adjusting the exposure time and the saving interval, the user can mark the cells visible in the microscope view for post-injection monitoring, check the intensity level of the current view and control the microscope lamp and the motorized focus remotely. The main window of the Genomanda software is shown in Figure 4.6.

Figure 4.6: Genomanda main window.

The basic adjustments such as taking pictures and changing the exposure time or saving are seen in the top of the screen and the post-injection monitoring commands are seen in the right edge of the screen.

4.1.2. Pipettes

Five different pipette sizes are used in the fluorescence injection experiments to acquire enough data points for the model. The pipettes were commercial and their parameters are presented in Table 4.1.

Table 4.1: Parameters of the pipettes used in the injection tests.

Size/µm	Tolerance	Material	Manufacturer	Model
0.5	±0.2µm	Borosilicate glass	Eppendorf	Femtotip II
1	±20%	Borosilicate glass	WPI	TIP1TW1
2	±20%	Borosilicate glass	WPI	TIP2TW1
5	±20%	Borosilicate glass	WPI	TIP5TW1
10	±20%	Borosilicate glass	WPI	TIP10TW1

The Femtotip II pipettes by Eppendorf have a plastic attachment with threads, with which it can be fixed to the arm of the micromanipulator. The pipettes manufactured by WPI need to be attached to a separate Teflon adapter with the threads before connecting to the manipulator. Figure 4.7 shows the pipettes and the connectors and Figure 4.8 illustrates a tip of a Femtotip II pipette imaged with scanning electron microscopy (SEM).

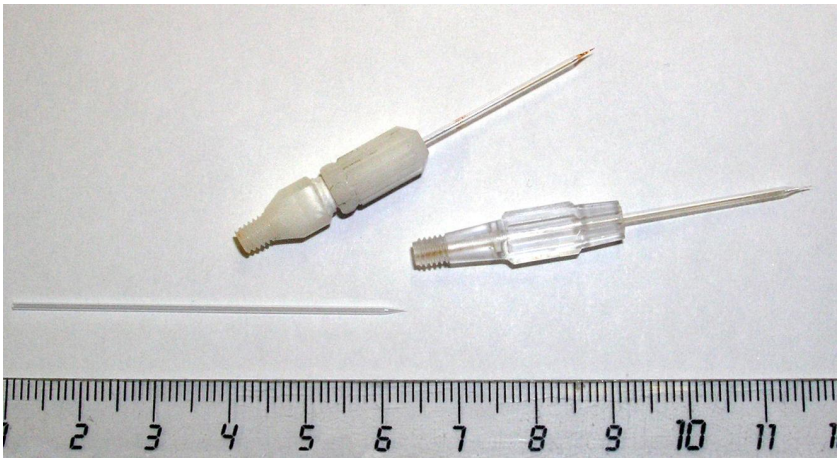

Figure 4.7: Pipettes used in the injection tests. From left to right: a pipette manufactured by WPI, a pipette manufactured by WPI attached to a capillary holder and an Eppendorf Femtotip II pipette.

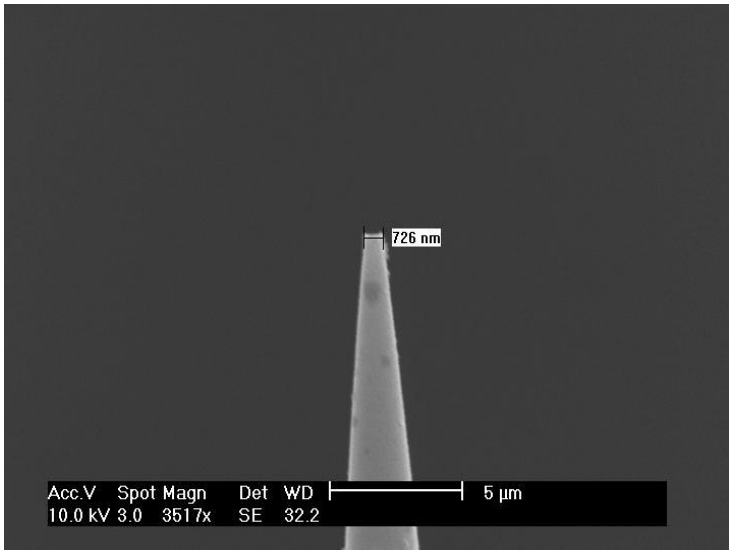

Figure 4.8: A SEM image of a Femtotip II pipette tip.

Some extra data was obtained using self-pulled pipettes. The pipettes were pulled out of Sutter Instruments quartz glass tubings with the inner diameter of 0.9mm, the outer diameter of 1.20mm and the length of 10cm. The pipette puller used was Sutter Instruments P-2000, which is presented in the next section. Appendix A describes the program used in pulling the pipettes. Figure 4.9 depicts a quartz glass tubing and two self-pulled pipettes.

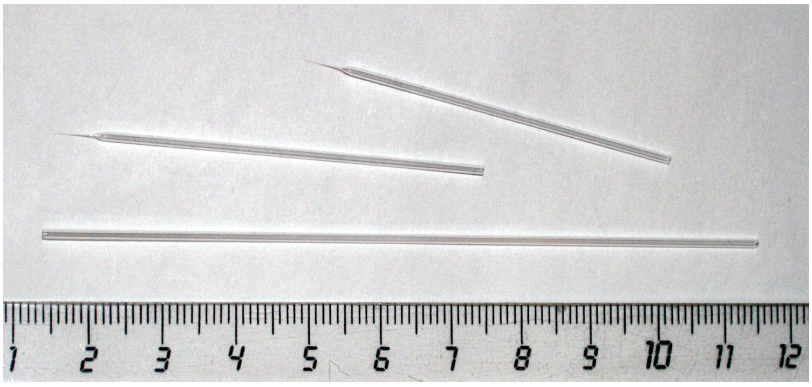

Figure 4.9: A quartz glass tubing and two self-pulled pipettes.

The tip diameters of the self-pulled pipettes vary from 15µm to 40µm and their length is around 5cm. For attaching the pipettes to the micromanipulator, a similar adapter to the one used with the pipettes manufactured by WPI was applied.

4.1.3. Pipette Puller

The pipette puller used in pulling the pipettes out of quartz glass tubings was Sutter Instruments P-2000. It is a laser-operated pipette puller capable of pulling pipettes out of borosilicate, aluminosilicate and quartz glass. The pipette puller is represented in Figure 4.10.

Figure 4.10: Sutter Instruments P-2000 pipette puller.

The tubing is attached from the both ends to the puller bars of the puller seen above the keyboard and the screen in Figure 4.10, a laser beam heats the middle parts of the tubing until it softens and finally the puller bars pull the ends apart producing two almost symmetrical pipettes. The parameters such as the heating power of the laser, the width of the laser beam and the power of the pull are defined in the program menu of the device. A set of parameters is called a pulling program and the user can save 100 different pulling programs to the memory of the pipette puller. Appendix A describes the different parameters of the programs and their effect.

4.1.4. Electrodes

The electrodes connected to the CDD were mostly Ag/AgCl electrodes made of 0.3mm thick silver wire. The wire is chloridized by connecting it to an 8.4V battery and immersing it in 0.15M KCl solution for 1–2 minutes. Also, in some later experiments 0.3mm thick platinum wire was used as the electrode material. Both electrode materials are seen in Figure 4.11.

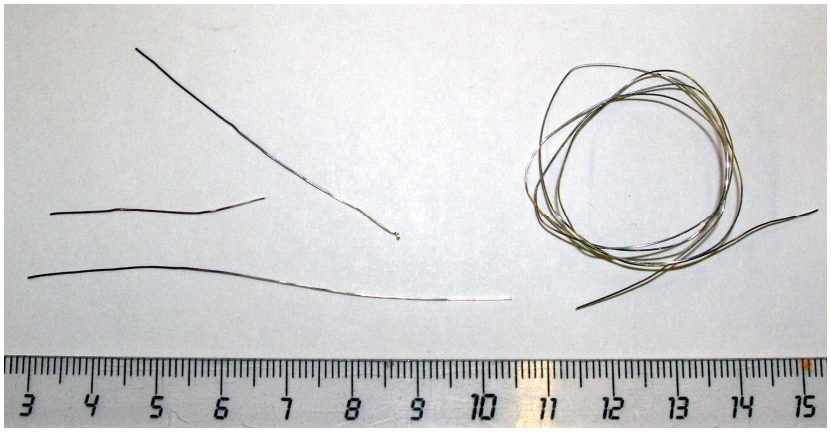

Figure 4.11: Three Ag/AgCl electrodes in the left (the dark end is chloridized) and some platinum wire in the right.

The silver wire has purity of 99.9% and it was purchased from Sargenta. The purity of the platinum wire is also 99.9% and it was acquired from Laborexin.

The difference between the electrode materials is that the silver–silver chloride electrodes are non-polarisable and the platinum electrodes polarisable [43]. The polarisable electrodes pass the current between the electrode and the electrolytic solution by changing the charge distribution within the solution near the electrode whereas the non-polarisable electrodes allow the current to pass freely across the electrode–electrolyte interface without changing the charge distribution in the electrolytic solution [43]. Usually, the polarisable electrodes are used more for excitation and the non-polarised for measuring since the non-polarisable electrodes seem to wear out faster when used for excitation [personal discussions with researchers].

4.1.5. Fluorescent Dye and Medium

The fluorescence dye used in the tests is fluorescence isothiocyanate (FITC) with the concentration of 5mM. The concentration was chosen to maximize the range of pressures and pipette sizes possible to use in tests without the intensity of injections going below the detection limit of the CCD camera or saturating it. The cell culturing medium used in the experiments is L-15 Leibovitz medium. Both the dye and the medium have been previously used in many microinjection experiments in the MST-group laboratory and thus are well-known.

4.1.6. Pressure Sensor Unit

The pressure sensor unit consists of a Sensor Technics HCX series pressure sensor and a custom-made electronic circuit board. The sensor has two inlets, of which the first is connected to the silicone hose going from the pressure system to MANiPEN and the other is in the normal air pressure. The sensor unit gives voltage output proportional to the pressure difference between the inlets. The maximum pressure difference the sensor can measure is 35kPa and the voltage output of the unit varies between 0 and 5V. Pressure is calculated from the output voltage using the equation

$$p_{meas} = aU - b \qquad (4.3)$$

where p_{meas} is the measured pressure, U is the output voltage and x and a are constants. For the unit used, the pressure in Pascals is gained from the output voltage in Volts by applying the equation

$$p_{meas} = 8847.5U - 5215.0 \qquad (4.4)$$

The pressure sensor unit connected to the pressure hose of the microinjection system is shown in Figure 4.12.

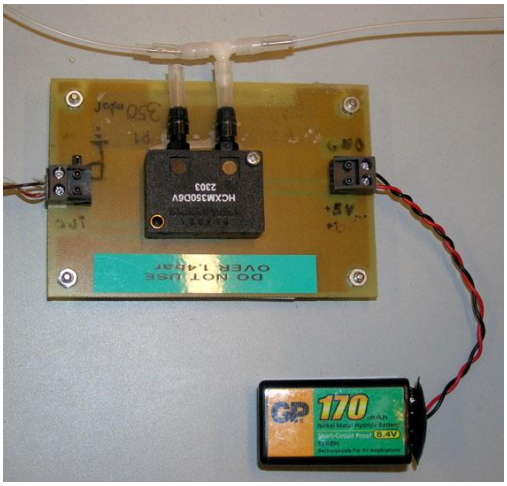

Figure 4.12: The pressure sensor unit used in the experiments.

As seen in the figure, a battery is used as a voltage supply for the sensor. This is done to reduce noise.

4.1.7. Computers and Software

Two computers are part of the microinjection system as discussed in the beginning of Section 4.1.1. The first one is used to control the manipulator and the pressure system with the program MART and the second one is a part of the vision system gathering the image data with the program Genomanda. Furthermore, a data acquisition system is needed for the CDD circuit and the pressure sensor and this system comprises two computers. Two computers are needed since the measurement program, which fulfilled the demands presented in the beginning of this chapter, utilizes a host computer and a target computer. The complete test bench architecture with all the computers and information flows is shown in Figure 4.13. The terms and the names of the information flows are described later in this section.

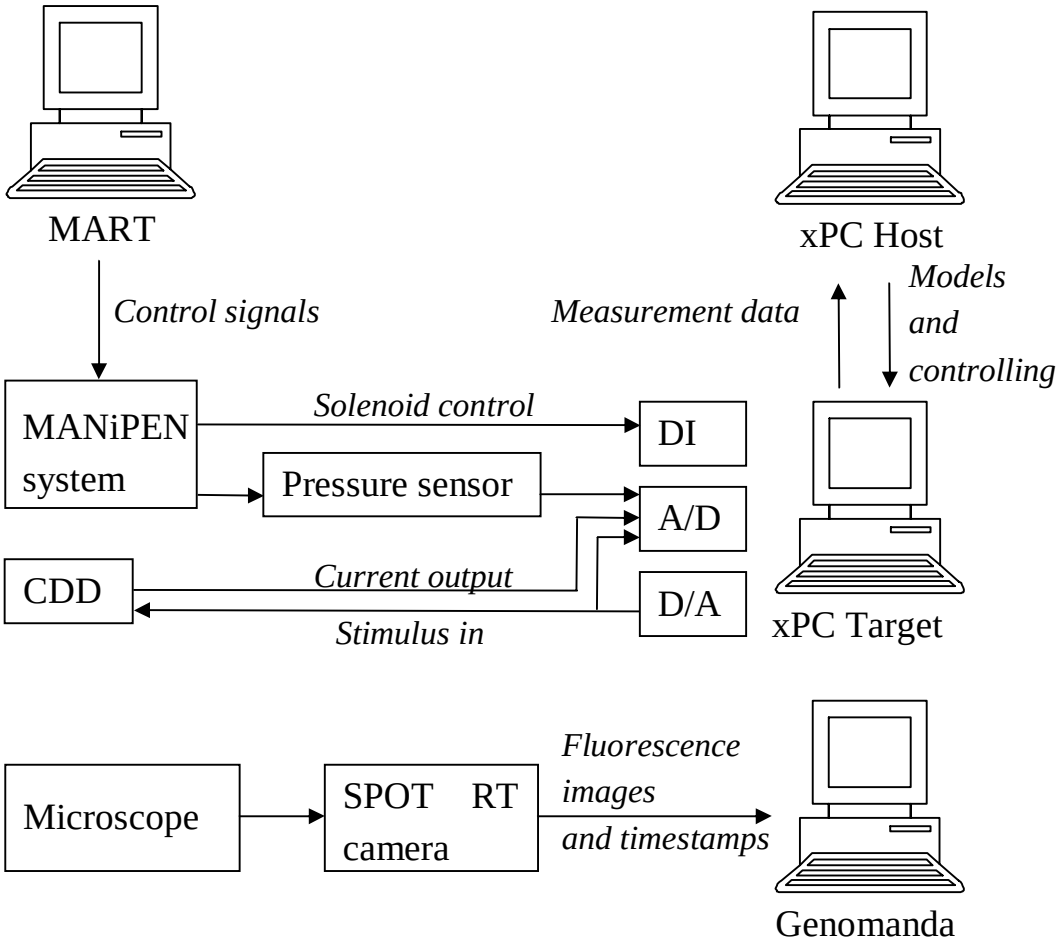

Figure 4.13: The test bench architecture and the information flows. DI means digital input, A/D analog-to-digital converter and D/A digital-to-analog converter.

Measurement Computers

The data acquisition software used needs two computers: one for performing the actual measurements by communicating with the measurement board and the other for controlling the first computer and gathering the data from it after the measurements. The computers are connected to each other via Ethernet. The computer with the measurement board is a 1.5 GHz Pentium 4 with 500 MB of RAM. The measurement board is National Instruments PCI-6052E, which is a 16-bit data acquisition board with 16 analog input channels, 2 differential analog output channels, 8 differential digital input/output channels and a maximum sampling rate of 333 kHz.

Measurement Software

The software used for data acquisition from the measurement board is MATLAB xPC Target toolbox. It is a real-time measurement application, which can sample multiple channels with a maximum frequency of 50 kHz and show the measurement results in graphs in real-time. It was chosen because it fulfills the requirements presented in the beginning of this chapter: it can perform long measurements with high frequencies and

the operator can monitor the measurements during the experiments. For example, the LabVIEW software is not reliable at high frequencies and long measurements with real-time monitoring of the measurement data are problematic with MATLAB Data Acquistion Toolbox. As mentioned above, xPC Target uses two computers. The user interface of the host computer is MATLAB xPC Target Explorer, which is started from MATLAB. With the program, the user can upload the preferred measurement application to the target computer, start and stop the measurements and gather the data from the target computer to the MATLAB workspace of the host computer. Also, some parameters such as the length of the measurement and the sampling frequency can be changed in xPC Target Explorer. Figure 4.14 presents the main window of xPC Target Explorer.

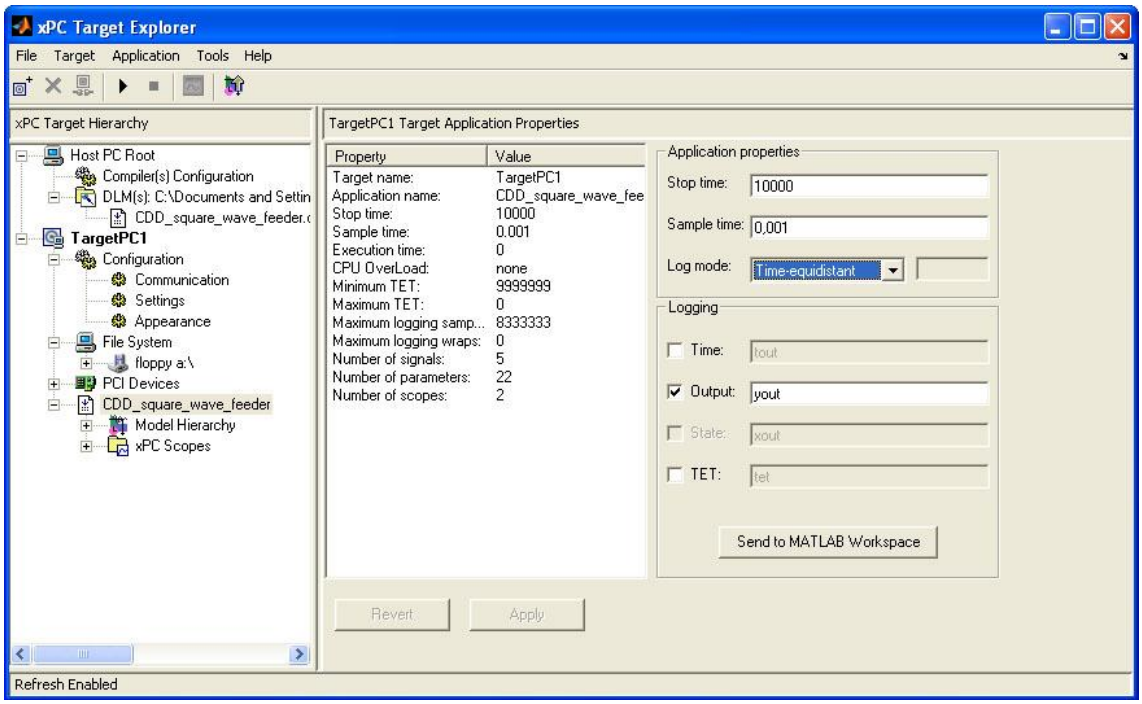

Figure 4.14: xPC Target Explorer main window.

The target computer has its own operating interface and it is booted from a floppy disk. The floppy disk is made with the host computer and it is host-specific. The actual graphical user interface is really simple and it is just for monitoring the tests progress. It shows the name of the measurement application, informs if the application is running or not, reports of the possible errors and – if needed – shows the measurement results in graphs in real-time. As a default, the user cannot give any commands to the interface. The graphical user interface is shown in Figure 4.15.

Figure 4.15: The graphical user interface of the target computer.

The actual measuring application loaded to the target computer is a MATLAB Simulink block model, which is compiled to C language by MATLAB Real-Time Workshop. The measurement board used, the signals going from and coming to the measurement board and the sampling frequency are described to the program in the block diagram. Figure 4.16 illustrates the block diagram used in this work.

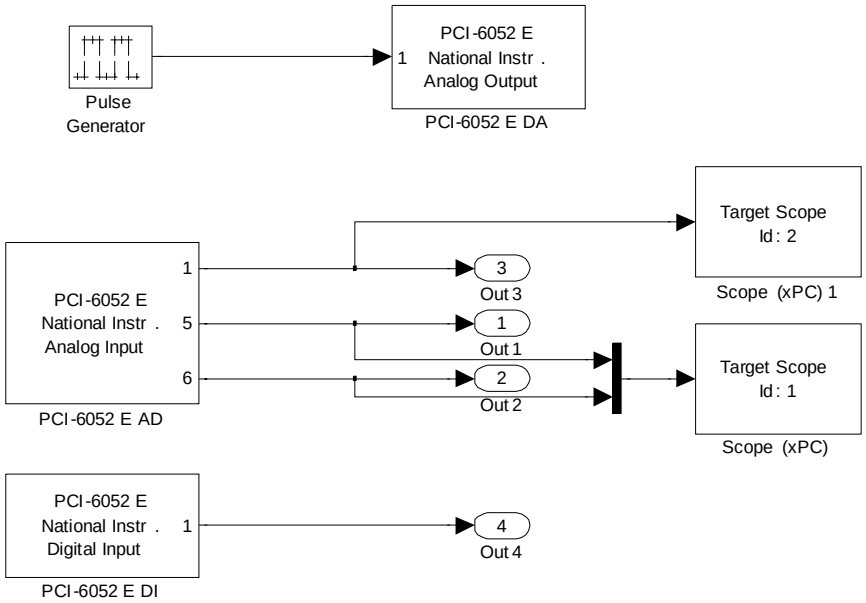

Figure 4.16: The Simulink model describing the connections for measuring.

The pulse generator block in Figure 4.16 is generating the square wave used as the stimulus signal in the CDD. The input of the CDD is connected to the first analog output of the measurement board and therefore the pulse generator block is connected to

the analog output block. The output of the CDD is connected to the differential analog input channel number 5 and the input channel number 6 measures the input signal going to the CDD. The analog input channel number 1 measures the output of the pressure sensor unit. The channels 5 and 6 are both channels for grounded signal sources whereas channel number 1 is for floating signal sources. Since the pressure sensor uses a battery as its power supply as mentioned in Section 4.1.6, the channel for floating sources has to be used. The control signal of the solenoid valve is measured by the digital input channel number 1.

The elliptical 'out' blocks describe, which data is saved and where. xPC Target saves the measurements into an array named 'yout'. The number inside the elliptic block tells the column of the array the data is saved to. Therefore, the resulting measurement data array is an *X**4 matrix, where *X* is the sampling frequency used in Hertz times the length of the measurements in seconds.

4.2. Possible Errors

In model building where the mission is to discover the effect of the injection pressure and the pipette electrical resistance on injection intensity, errors can occur in the actual injection procedure and also in every step of the measurement process. Faults in the system and careless preparation of the experiments may cause unsuccessful injections, which do not provide any useful data. Also, disturbances in the resistance measurement of the pipette, the measurement of the injection pressure and imaging and image processing provide erroneous data for the modelling. The disturbances linked to the different parts of the measurement and modelling procedure are presented in Figure 4.17. All of them are discussed briefly in this section.

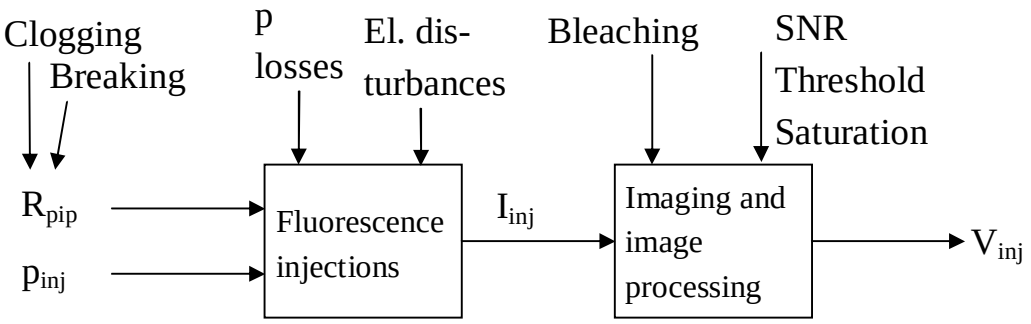

Figure 4.17: Block diagram describing the parameters of the model and the disturbances occurring in the different phases of the measurements.

4.2.1. Pressure Losses

The pressure inside the capillary is not exactly the same as the pressure measured from the hose with the pressure sensor unit since the pipette connector leaks a bit. Also, the really narrow pipette causes some pressure drops.

4.2.2. Electric Disturbances

Electric disturbances such as noise and electric and magnetic fields caused by the other devices in the laboratory disturb the contact detection device and cause errors in the measurement of the pipette resistance. Taking average of the measurement signal is used to reduce the effect of the noise but it still lowers the precision of the resistance measurement.

4.2.3. Bleaching

Since the tip of the pipette is exposed to the excitation light during the whole test, bleaching occurs in the fluorescence liquid inside the pipette. This causes the intensity of the fluorescent liquid drop by time and furthermore the intensity of similar injected volumes to drop by time. In equation form this is expressed as

$$I(V_{inj}, t_2) < I(V_{inj}, t_1), \qquad t_2 > t_1 \tag{4.5}$$

where $I(V_{inj},t_1)$ means the intensity caused by the volume V_{inj} at the time t_1 and $I(V_{inj},t_2)$ the intensity caused by the same volume V_{inj} at the time t_2.

4.2.4. Camera Properties

Other possible errors are caused by the CCD camera used. A certain amount of photons is needed before the CCD gives any output. Due to this threshold, small amounts of fluorescence will not become detected. In addition, noise and the signal-to-noise ratio of the camera limit the minimum number of photons possible to detect. The camera in use (SPOT RT Monochrome) has a SNR of 60 dB. High number of fluorescent particles in one place can also saturate the camera.

4.3. Measurement Algorithm

Before the measurements, the parameters such as the sampling frequency of xPC Target and the saving interval of Genomanda are adjusted. Then the microinjection tests are performed and the measurements are done in the following means:

- Square wave voltage signal with the frequency of 10Hz and the amplitude of 1–5mV is fed to the pipette by using xPC Target toolbox and the contact detection device. Measurement signal coming from the contact detection device as well as the actual stimulus signal fed to the contact detection device is gathered by xPC Target.
- The measurement signal from the pressure sensor unit is gathered by xPC Target
- The images taken by the microscope camera are saved by Genomanda

After the measurements, the measurement data gathered is processed in MATLAB to find the injection pressures, the pipette resistances before the injections and the intensity changes caused by the injections. The next chapter covers processing the measurement data.

5. MEASUREMENT DATA

The Simulink model seen in Figure 4.16 produces a *X* x 4 matrix as its output where the first column is the output of the CDD, the second column is the input of the CDD, the third one is the output of the pressure sensor and the last column is the control signal of the solenoid valve of the pressure system. The two first columns are used for calculating the resistance of the pipette by applying Equation (3.5), the third one is for calculating the pressure using Equation (4.4) and the last one is used for finding the injection moments from data and synchronization of the visual data and the resistance data and the pressure data.

The amount of data gathered in the experiments is really high since the sampling frequency of xPC Target may be in kilohertzs, the sampling interval employed with the Genomanda software is in scale of hundreds of milliseconds and the test can last several minutes, often even over 10 minutes. Therefore, an automated algorithm is essential for handling the data efficiently, adding extra information to the data, organizing the results clearly and saving them systematically. A MATLAB function is made for this purpose. It takes the output matrix of xPC Target as its input, asks some parameters from the user, performs the calculations and saves the results in a data structure, which the function gives as its output. The data structure is presented in details in Section 5.2 and the operation of the function is described in Section 5.3. Before them, synchronization of the data is discussed in Section 5.1.

5.1. Synchronizing the Data

As discussed in the previous section and described in Figure 4.13, there are two separate measurement computers in the test setup, of which the first measures the pressure and the pipette resistance and the second records the image data. Since it is impossible to start the measurements precisely at the same time, the image data has to be synchronized with the other measurement data after the experiments.

The filenames of the images saved by the Genomanda program contain the time instants the images have been taken with precision of one hundredth of second as mentioned in Section 4.1.7. The image names are in form *YYYY_MM_DD_hh_mm_ss_ff.jpg*. Due to delays in processing, the timestamps are not always equal to previous timestamp plus the imaging interval. For this reason, the timestamps in the image names are used for synchronization of image data and measurement data later in data processing instead of the imaging interval.

The control signal of the solenoid valve of the pressure system is used as the counterpart in synchronizing. The operating principle of the valve is the following: One

digital output controls the solenoid valve. Logical one opens the valve and logical zero closes the valve. The valve is open during injections and when the back pressure is maintained, and closed when the pressure is increasing from the back pressure to the injection pressure before an injection or decreasing from the injection pressure to the back pressure after an injection. [15]. Therefore, the precise times for the beginning and the ending of an injection can be acquired from the control signal of the solenoid valve. Figure 5.1 presents the voltage input of the valve as a function of time during an injection.

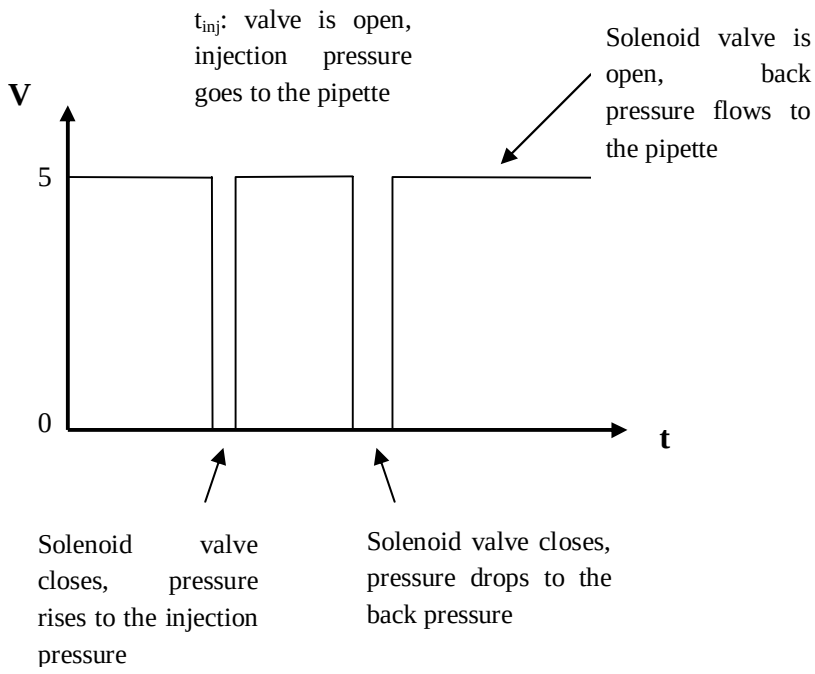

Figure 5.1: The control principle of the solenoid valve of the pressure system.

The image data and the other measurement data can be synchronized by first manually finding an image taken in the beginning of the first injection. The timestamp of that image corresponds to the time instant the solenoid valve opens after a short closure for the first time. The rest of the injection starts and ends in the image data are easily automatically found after that by using the control signal of the solenoid valve. This is described more in details in Section 5.3.4. The synchronization error is defined

$$synchronization\ error < \frac{1}{2} * imaging\ interval + injection\ delay \qquad (5.1)$$

where *injection delay* means the delay from the change in the control signal of the solenoid valve to the start of an injection.

5.2. Measurement Data Structure

The data structure of measurement results and information generated by the MATLAB algorithm is a structure array having separate fields for the data from the different sources. The advantage of the structure arrays is that different types of data can be saved to them, named descriptively and organized consistently. Structure arrays contain data fields, which may further contain subfields and so on. This allows one single MATLAB variable to contain all the test information in similar form to directory trees in a hard drive. If a structure array contains fields and subfields, the information in subfields can be accessed by typing *structure_name.field_name.subfield_name*. By typing *structure_name*, the user can see all the fields, and by typing *structure_name.field_name*, all the subfields of the particular field are shown.

The experiment data processed by the MATLAB function is divided to six sections: general information, pipette information, raw data, resistance data, fluorescence data and pressure data. Except the first section, all of them are saved in own fields in the structure array. A field consists of parameters linked to the experiment, data processing, calculated results or all of them. All the fields and sections are discussed below.

5.2.1. General Information

The general information about the test is saved to the root of the data structure to make it easily seen at the first glance by the user. It contains the fields *date*, *name of the operator*, *target*, *total duration of the test*, and *notes*. *Target* means the target of the injections and it may be a specific cell growth medium or actual living cells. *Notes* is an optional field for typing information of special errors occurred during measurements or important remarks. The function automatically calculates the duration by using the timestamps of the image data but the values for the other fields are asked from the user while the function is running.

The contents of the fields of *general information* are not used in the actual data analysis performed by the function but they provide useful information about the testing conditions and the type of the experiment, which define the comparability of the results. For example, the target can be a dish full of cell growth medium, living cells or something resembling living cells like drops of oil. The data gained from these different circumstances can vary to a great extent and that is why the testing conditions should be clearly stated in the data.

5.2.2. Pipette Information

This field comprises the information of the pipette used in the test. If the pipette is commercial, its model is typed to a field *model*; if it is self-pulled, the parameters of the program of the pipette puller used in making the pipette are saved to a field *program*. The other parameters of this field are *tip diameter given by the manufacturer*, *measured tip diameter*, *tubing outer diameter*, *tubing inner diameter* and *material*. Tubing means

the glass tube of which the pipette is made. The most common pipette material is borosilicate glass but sometimes also quartz glass is used to achieve a more durable structure.

Pipette information is totally user-given field and as with *general information*, any piece of the information saved here is not used in the actual calculation of results performed by the function. However, these parameters give huge amount of valuable information when analyzing the results. Firstly, the connection between the pipette resistance and the tip diameter can easily be seen by using this field. Furthermore, different manufacturers have different tip geometries and that may have an impact on the pipette resistance as well. By utilizing this field, it can be seen how universal the tip diameter – pipette resistance relationship is. Secondly, the effect of the pipette material on the measurements can be detected and also the durability of different materials may be seen by doing statistical analysis to the resistance data gathered. The capillary breakages should be seen in resistance drops, thus the probability of breakages with different materials could be possible to find out. Moreover, the true tolerances of different manufacturers and pipette types can easily be seen by comparing fields *tip diameter given by manufacturer* and *tip diameter measured*.

5.2.3. Raw Data

The four columns of the measurement data matrix generated by xPC Target are saved here to four data arrays named as *stimulus input*, *stimulus output*, *pressure sensor output* and *solenoid control*. This way, the original data is easily found and accessible for searching for measurement errors or for recalculation with the possible new versions of the algorithm.

5.2.4. Resistance Data

This field contains the information of the parameters used in the resistance calculation as well as the calculated resistance of the pipette at different time instants. Firstly, the parameters *sampling frequency* and *excitation frequency* are included in this field. Sampling frequency means the sampling frequency used in xPC Target during the test, thus in addition to the resistance calculation it is essential in the computation of the pressure data and finding the injection moments from the solenoid control signal. *Excitation frequency* is the frequency of the square form stimulus signal used as the input of the CDD. Both of these parameters are given by the user when the data handling function is driven.

Last parameters of this field are two arrays called *resistances* and *injection resistances*, which both are calculated by the function. In the former, a resistance value for the pipette is calculated at each period of the square form stimulus signal by comparing the stimulus signal going to the CDD with the measurement signal coming from the CDD. The latter contains only the resistances calculated from the last whole periods of the excitation signal before each injection pulse of the experiment. The

solenoid valve control data is used in finding the injection moments. Section 5.3.2 describes the resistance data calculation in more details.

5.2.5. Fluorescence Data

The information of the fluorescent dye and the imaging used in the experiments as well as the fluorescent measurement results are stored in this field. The user-given parameters of the field are *fluorescence type, concentration, exposure time, lamp age, magnification used* and *image folder*. *Type* means the type of the fluorescence dye, for example, FITC or Texas Red and *concentration* is its concentration in mM. *Exposure time* is the exposure time used in the Genomanda software, *magnification used* is the total magnification of the microscope employed in the experiment and *image folder* means the folder containing the microscope images of the test in the host computer. Due to the large amount of image data it is not possible to save them in matrix form to the data structure. The lifetime of the mercury lamp utilized for excitation of the fluorescence dyes with the microscope is 100 hours and it is bit uncertain if the properties of the lamp remain constant over its life. For this reason, also the reading of the power supply of the lamp is saved in the field *lamp age* in the data structure for comparison. *Type*, *concentration, exposure time* and *magnification used* naturally all affect the intensity of the image data, and therefore they have to be same in the experiments, whose results are compared with each other. It is possible to compensate some of the differences computationally but that produces one error source more.

The parameters in the field calculated by the computer are *image intensities, injection intensities, injection saturations, resolution, imaging interval* and *threshold used*. Prior experiments show that an intensity change in the pipette may occur during an injection. It disturbs the image-based injection intensity calculation since the algorithm assumes that all the intensity change is caused by the outflow of fluorescence. Thus, the micropipette is masked out from the images. This is done based on the first image in the folder since there is no injection going on. The user defines the threshold for the mask, meaning the pixel value, above which every pixel is changed to value 0. The images taken with the microscope camera are grayscale images having pixel values from 0 to 255 where 0 corresponds to black and 255 means white. Therefore, the mask changes the parts of the pipette brighter than the given threshold to black. The threshold value used is saved to the parameter *threshold used*. *Image intensities* is an array with an element for each image in the given image folder. Each element contains the mean pixel value of the picture with the pipette masked out. Thus, their mean pixel values are also in the range from 0 to 255. *Injection intensities* is an array having an element for each injection. Each element describes the intensity change during that particular injection and is calculated by subtracting the mean pixel value of the image taken just in the beginning of the injection from the mean pixel value of the image taken at the end of the injection. The pipette is again masked out from the both images before taking the mean. The array *injection saturations* is a qualitative marker of the reliability of the fluorescence measurements. It has elements equal to the number of injections and it

announces how many pixels with value 255 there is in average among the images taken during an injection. If the pixel value is 255, it is probable that the CCD of the camera has been saturated. Therefore, if the *injection saturation* value of an injection is high, the *injection intensity* of that particular injection is too small and faulty. Hence, the data from injections with high saturation value should not be used in the model generation. *Resolution* declares the width and height of the images in pixels and *imaging interval* tells the imaging interval used with the Genomanda software calculated by taking a mean from the differences in the timestamps of the images.

5.2.6. Pressure Data

Pressure data consists of the information from the pressure sensor and the solenoid valve control signal. It holds parameters *pressure*, *injection pressures*, *back pressures*, *injection starts* and *injection ends*. The pressure values calculated from the data given by the pressure sensor at each sampling moment are saved to the array *pressure*. The mean pressures during each injection are saved in the array *injection pressures* and the pressures in the system just before each injection are saved to the parameter *back pressures*. All the pressure values are saved in pascals. Starting points of injections measured in seconds from the beginning of the experiment are saved to the array *injection starts* and the time instants of ending points of injections are similarly saved to the array *injection ends*. The time instants are calculated using the solenoid control signal and sampling frequency.

Figure 5.2 illustrates the measurement setup architecture with information flows as well as the data handling routes described.

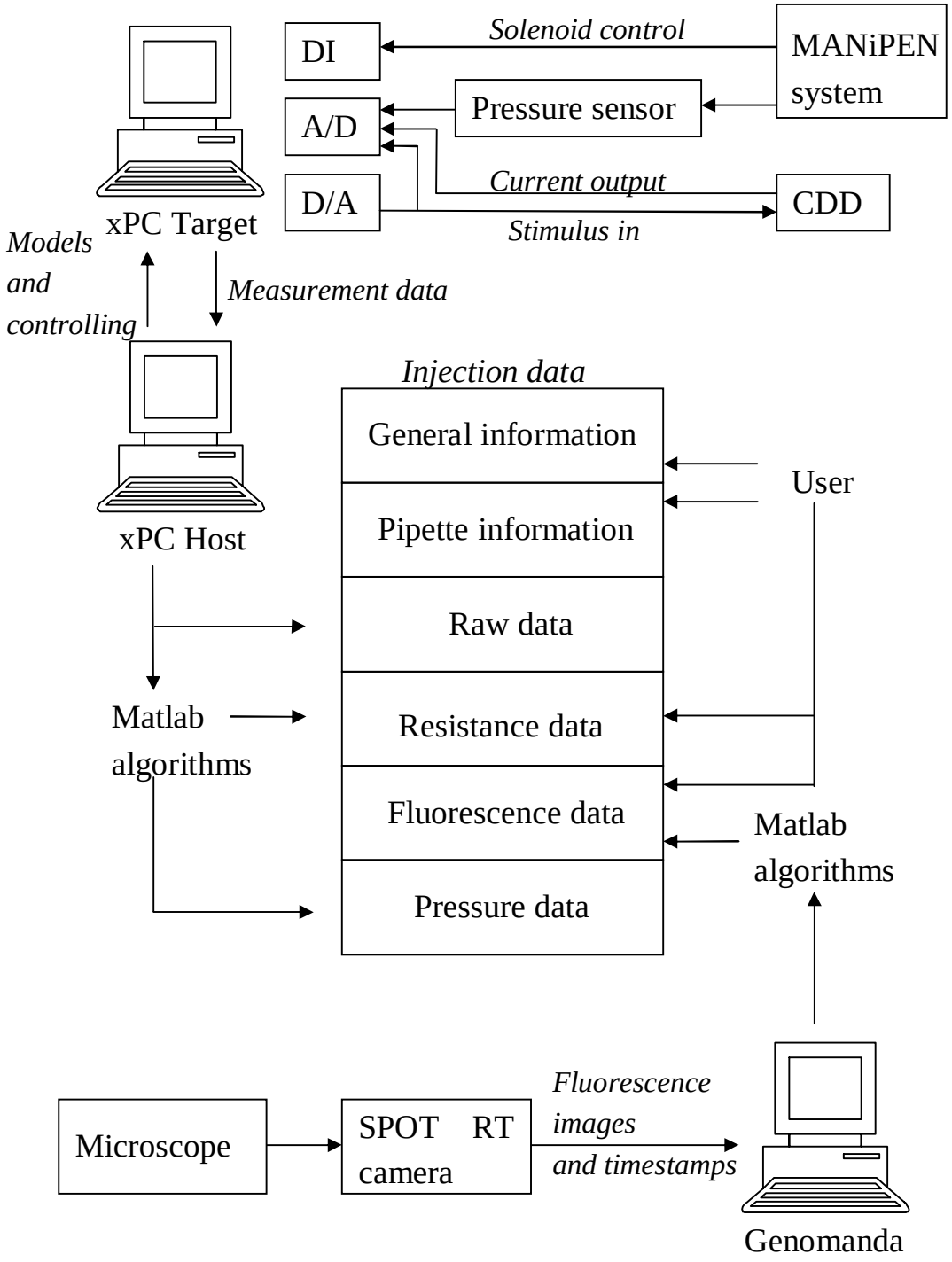

Figure 5.2: Measurement setup with information flows and measurement handling routes.

5.3. Operation of the Data Handling Algorithm

This section describes the operation of the MATLAB algorithm handling the measurement data and making the data structure described in the previous section step by step. As a prerequisite work, all images before the first injection are deleted manually, thus the first timestamp in the image folder is the beginning of the first injection.

5.3.1. Preparative Procedures

First, the structure array is initialized and the general information and the pipette information are asked from the user and saved in the corresponding fields in the structure array. Then, the location of the measurement data matrix given by xPC Target in the hard drive is asked from the user and the measurement data is loaded as a local variable of the function. The raw data from the data matrix is saved to the field *raw data* of the structure array. Then, the sample indexes of injections are found from the solenoid valve control signal as shown in Figure 5.3 for later use.

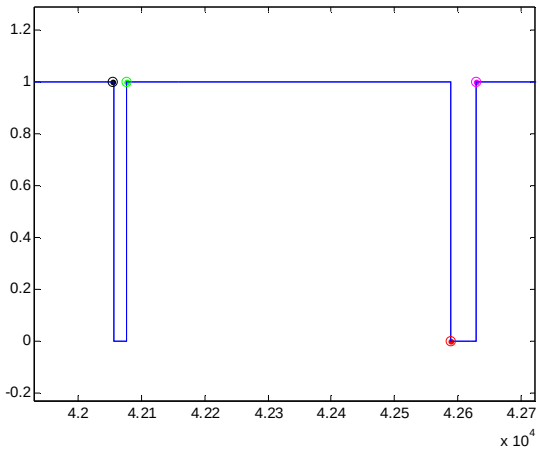

Figure 5.3: Solenoid valve control signal plotted in MATLAB. Start of an injection marked with a green dot, end of an injection with a red dot, start of a pause with a purple dot and end of a pause with a black dot.

As seen in Figure 5.3, the injection moments – starts and ends of an injection and a pause – are straightforward to find from the changes in the binary control signal.

5.3.2. Resistance Data Calculation

The sampling frequency used in the measurements (F_s) and the frequency of the square form excitation signal (f_{exc}) are asked from the user and saved to the corresponding fields in the field *resistance data*. The pipette resistance is calculated from the CDD signals using these parameters and the pre-known information of the CDD circuitry. Figure 5.4 presents an example of the CDD signals to clarify the operations. First the

signals are preconditioned and the values of some important parameters are found from the signals as follows.

1. The actual excitation signal going to the pipette and the current signal coming from the pipette are calculated from the measured excitation signal and measurement signal by using the scaling, the value of the feedback resistor of the current-to-voltage converter and amplification as shown in Equation (3.5)

$$x_{prec}(n) = \alpha_{scale} x(n), \qquad n = 0,1,2,.. \tag{5.2}$$

$$y_{prec}(n) = \frac{y(n)}{\alpha_{ampl} R_{i2v}} \tag{5.3}$$

where *x(n)* is the measured excitation signal and *y(n)* is the measurement signal and *n* means the sample index.

2. The period of the excitation signal is calculated using the following formula:

$$\mathrm{T}_{exc} = \frac{F_s}{f_{exc}} \tag{5.4}$$

where T_{exc} is the period of the excitation signal.

3. The amplitude of the preconditioned excitation signal is found by taking the mean of the part the signal is high for the first time

$$a_{exc} = \frac{\sum_{i=\frac{\mathrm{T}_{exc}}{2}}^{\mathrm{T}_{exc}-1} x_{prec}(i)}{\frac{\mathrm{T}_{exc}}{2}} \tag{5.5}$$

Then the resistance value for every pulse of the preconditioned measurement signal $y_{prec}(n)$ is calculated in a loop and saved in the array *resistances* in the field *resistance data*. The loop contains three steps, which are repeated as long as there is data to handle:

1. Offset of the pulse *q* is detected from its first half (signal is low)

$$o_{meas}(q) = \frac{\sum_{i=\mathrm{T}_{transient}}^{\frac{\mathrm{T}_{exc}}{2}-1} y_{prec}\left(i + q\mathrm{T}_{exc}\right)}{\frac{\mathrm{T}_{exc}}{2} - \mathrm{T}_{transient}}, \qquad q = 0,1,2,... \tag{5.6}$$

where $T_{transient}$ is the transient estimate in samples and q is the pulse index.

2. The level of the pulse q is detected from its last half (signal is high) and the amplitude is obtained by subtracting the offset from the signal level

$$a_{meas}(q) = \frac{\sum_{i=\frac{T_{exc}}{2}+T_{transient}}^{T_{exc}-1} y_{prec}(i + qT_{exc})}{\frac{T_{exc}}{2} - T_{transient}} - o_{meas}(q) \tag{5.7}$$

3. The pipette resistance of the pulse q is calculated by dividing the amplitude of the excitation pulse by the amplitude of the measurement pulse as shown in Equation (3.5)

$$R_{pip}(q) = \frac{a_{exc}}{a_{meas}(q)} \tag{5.8}$$

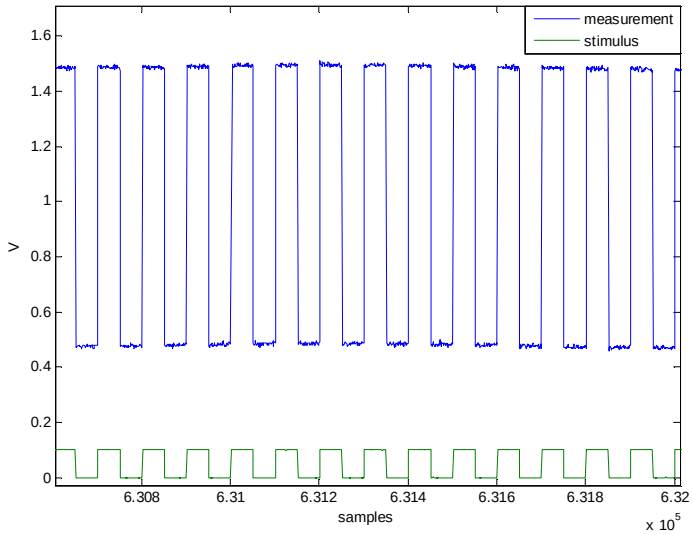

Figure 5.4: Stimulus signal going to CDD (green) and measured output from CDD (blue).

Finally, the pipette resistance values just before the injection moments are found by utilizing the sample indexes of the injection starts found in Section 5.3.1 and taking the resistance values calculated from the last whole pulses prior to injections. This information is used to describe the condition of the pipette just before the injections. The results are saved to the array *injection resistances* in the field *resistance data*.

5.3.3. Pressure Data Calculation

The pressure at every sample moment is calculated by applying Equation (4.4) to the pressure sensor output signal and it is saved to the array *pressures* in the field *pressure data*. The pressures during injections are found by taking the mean of the pressure values between the start and the stop of an injection found in Section 5.3.1. The first quarter is neglected since there might be some transient. The results are saved to the array *injection pressures* in the field *pressure data*.

The back pressures are calculated by taking means of the pressure values during one second before each injection and saving them to the array *back pressures* in the field *pressure data*. The whole pause time between two injections is not used since sometimes the back pressure needs to be adjusted during an experiment. During the last second, the back pressure should stay unadjusted.

5.3.4. Intensity Data Calculation

Information of the fluorescence dye, the fluorescence microscope system and the parameters used in the measurement software is asked and saved to the field *fluorescence data*. The location of the image data in the hard drive is asked and saved to the field *image folder*. The first image in the folder is taken as the beginning of the first injection as mentioned in the beginning of Section 5.3, and it is used in the mask generation.

1. A threshold estimate σ is asked from the user
2. The mask is generated by changing the values of all the pixels in the image with a value above the threshold to 0 and all the pixels with a value below the threshold to 1.

$$g(u,w) = \begin{cases} 1, & f(u,w) < \sigma \\ 0, & f(u,w) \geq \sigma \end{cases} \qquad (5.9)$$

where *g(u,w)* is the mask and *f(u,w)* is the original image.

3. The image is masked with the mask by multiplying the image element by element with the mask

$$h(u,w) = g(u,w) \bullet f(u,w) \qquad (5.10)$$

4. The original image *f(u,w)* and the masked image *h(u,w)* are printed next to each other as shown in Figure 5.5 and the user is asked if the mask is sufficient. A mask is good if the pipette and only the pipette is masked out of the picture.
5. If the mask is sufficient, the user accepts it and the threshold value is saved to the field *threshold used* in the field *fluorescence data*. The mask is then used to

all the images in the folder. If the user does not accept the mask, the function returns to the step 1.

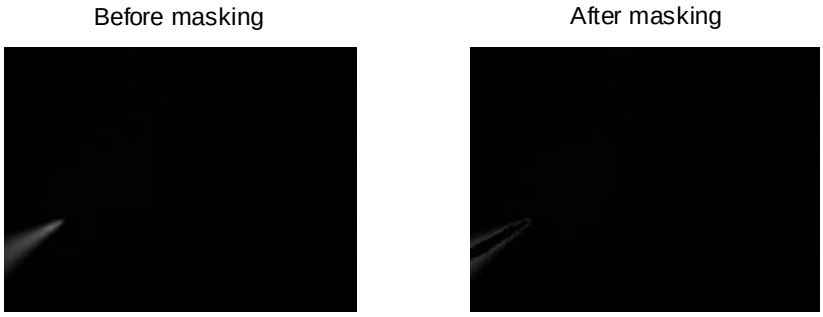

Figure 5.5: Masking the pipette out. The original image shown in the left and the masked image shown in the right. For illustration purposes, a good mask is not applied and the borders of the pipette are clearly visible.

The images the given folder contains are loaded to MATLAB in a *for* loop one by one, masked with the mask generated in the previous phase and their mean pixel values are calculated and saved to the array *image intensities* in the field *fluorescence data*. In addition, the number of the pixels with a value 255 in each image (the saturated pixels) are calculated and saved to a temporary array variable. Then, the image data and the measurement data from the xPC Target computer are synchronized for detecting the intensity changes occurring during individual injections. First, the timestamps of the image data are anchored to the beginning of the first injection by performing the following steps:

1. The hours, minutes, seconds and hundredths of seconds from the time the images are taken are separated from the names of images, converted to milliseconds and saved to a temporary array here denoted as $t_{im}(r)$, where r is the number of the image.
2. The time differences between the images and the beginning of the first injection are calculated by applying the equation

$$\Delta t_{im}(r) = t_{im}(r) - t_{im}(0) \qquad (5.11)$$

Figure 5.6 clarifies these two steps.

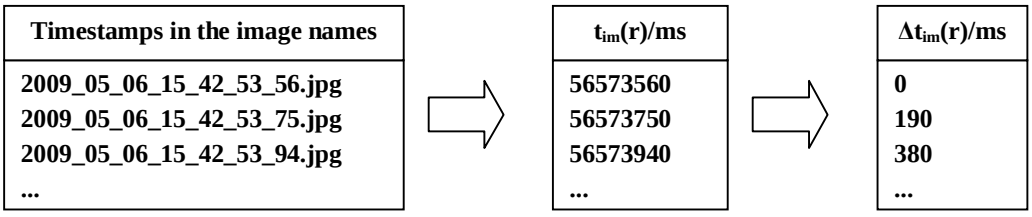

Figure 5.6: Schema of acquiring the time differences between images.

After this, the true imaging interval is obtained by taking the mean of the differences of the elements in the time difference array shown in the rightmost block in Figure 5.6, and saved to the field *imaging interval* in the field *fluorescence data*. The next step is to synchronize the time difference array with the data gathered with xPC Target. It is done by following the steps below

1. The relative time instants for the starting and ending points of the injections in milliseconds are calculated using the start of the first injection as the zero point by applying the following equations

$$t_{start}(k) = \frac{s(k) - s(0)}{Fs} \times 1000, \qquad k = 0,1,2,... \tag{5.12}$$

$$t_{end}(k) = \frac{e(k) - s(0)}{Fs} \times 1000 \tag{5.13}$$

   where $s(k)$ and $e(k)$ are the arrays containing the sample indexes of the beginnings and ends of the injections found in Section 5.3.1 and k is the number of the injection.
2. The images taken from the beginning and end of individual injections are found by comparing the arrays $t_{start}(k)$ and $t_{end}(k)$ with the array $\Delta t_{im}(r)$.

The intensity differences caused by the injections are calculated by subtracting the mean pixel values of the images taken in the beginnings of the injections from the mean pixel values of the images taken in the ends of the injections. The resulting array is saved in the field *injection intensities* of the field *injection data*. Injection time instant arrays $t_{start}(k)$ and $t_{end}(k)$ are converted to seconds and saved to the field *pressure data* with names *injection starts* and *injection ends*, respectively. The average number of saturated pixels per injection is calculated utilizing the saturation array generated earlier and synchronization done in previous two steps and saved to the field *injection saturations* in the field *fluorescence data*.

5.3.5. Plotting the Results

At the end of the operation of the function, three qualitative graphs are printed to allow the user to verify successful computation and the results of the test. The graphs are the following

1. *Image intensities* with marks in the beginning and end of the injections to ensure that the synchronization of the image data and measurement data is credible. The starting points should be in or near the dips of the graph and the ending points in or near the peaks. This is shown in Figure 5.7.
2. *Injection saturations* to show how trustworthy the fluorescence measurement is as shown in Figure 5.8

3. *Injection intensities* versus *injection pressure* to see the pressure – volume flow relationship presented in Figure 5.9

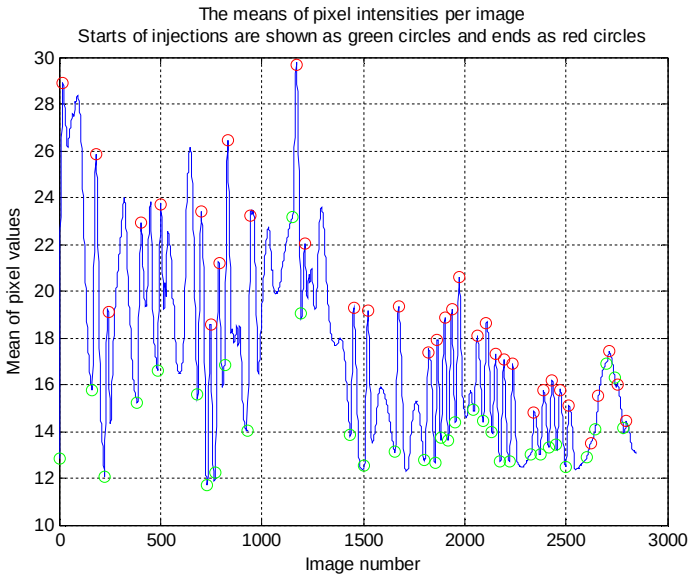

Figure 5.7: Mean pixel intensities of images with markers in the starts and ends of injections.

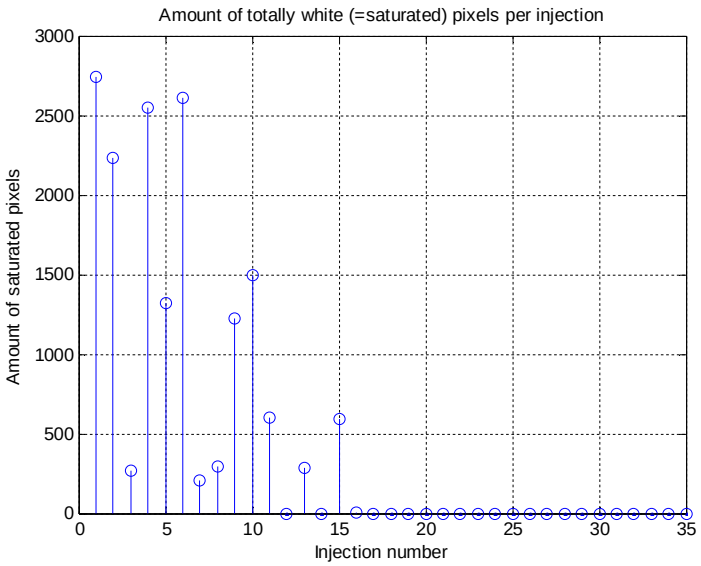

Figure 5.8: Average number of saturated pixels per image during injections.

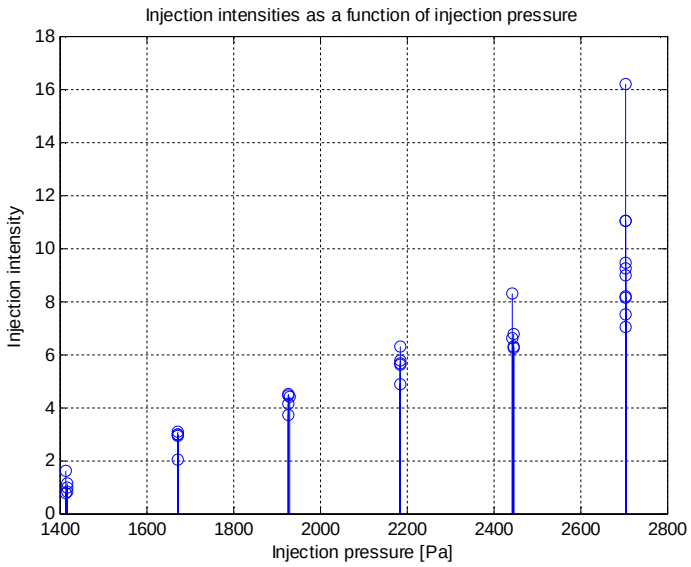

Figure 5.9: Injection intensities as a function of injection pressure.

After showing the figures, the user is asked if the generated structure array is wanted to be saved as a *.mat*-file. There are more data visualization algorithms for the saved structure arrays as it is discussed in the next section.

5.4. Visualization of Data

Even though the measurement data in the data structures described in Section 5.2 is logically sorted, it consists only of numbers and therefore is not the most illustrative for a human being. Hence, functions to visualize the measurement data in the data structures are generated in MATLAB. The user just gives the data structure of interest as an input to the function and the function presents the data visually. The algorithms for making video files and graphs out of the measurement data are generated. This section will discuss those forms of visualization. The video files are presented in Section 5.4.1 and the graphs are described in Section 5.4.2.

5.4.1. Video Files

Video files are generated out of measurement data structures to enable monitoring of the test progression afterwards, check the synchronization of the data and to clarify the test process for presentation purposes. The video files are generated with a MATLAB algorithm. Figure 5.10 presents an example of the video files and an explanation to the figure is given below.

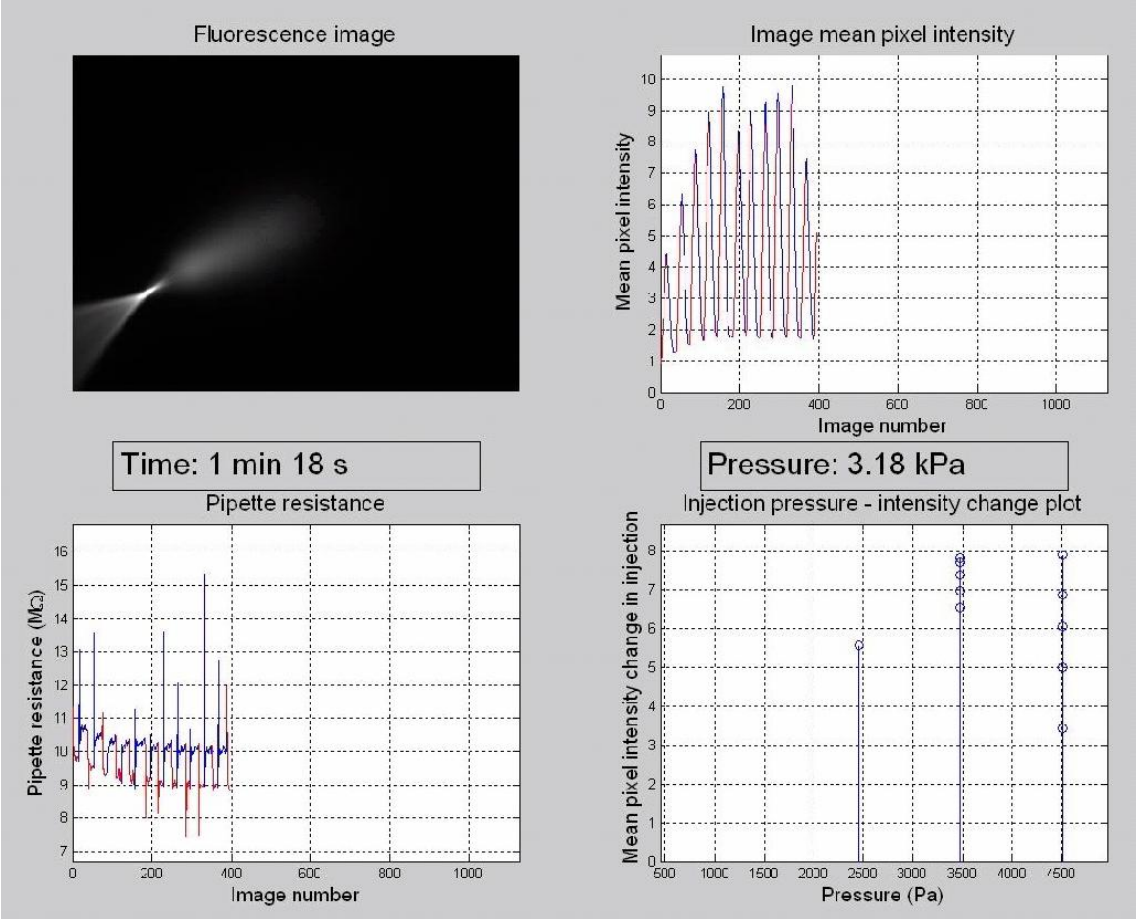

Figure 5.10: An example of the video files generated out of the measurement data. The data shown was gathered from injection experiments with Femtotip II pipettes.

In the video files, time is running in the mid-left, the images taken with the microscope at each time instant are seen up left and the mean pixel intensity of each image is plotted in up right. Whenever an injection is going on, the graph is coloured to red. The pressure in the system is seen in mid-right, and after each injection a stem describing the change of intensity with the injection pressure used is plotted down right. The resistance of the pipette is seen as a graph in down left and – as with the mean pixel intensity graph – the colour of the graph is changed to red each time an injection is going on.

5.4.2. Graphs

Naturally, graphs representing the intensity as a function of the injection pressure and the pipette resistance are drawn out of data from all pipette sizes. Also, graphs describing the pipette resistance – tip diameter relationship are plotted.

6. MEASUREMENTS AND RESULTS

The following chapter discusses the measurements done with the test bench and the results gained. The chapter is divided to five sections. Section 6.1 describes the test procedure. It presents the preparations done for an experiment and the actual practice of the experiments. Section 6.2 discusses the observations done during the tests or during the analysis of the measurement data. Among others, common problems encountered and remarks done during the data handling are considered. Section 6.3 presents the actual results achieved. It describes the relationship between the measured parameters: the injection pressure, the pipette electrical resistance and the injection intensity. Some more testing was required after the original experiments since new questions arose from the measurement data. Section 6.4 depicts the additional tests performed and discusses their results. Finally, Section 6.5 is for discussion of the contents of this chapter.

6.1. Test Procedure

The mercury lamp of the microscope was warmed up approximately half an hour before starting the tests. A 6 well plate with one well filled with the Leibovitz medium was fixed on the microscope placing the well with medium above the objective. A micropipette to be measured was first attached to the adapter if needed and then 5–7µl of 5mM FITC was dozed inside the micropipette using a manual pipettor. The pipette was attached to the arm of the micromanipulator and the measurement electrode of the CDD circuit was put inside the pipette in contact with the liquid column of FITC. The micropipette was moved to the medium near the bottom of the well plate with the micromanipulator and the microscope was focused to the tip of the micropipette. With the Femtotip II pipettes, the 20x objective was used but with all the other pipettes, the 4x objective was employed. After focusing, the microscope lamp was turned off and the filter cube for FITC was put in. The exposure time was set to 100ms in Genomanda.

A couple of injections were performed prior to the actual tests to ensure that the micropipette was not clogged and to adjust the back pressure using the MART program for controlling the pressure and the Genomanda software for feedback. The back pressure was suitable when there was not a visible outflow from the tip while not injecting but the interface of the FITC was in the very tip of the micropipette.

After adjusting the back pressure, the measurement was started with xPC Target and the saving interval in the Genomanda software was set to 100ms. The injection pressure was set to a starting value in MART, five injections were made with that value and then the injection pressure was changed and again five injections were made and so on. Often the starting value was 10kPa in MART, which corresponded around 6–7kPa in

the pressure sensor data, and then the injection pressure was lowered in 1kPa or 2kPa steps in MART. In the early tests, 10 different injection pressures were used but in the later tests, only five different injection pressures were used to shorten the experiments and decrease the probability of clogging the micropipette. The measurement signals from xPC Target and the image data were monitored for abnormalities during the experiment. After a successful test, the data was saved and handled with the algorithm presented in Section 5.3 and the pipette used in the test was stored for SEM measurements to measure its exact size. For the SEM measurements, the pipettes have to be coated with a thin layer of gold.

6.2. Observations from the Tests

This section discusses different observations done from the tests. First, the problems encountered during the measurements are described. Some remarks on the possible limitations and usability of the method could be already made based on the early measurement data. These remarks are presented next. Finally, other observations made during the measurements or data handling are depicted.

6.2.1. Problems Encountered

Problems arose in the resistance measurement and functioning of the micromanipulator. Also, pipette clogging was a frequent source of error. These all three points are discussed below.

Problems in Resistance Measurement

Problems in resistance measurements occurred in many experiments. The Ag/AgCl electrodes wore sometimes down rapidly or had unequal properties, which caused their half-cell potentials to be different thus producing offset and finally causing the current-to-voltage converter in the CDD circuit to saturate. In this case, the measurement signal from the CDD was either 10V or -10V. Sometimes the measurement signal was not totally saturated but the offset was large enough to cause cutting of the peaks or the dips of the measurement signal thus distorting the signal.

Once, the whole head stage of the CDD circuit had to be built again since it seemed to be out of order. The head stage contains the most sensitive and thus the most vulnerable component of the circuit – the current-to-voltage converter – which may broke down even from a relatively small static electricity discharge and should therefore be handled with extra care. Also, it was noticed that the positioning of the head stage had great effects on the measurement noise.

Manipulator Problems

Every now and then the MANiPEN 4 micromanipulator had slipped out of calibration between the tests. The reason was the relatively soft piezo bender actuators, which easily deformed while attaching or detaching the pipette and sometimes seemed to drift

during or between the experiments. Due to the small motion range of the benders, it was not possible to move the pipette to a suitable point in the microscope view and thus the image data was not possible to be gathered when the manipulator was out of calibration. Recalibration of the benders is time-consuming and really difficult work since it has to be done manually.

Finally, errors occurred in the linear motor of the MANiPEN 4 micromanipulator and the SmarAct micromanipulator had to be used instead. However, the majority of the tests was done with MANiPEN 4.

Clogging

Many experiments had to be finished prematurely due to clogging of the pipette. In the desired measurement data, the only changing parameter during the test should be the injection pressure. Thus, the changes in the pipette properties were unwanted. Figure 6.1 shows a picture of a clogged pipette tip. The clogging particle seen in the picture is relatively big.

Figure 6.1: A clogged pipette with a tip diameter of 2µm.

Naturally, the data gathered from clogging situations offers valuable information on the resistance and intensity changes caused by clogging, with which the generality of the relationship between the pipette resistance and the injection intensity can be assessed. However, first it is essential to gather data only from clean pipettes to form a so-called zero-point.

6.2.2. Limitations and Usability of the Method

It was soon noticed from the clogging data that the effect of clogging cannot be compensated with the injection pressure since the increase in resistance is relatively small even when the clogging affects outflow radically. Table 6.1 shows the resistance and the injection intensity data from a clean 1µm pipette, a clean 2µm pipette and the same 2µm pipette clogged to clarify this.

Table 6.1: Comparison of electrical resistance and relative injection intensity change of two clean and one clogged pipette.

	Clean 1µm	**Clean 2µm**	**Clogged 2µm**
Resistance / MΩ	1.9	1.0	1.1
Relative injection intensity change (pressure used)	0.3 (3.7kPa)	3.5 (3.8kPa)	0.1 (3.8kPa)

As seen in Table 6.1, the resistance of a clean 1µm pipette is considerably higher than the resistance of a clogged 2µm pipette even though the injection volume is also higher. The reason for this is that although the tip diameter decreases when a particle partially clogs the tip, the particle cannot be considered as an electrical insulator like the pipette glass but as an electrical RC circuit with a certain impedance. Thus, while the liquid flow cannot pass through the clog, the electrical current can. Therefore, the circuit model in Figure 3.3 cannot be used to model the clogged pipette and Equation (3.1) does not apply to the resistance of the clogged pipette anymore. The correct way to model the clogged pipette is adding a component describing the electrical properties of the clog as shown Figure 6.2.

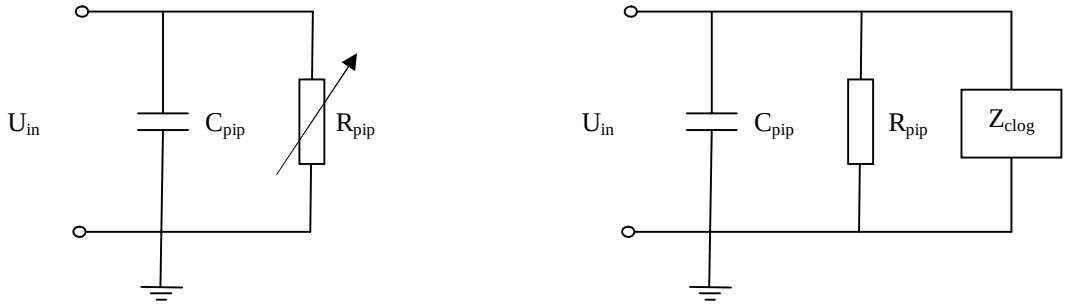

Figure 6.2: An incorrect way to model a clogged pipette with a changing pipette resistance value (in the left) and the correct way to model the clogged pipette with a parallel connection of the pipette circuit and impedance of the clog, Z_{clog} (in the right).

The actual use of the model presented in Figure 6.2 is not feasible since the electrical properties or the material properties of the clogging particles are not known and they can vary. Also, the clogs with different size can cause a similar change in the tip opening but – since the electrical properties are dependent of the geometrical properties of the object – the electrical resistances of the clogs are different. Figure 6.3 illustrates this.

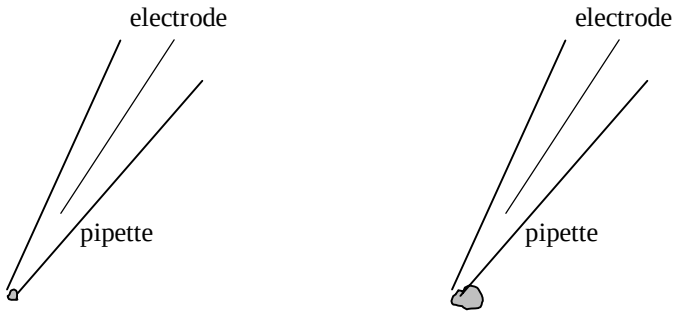

Figure 6.3: Similar pipettes clogged by particles of different size and having similar tip opening after clogging.

This all can be summarized that the same model that is used to model the volume flow as a function of the injection pressure and the pipette resistance cannot work if the pipette is clogged. However, clogging of the pipette can be detected from the resistance data relatively reliably. The impedance measurement, which takes also the capacitive part in account, might improve the detection still. Table 6.2 presents the relationship between the changes in the pipette resistance and the changes in the injection intensity or injection volume in the experiments done. All 10 cases where notable changes occurred are analyzed and the data is divided to four categories based on the connection between the resistance changes and the intensity changes.

Table 6.2: Relationship between the changes in the pipette resistance and the changes in the injection intensity in the measurement data.

	Increase in the pipette resistance → clearly observable decrease in the injection intensity	Increase in the pipette resistance → not detectable decrease in the injection intensity	Uncertain	The pipette resistance remains almost stable, the injection intensity decreases
Number of cases	7	1	1	1
Percentage	70%	10%	10%	10%

From the data it can be seen that if – for example – a 10% change in pipette resistance is interpreted as clogging, in seven cases out of nine the interpretation is correct and only one false positive is gained. The data also shows that in 1 case out of 10 the clogging was not detected. However, it is not sure that the detected intensity change was not caused – for example – by photobleaching of the fluorescence instead of a clogging particle.

6.2.3. Other Observations

The injection moments are clearly visible in the pipette resistance data. The resistance drops significantly in the beginning of an injection, remains lower during the injection, increases rapidly causing a huge peak in the end of the injection and settles down to approximately the same value as it was before the injection afterwards. This is shown in Figure 6.4.

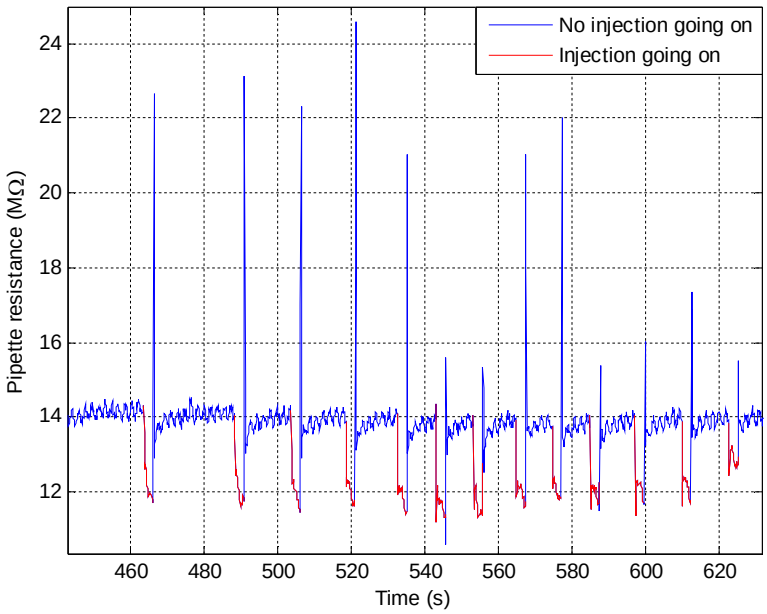

Figure 6.4: Pipette resistance changes during injections. The resistance measured with Ag/AgCl electrodes.

The data shown in Figure 6.4 is measured from a Femtotip II pipette and an Ag/AgCl electrode is used in the measurements. As it can be seen, the resistance drop during an injection is over 15% and the peak after the injection can be almost 100% of the original value. Sometimes, there can be seen difference in the resistance drops during injections with different injection pressures but there is no evidence of correlation between the resistance drops and the injection pressure or the injection intensity.

Actually, the injection moments are seen already in the raw measurement data as presented in Figure 6.5.

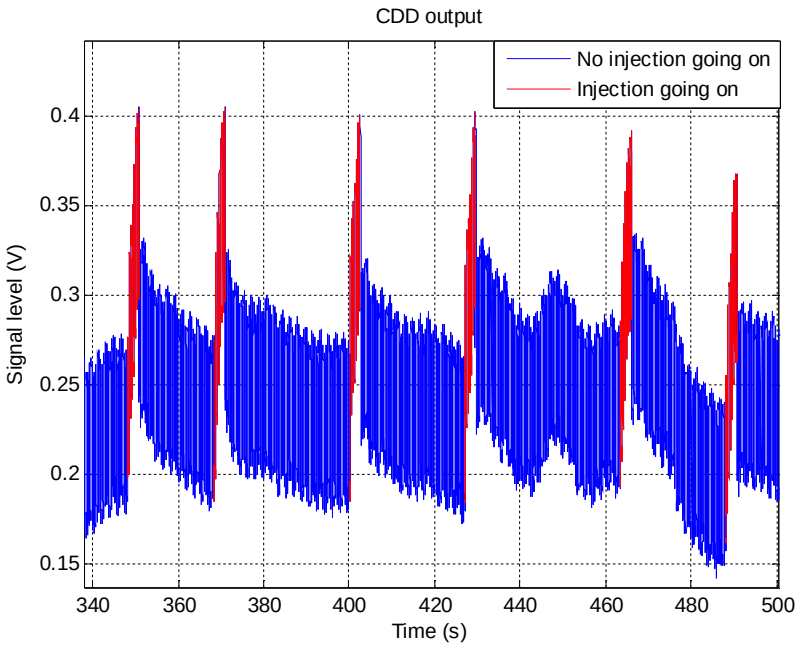

Figure 6.5: Raw CDD measurement signal changes during injection. Ag/AgCl electrodes were used in the measurement.

As it can be seen, the offset of the measurement signal from the CDD circuit changes dramatically during an injection. The offset does not remain exactly steady after the injection either but the drift is smoother compared with the sudden changes occurring at the injection moments.

Figure 6.4 and Figure 6.5 were drawn of the data measured with Ag/AgCl electrodes as discussed earlier. The injection moments are seen also in the resistance data measured with platinum electrodes but the resistance drops look bit different as can be seen in Figure 6.6.

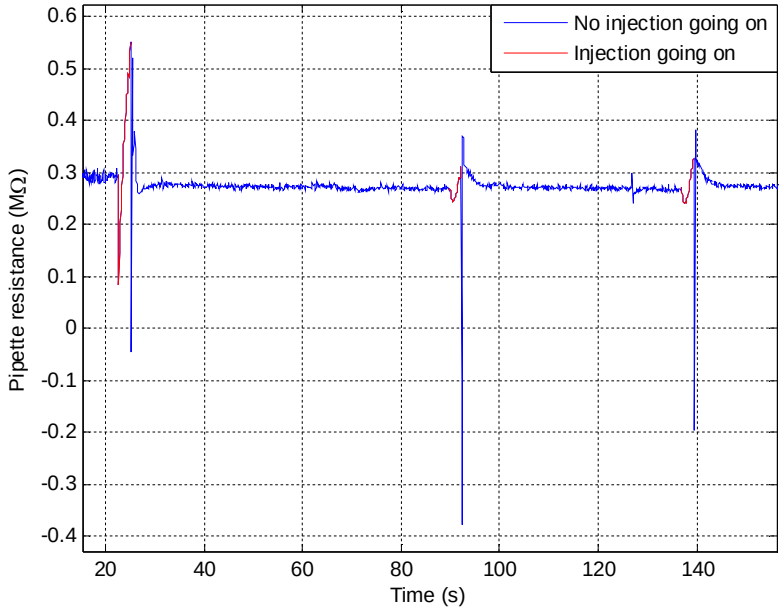

Figure 6.6: Pipette resistance changes during injections. The resistance measured with platinum electrodes.

Also, the raw measurement signal from the CDD differs slightly from the one presented in Figure 6.5. This is shown in Figure 6.7.

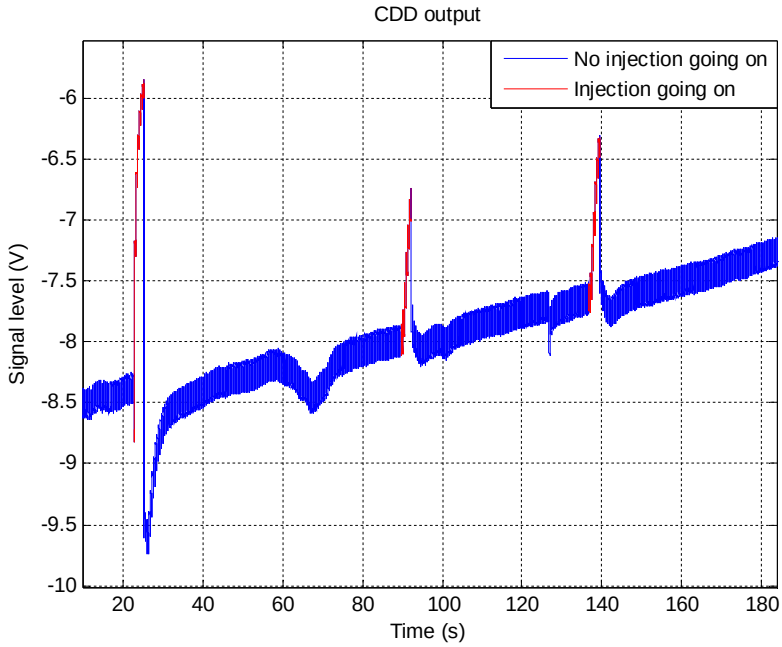

Figure 6.7: Raw CDD measurement signal changes during injection. Platinum electrodes were used in the measurement.

The reason for the differences in Figure 6.4 and Figure 6.6 and in Figure 6.5 and Figure 6.7 is most probably the different operation principle of the polarisable and non-polarisable electrodes, which was presented in Section 4.1.4.

6.3. Results

The results of the experiments are presented in this section. First, the relationship between the injection pressure – pipette electrical resistance – injection intensity, determining of which was the main goal of this thesis work, is discussed. Secondly, the relationship between the pipette tip diameter and the pipette resistance is described.

6.3.1. Injection Pressure – Pipette Electrical Resistance – Injection Intensity Relationship

The injection pressure – pipette electrical resistance – injection intensity relationship is observed using the values for each parameter saved to the injection measurement data structure described in Section 5.2. The pipettes used in the measurements had manufacturer-given tip diameters of 0.5µm, 1µm, 2µm, 5µm and 10µm as presented in Table 4.1. Since measurement data from the tests where pipette was clogged was not suitable for modelling as discussed in Section 6.2.2., only data without great variance in the pipette resistance values over the test was utilized. Also, measurement data with significant saturations or other errors was omitted. If some smaller errors in individual injections were detected, the data from those injections only was excluded from the analysis.

In the final analysis, results from one test with each pipette size were utilized. The injection intensity and the pipette resistance values gained with the same pressures and the same pipette were averaged. Figure 6.8 presents the pressure – resistance – intensity plot gained. The standard deviations are shown in the data with crosses. Since the intensities achieved with the 10µm pipette were considerably larger than those gained with the other pipette sizes, Figure 6.9 shows the data again without the data from the 10µm pipette to make the comparison between the intensities of the smaller tips easier.

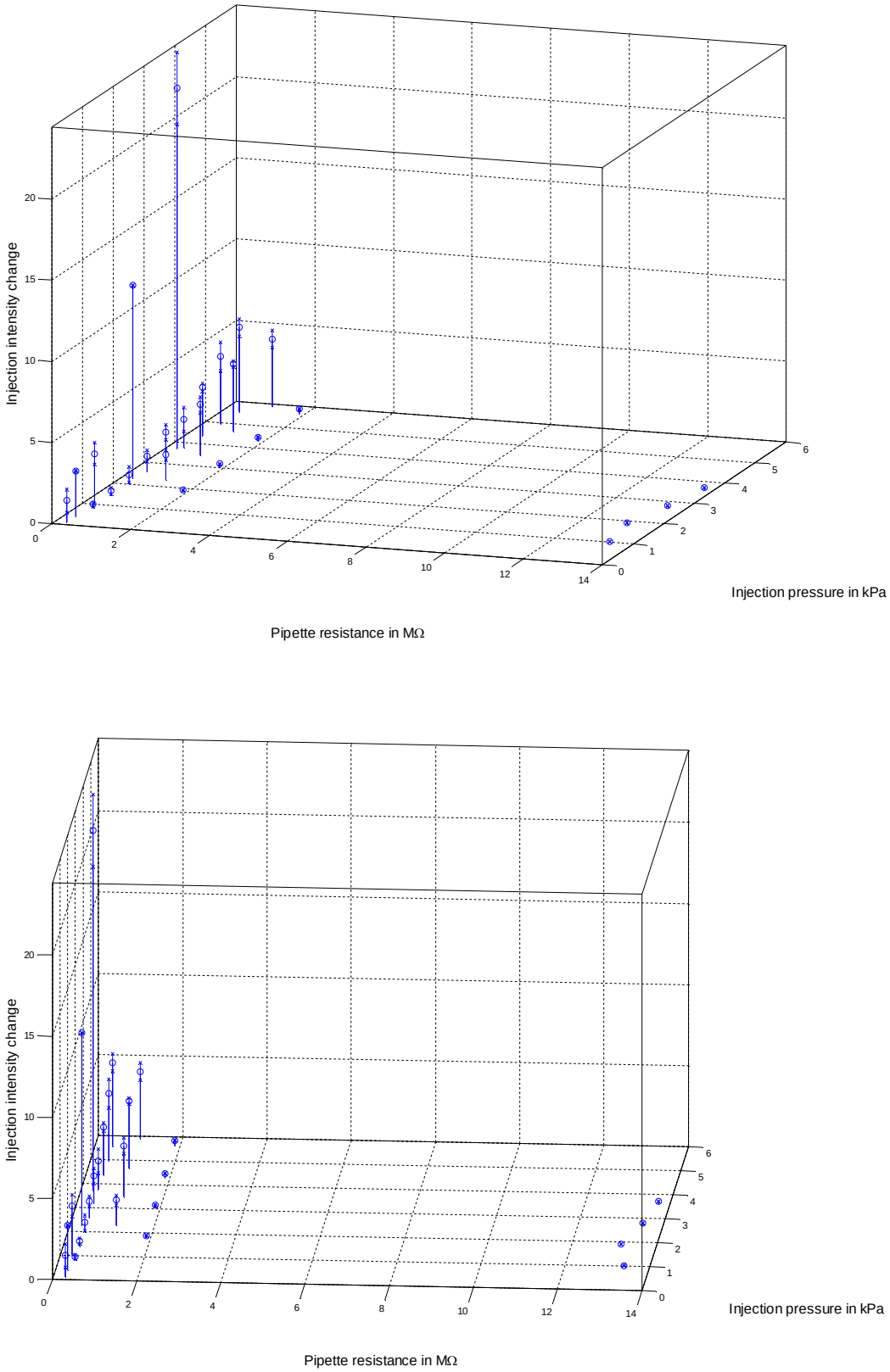

Figure 6.8: Injection intensity change as a function of the injection pressure and the pipette resistance with 0.5µm, 1µm, 2µm, 5µm and 10µm pipettes (values given by the manufacturers).

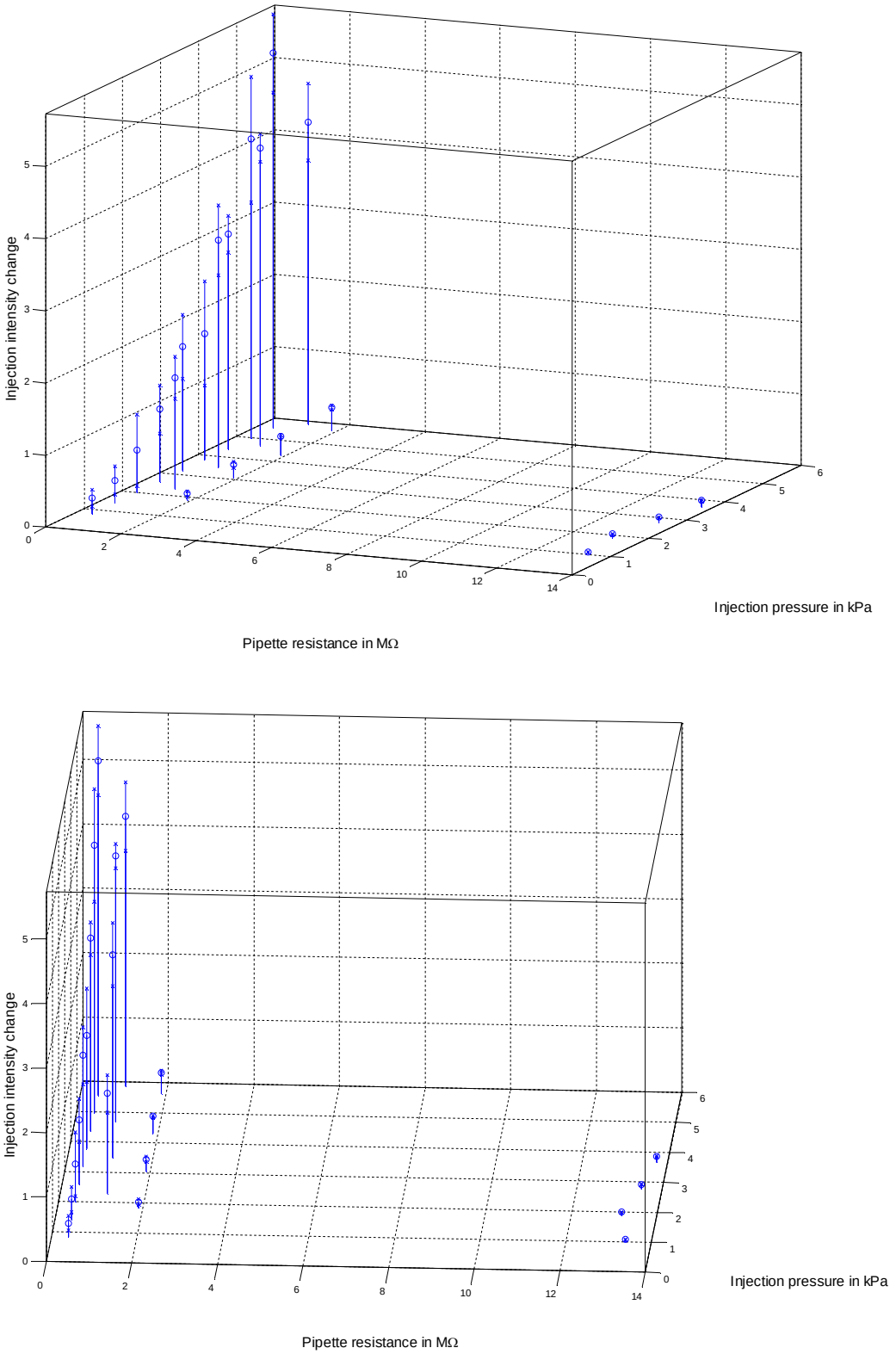

Figure 6.9: Injection intensity change as a function of the injection pressure and the pipette resistance with 0.5µm, 1µm, 2µm and 5µm pipettes (values given by the manufacturers).

It can be seen in the figures presented, that as the injection pressure increased also the injection intensity – the indicator of the injection volume – increases, which is of course logical and expected behaviour. Also, as the pipette resistance increases, the injection intensity decreases, which is a proof supporting the theory that the pipette size or the hydraulic resistance affecting the outflow from the pipette is proportional to the pipette electrical resistance.

However, the relationship between the parameters does not look too easy to express as an equation since it is hard to fit a curved plane to the data. The intensities measured from the 2µm pipette (points near 1.0MΩ) and from the 5µm pipette (points near 0.5MΩ) seem to be too close to each other. Nevertheless, the trend shows that the effect of the injection pressure on the injection volume is somewhat linear whereas the effect of the pipette resistance on the injection volume seems to be more hyperbolic.

This all is seen more clearly in Figure 6.10 and Figure 6.11. Figure 6.10 shows the injection pressure – injection intensity plot for each pipette resistance separately. The somewhat linear trend is seen in the figures even though there is clear error in some of the values. Figure 6.11 presents the pipette resistance – injection intensity plot for two different injection pressures: 2kPa and 5kPa. Since the control of the injection pressure with MART was not precise as mentioned in Section 6.1, inter- and extrapolation was used in some cases to achieve the data points for the mentioned pressure values. Also, for clarification, best-fitting trendlines are fitted to the graphs Figure 6.11.

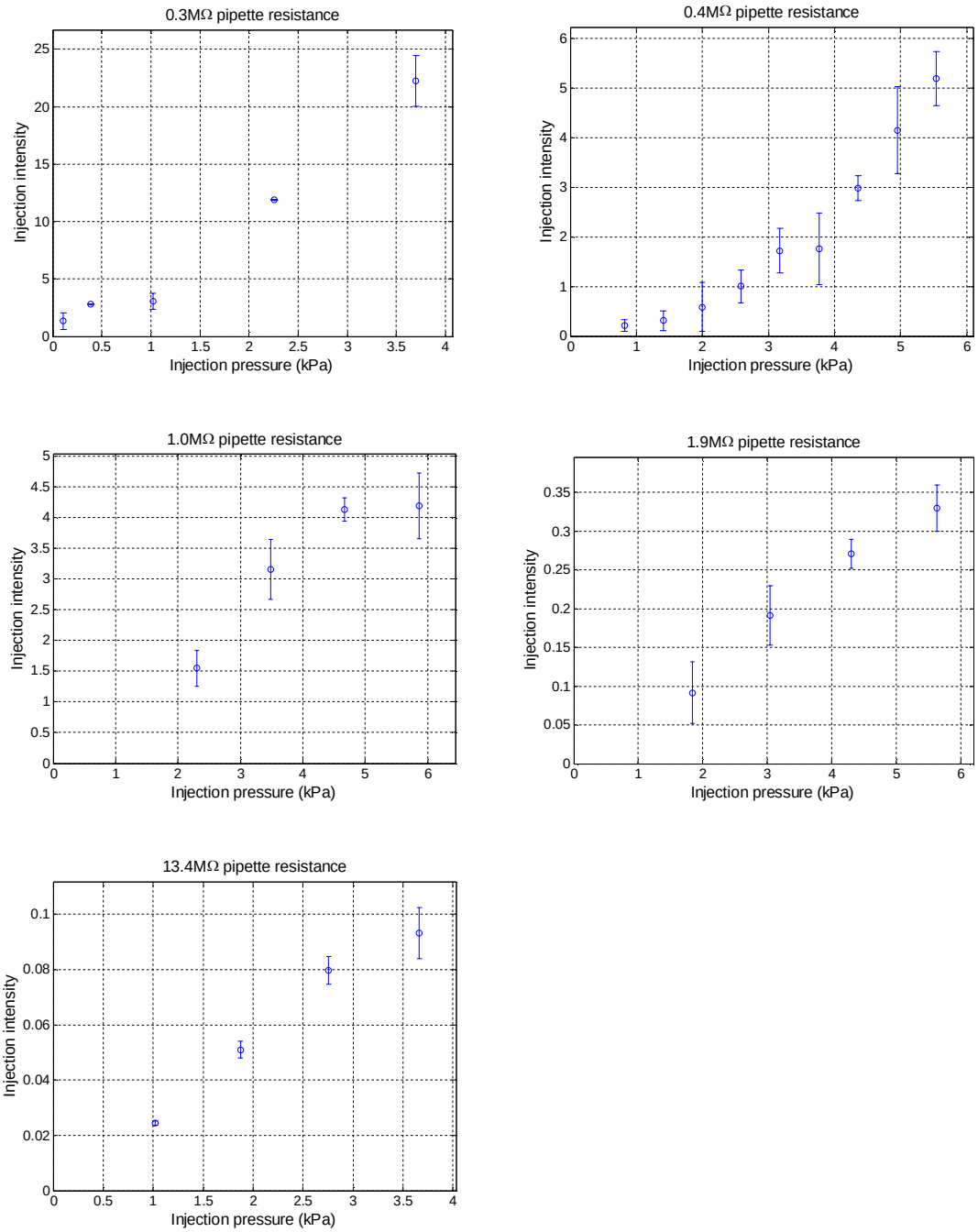

Figure 6.10: Injection intensity as a function of injection pressure for all the five pipettes (pipette resistances). The standard deviations are shown as well.

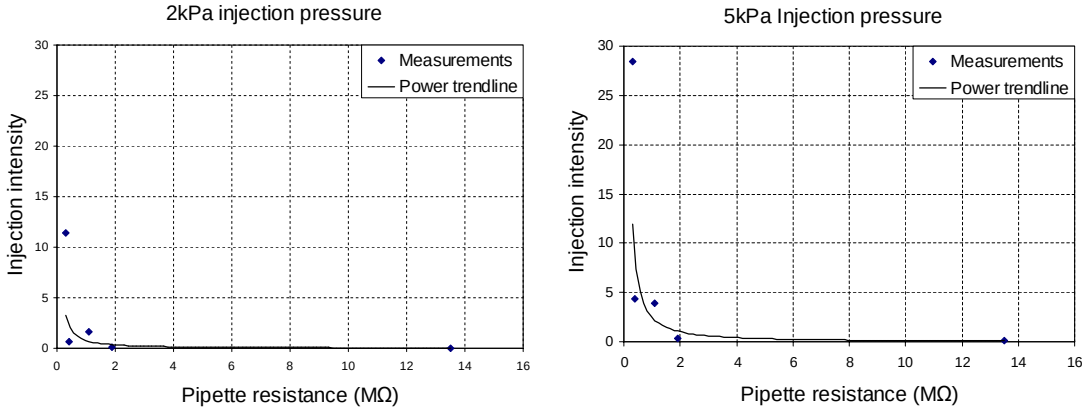

Figure 6.11: Injection intensity as a function of pipette resistance with the injection pressure of 2kPa (in the left) and 5kPa (in the right).

When the data shown in Figure 6.8 is fitted with a MATLAB `polyfitn` function available in the Mathworks pages to acquire a second order model, the following result is obtained with the presented variances and standard deviations for each term.

$$I_{inj} = -0.3072\,p_{inj}^2 - 0.1465\,p_{inj}R_{pip} + 2.9277\,p_{inj} + 0.2896R_{pip}^2 + 4.0082R_{pip} + 1.3342 \quad (6.1)$$

var:	0.0958	0.0304	5.0879	0.0171	3.4132	8.4605
std:	0.3095	0.1745	2.0218	0.1307	1.8475	2.9087

As it can be seen, the variances are quite large and thus the model produced is not really practical. Also, the form of the equation is not intuitive and it is hard to justify why the equation describes the injection process.

Even though the data gained in the tests was not good enough for model generation, the measurements provided valuable information on the sensitivity of the microinjection process for changes in the pipette properties and thus the need for the model of the injection volume. Figure 6.10 shows how drastic changes there are in the injection intensity between different pipette sizes. For example, if a 1µm pipette tip is used in injection and it gets broken increasing the tip opening to 2µm, the injection volume increases tenfold if the injection pressure remains the same. If a 0.5µm pipette breaks down to a 1µm pipette, the corresponding change is 3–5-fold. On one hand, this produces a considerable increase in the stress caused to the cell and on the other hand, the repeatability of the injections in that test is lost. Thus, the microinjection system should be able to detect the breakages and re-adjust the injection pressure. Furthermore, the relatively high tolerances in the pipette sizes mean that a feedback is needed.

6.3.2. Pipette Resistance – Pipette Diameter Relationship

Equation (3.1) proposed a relationship between the pipette tip diameter and the pipette resistance. To examine the validity of this relationship, a regression model is fit to the

data describing pipette tip diameters and the corresponding measured pipette resistances. Seven pipettes are used in the analysis. Five of them are the same as used in the previous section and two are self-pulled pipettes manufactured with the pipette puller presented in Section 4.1.3. Microsoft Excel is used in the regression model fitting.

With the pipettes used in the injection tests, a resistance value measured in the beginning of the tests is used in this analysis, and with the self-pulled pipettes, the resistance is measured similarly to the actual injection tests for the analysis. The pipette diameter is a more problematic parameter since – as shown in Table 4.1 – the tolerances are relatively big and thus the diameters announced by the manufacturer are not trustworthy. A scanning electron microscopy (SEM) measurement of new WPI tips showed that the tolerance can actually be as high as 90%. Determining the real diameters with microscopy is rather difficult. Measurement the pipette tips with a conventional light microscope before or after the tests is not possible because of the very small tip diameters that are not visible for the microscopes of our laboratory. SEM measurements before the tests are not feasible since the pipette has to be coated with a thin gold layer before the measurement. This changes both the geometrical and the electrical properties of the pipette. SEM measurements after the tests are not straightforward either since the injection liquid and cell cultivation medium dry on the pipette tip and change its geometry. Cleaning the pipette with alcohol after the tests might help the situation but it is not certain that the entire residue can be removed.

The first results presented are done using the diameter values given by the manufacturers for the commercial pipettes. The self-pulled pipettes were relatively large and their diameter was possible to be measured with a zoom lens. Table 6.3 and Figure 6.12 show the results.

Table 6.3: The tip diameters and the resistances of seven pipette sizes.

Type	Resistance / MΩ	Diameter / µm	Diameter by
Eppendorf Femtotip II	14.00	0.5	Manufacturer
WPI TIP1TW1	1.88	1	Manufacturer
WPI TIP2TW1	1.02	2	Manufacturer
WPI TIP5TW1	0.43	5	Manufacturer
WPI TIP10TW1	0.29	10	Manufacturer
Self-pulled	0.26	17	Measured with a zoom lens
Self-pulled	0.23	27	Measured with a zoom lens

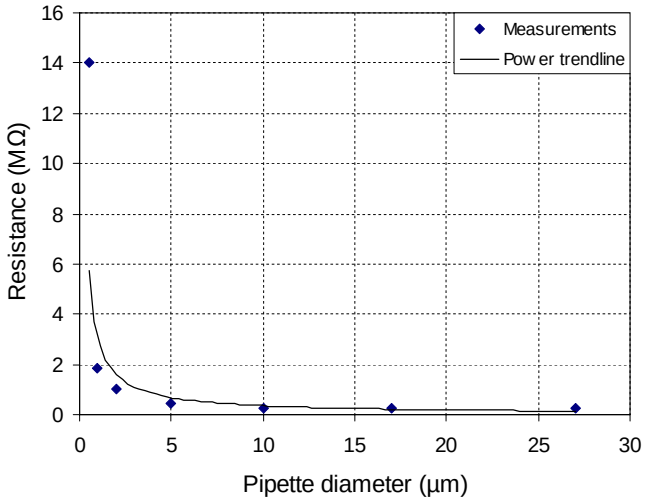

Figure 6.12: Pipette resistance as a function of its diameter. The diameters given by the manufacturers were used.

The best-fitting regression trendline was a power trendline and it had the following equation

$$R_{pip} = \frac{3.01}{d_{pip}^{0.93}} \qquad (6.2)$$

for R_{pip} given as MΩ and d_{pip} given as µm. Compared with Equation (3.1), the form is somehow similar but the exponent of d_{pip} should be 2. The exact values for ρ_{liq} and l_{pip} are not known and therefore the value of the constant in Equation (6.2) is hard to evaluate.

The commercial pipettes used in Figure 6.12 were measured with a Philips XL30 SEM microscope to determine their exact diameters. However, as discussed above, the dried medium and FITC residues caused error in the measurements. Therefore, the measured values appeared realistic and usable for only three of the pipettes. Table 6.4 presents the parameters in Table 6.3 corrected with the SEM measurements.

Table 6.4: Pipette diameters and resistances of seven pipette sizes. SEM measurements presented in bold.

Type	Resistance / MΩ	Diameter / µm	Diameter by
Eppendorf Femtotip II	14.00	0.5	Manufacturer
WPI TIP1TW1	1.88	**2**	**SEM**
WPI TIP2TW1	1.02	**3.3**	**SEM**
WPI TIP5TW1	0.43	5	Manufacturer
WPI TIP10TW1	0.29	**16.6**	**SEM**
Self-pulled	0.26	17	Measured with a zoom lens
Self-pulled	0.23	27	Measured with a zoom lens

The diameter for WPI TIP10TW1 appears to be more in line with the resistance value if compared with the self-pulled pipette with the tip diameter of 17µm. When Figure 6.12 is redrawn using the diameter values presented in Table 6.4, some changes happen. The results are presented in Figure 6.13.

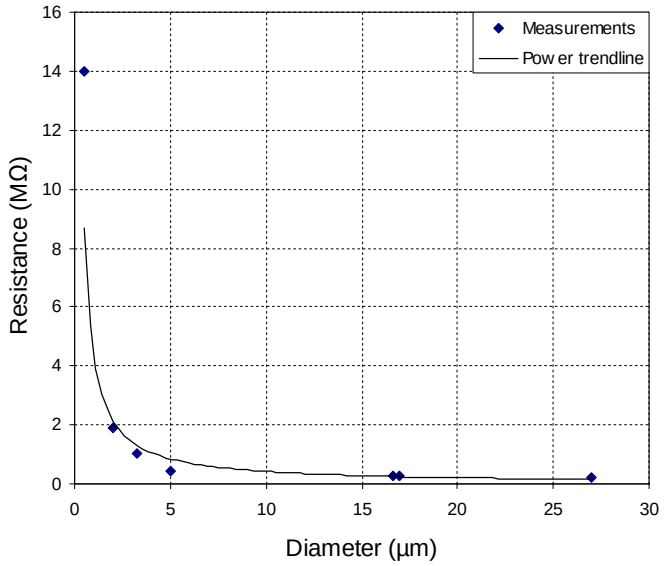

Figure 6.13: Pipette resistance as a function of its diameter. With three commercial pipettes, SEM measurements are used instead of the diameter given by the manufacturer.

Again, the best-fitting regression trendline was a power trendline. As it can be seen, it fits to data bit better than in Figure 6.12. This time, the trendline is described with the following equation

$$R_{pip} = \frac{4.32}{d_{pip}^{1.01}} \qquad (6.3)$$

This equation differs only slightly from Equation (6.2). However, the change is towards Equation (3.1).

6.4. Additional Tests

Since some new questions arose while performing the experiments and analyzing the results, additional tests were required. Two types of additional tests were made: pipette moving tests and electrode tests. This section presents the additional tests and their results.

6.4.1. Pipette Moving Tests

It was observed that when the higher pressures were used in the injection tests the pipette tip moved a bit. This movement was seen only when the 20x objective was used and the amplitude of the movement was less than 10µm. In order to detect if this movement was the origin of the resistance peaks presented in Section 6.2.3, experiments where the pipette was moved back and forth while the resistance was measured were performed. The micropipette used in the tests was Femtotip II and it was filled with FITC similarly to the original injection experiments. Pipette tip was immersed in a well plate well filled with Leibovitz medium, resistance measurement was started and the pipette was moved ±50µm in 10µm steps in one direction using the SmarAct micromanipulator. One experiment to each direction was done. A simple switch connected to the digital input of the measurement board was used to mark the beginning and the end of moving the pipette. The results are presented in Figure 6.14 and Figure 6.15.

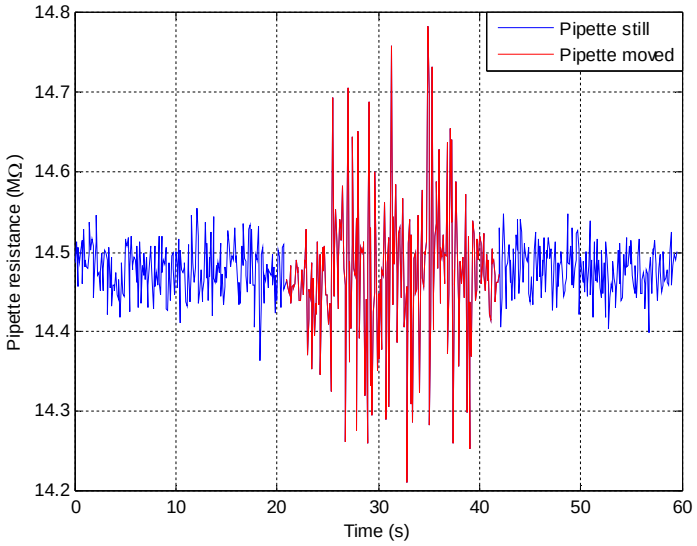

Figure 6.14: Pipette resistance while the pipette is moved several times ±50µm in 10µm steps vertically.

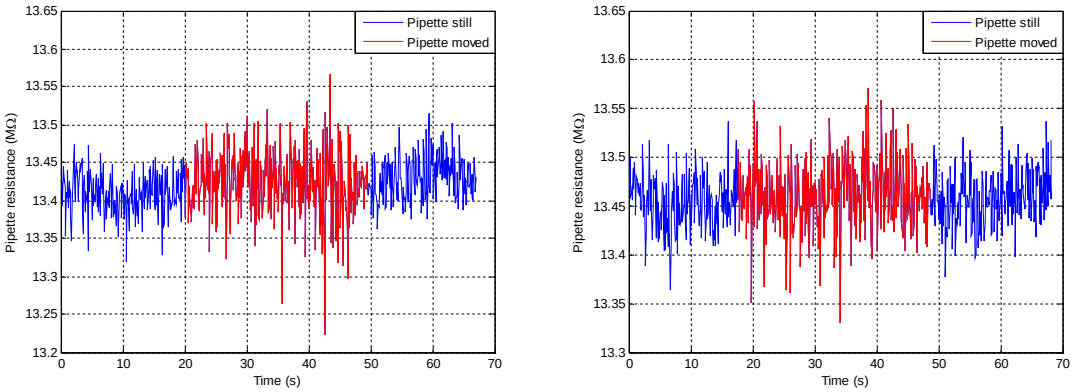

Figure 6.15: Pipette resistance while the pipette is moved several times ±50µm in 10µm steps horizontally. Parallel to the x-axis (in the left) and parallel to the y-axis (in the right).

The figures show that the noise is bit higher during the motion. It seems that the resistance measurement is most sensitive to vertical movement. However, when the tests were repeated using ±500µm movement in 100µm steps, same result was not obtained. In first experiment, the noise remained the same during the motion, and in the second one, the noise even reduced during the motion. Some higher peaks were gained in the beginning of the motion, though. Nevertheless, given that the movement of the pipette is only less than 10µm in injections, the movement alone cannot explain the resistance peaks seen in the injection moments.

6.4.2. Electrode Tests

Wearing out of electrodes caused often errors in resistance measurement as discussed in Section 6.2.1. As mentioned, wearing out can be seen as the change of offset and finally as saturation of the current-to-voltage converter. Wearing out should be a bigger problem with the silver – silver chloride electrodes than with the platinum electrodes since the chloride layer disappears from the pipette electrode as the result of wearing and causes the electrode to change to a silver electrode. The silver electrode has different properties and a different half-cell potential than the Ag / AgCl electrode and this causes errors in the measurement. The platinum electrode remains as a platinum electrode also after wearing and it should therefore be more stable and durable.

An experiment was performed to study the stability and the durability of Ag / AgCl and platinum electrodes. The pipette resistance was measured for 12 hours first using a platinum electrode and then using an Ag / AgCl electrode. A femtotip II micropipette was filled with FITC and immersed in Leibovitz medium for the resistance measurement as in the actual injection experiments. The pipette and the liquids were changed between the measurements. The sampling frequency was 1kHz and the excitation signal was a 10Hz square wave signal as in the original injection experiments as mentioned in Section 4.3. The amplitude of the excitation signal going to the pipette was 2mV. Figure 6.16 shows the offset of the measurement signal as a function of time for both electrodes and Figure 6.17 presents the amplitude of the measurement signal.

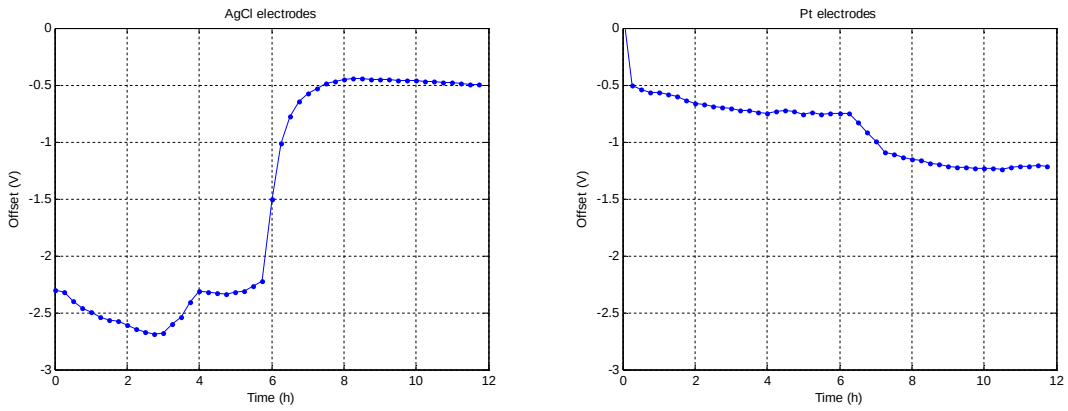

Figure 6.16: Offset as a function of time with the Ag / AgCl electrodes (in the left) and the platinum electrodes (in the right).

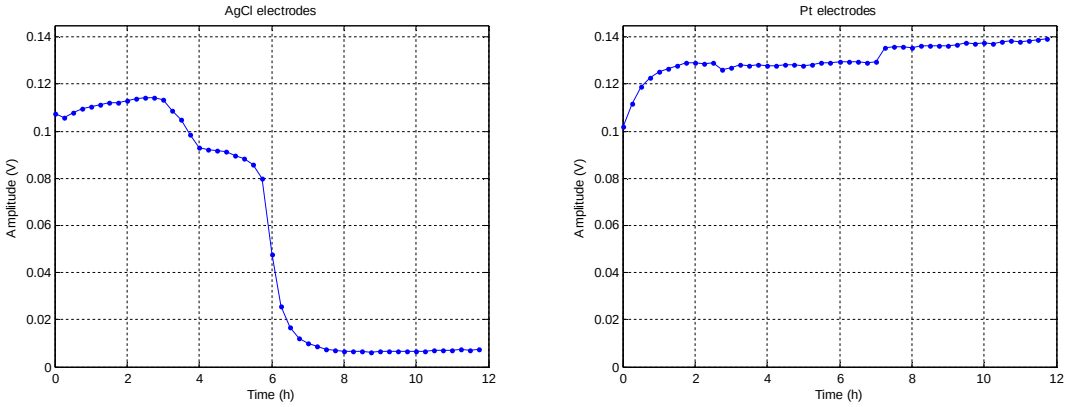

Figure 6.17: Amplitude as a function of time with the AgCl electrodes (in the left) and the platinum electrodes (in the right).

The figures show that in both cases the offset and the amplitude seem to be roughly inversely proportional to each other. When the offset decreases, the amplitude increases and vice versa. The pipette properties should remain constant during the test since nothing is done with the pipette thus the reason for the amplitude changes should be the changes of the offset. Figure 6.18 shows the amplitude as a function of the offset to clarify this.

It is also observed that during the first two hours, the Ag / AgCl electrodes are more stable than the Pt electrodes but after that the Pt electrodes are more stable. After five hours the offset of the measurement signal from the Ag / AgCl electrodes jumps and the amplitude drops dramatically whereas after two hours both the offset and the amplitude of the measurement signal from the Pt electrodes remain rather stable. There is only one notable fluctuation after seven hours.

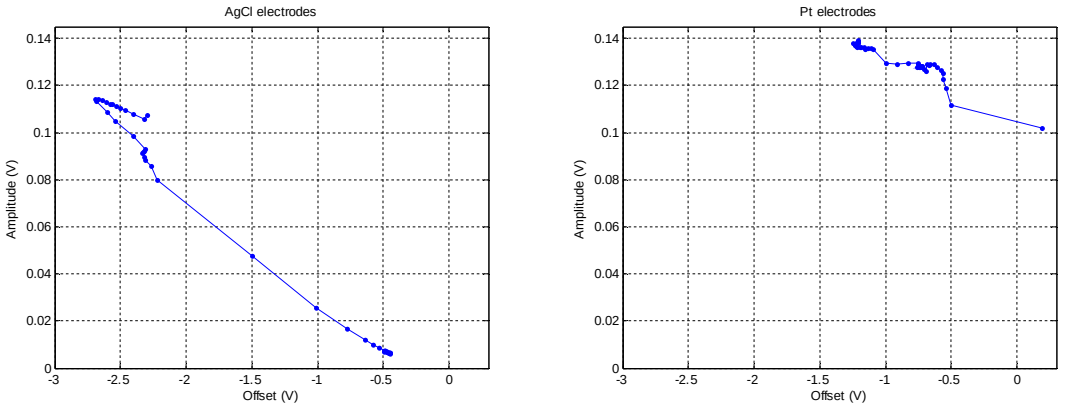

Figure 6.18: Amplitude as a function of offset with the Ag / AgCl electrodes (in the left) and the platinum electrodes (in the right).

Since the pipette resistance is calculated using the amplitude of the excitation signal and the amplitude of the measurement signal as shown in Equation (3.5), the changes of the amplitude of the measurement signal caused by the changes of the offset also change the measured pipette resistance value drastically. The measured resistance as a function of time is depicted in Figure 6.19.

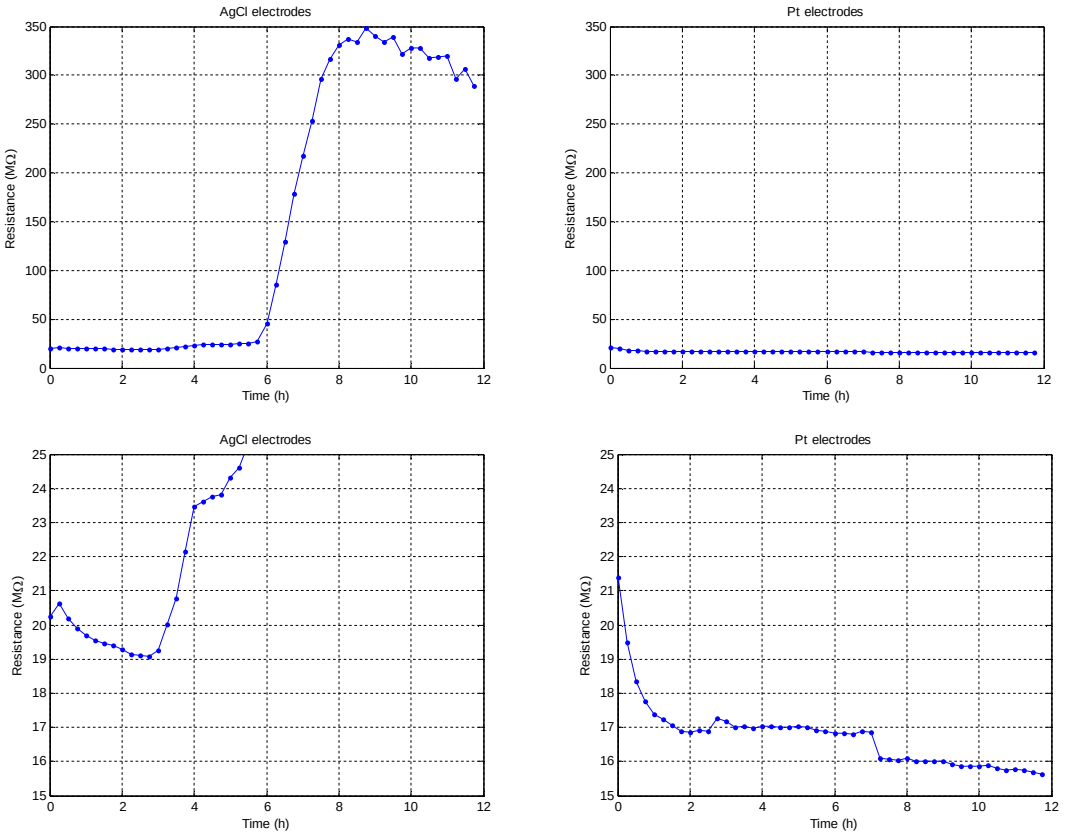

Figure 6.19: Measured resistance as a function of time with the Ag / AgCl electrodes (in the left) and the platinum electrodes (in the right). Figures scaled according to the measurements from the Ag / AgCl electrodes (up) and according to the measurements from the Pt electrodes (down).

Figure 6.19 illustrates that the error due to changes in offset can be as great as 1650% with the silver chloride electrodes. Offset changes in the beginning of the measurements with the platinum electrodes caused also notable 26% error.

Figure 6.20 shows the measured resistance as a function of the offset for both electrode materials. When the offset increases, the resistance increases but the relationship is not linear.

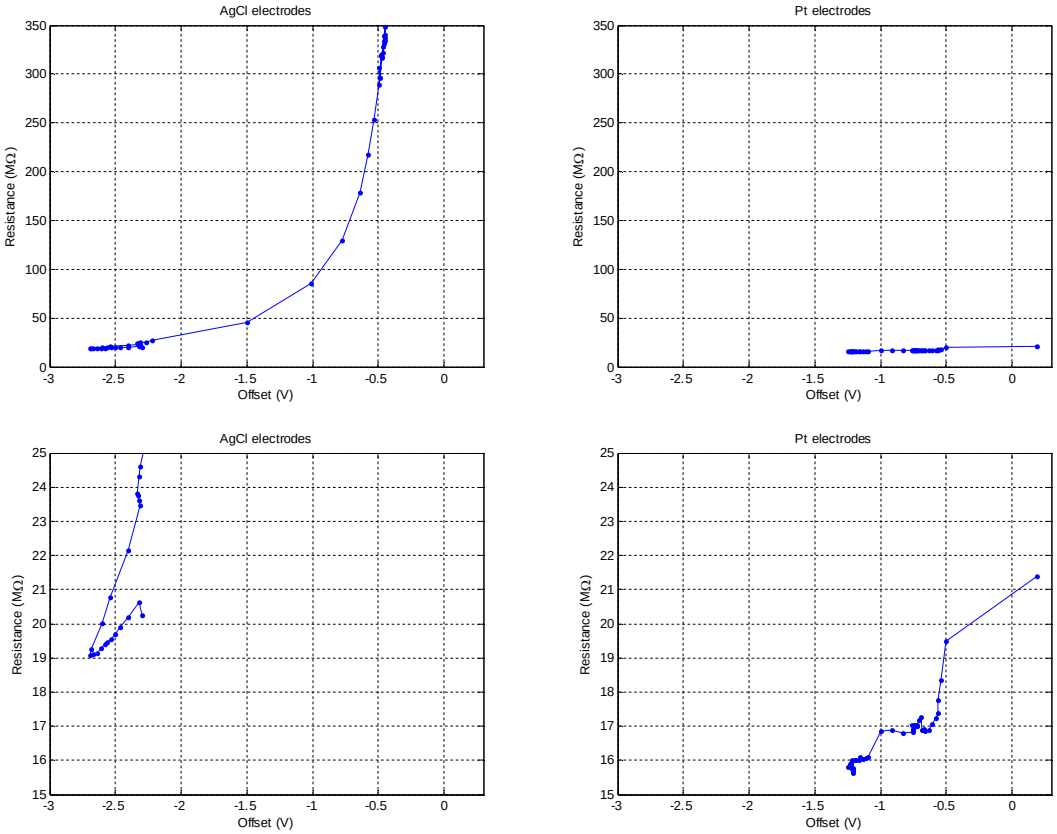

Figure 6.20: Resistance as a function of offset with the AgCl electrodes (in the left) and the platinum electrodes (in the right). Figures scaled according to the measurements from the AgCl electrodes (up) and according to the measurements from the Pt electrodes (down).

It can be concluded that according to these tests, platinum seems to be a more durable and stable electrode material than silver – silver chloride. However, remarkable offset changes occur also with platinum especially in the beginning of the measurements. Since there appears to be a relationship between the offset change and the change in the measured resistance, it could be possible to computationally compensate the measurement error caused by wearing of the electrodes. However, further experiments are needed to confirm the nature of the relationship to obtain the equations sufficient for compensation. At this point, it might be more feasible simply to monitor the condition of the electrode based on its offset changes, change the electrodes if drastic fluctuations in the offset are detected and omit the data where great variations arise.

In the data shown in Figure 6.8, the offsets in the resistance measurements varied from -8V to 2V from the pipette to pipette. The offset values were from the lowest pipette resistance to the highest the following: 0.5V, 1.5V–2.0V, -1.5V– -0.5V, 6.0V–6.5V and -8V– -4V. Thus, the largest offset oscillations during the measurement were with the largest tip, WPI TIP10TW1, and a platinum electrode. As it can be seen from the data presented in Figure 6.8, the changes in the measured resistance caused by the changes in the offset seem not to be always as radical as in Figure 6.20 and therefore extra experiments on the electrode behaviour are justified. It is hard to estimate what

was the effect of the different offsets on the measurement data shown in Figure 6.8 but at least the resistance variations during the measurements were small.

6.5. Discussion

Actual reliable mathematical model describing the relationship between the injection pressure, the pipette electrical resistance and injection volume could not be built based on the measurement data. A second-order polynomial model was generated but it did not work well even for the data used in its development. However, the experiments proved that the pipette electrical resistance is connected to the hydraulic resistance or the tip diameter of the pipette and thus the same pressure produces a lower injection volume with a pipette whose electrical resistance is higher. In addition, the tests revealed that the relationship seems to be hyperbolic whereas the relationship between the injection pressure and the injection volume appears to be somewhat linear. However, the deeper understanding of the nature of the relationships and generation of a more reliable mathematical model require more measurement data.

As it was pointed out, many problems were encountered while gathering the data. The micromanipulator and the CDD circuit were not always functioning reliably, which hindered the measurements and caused wasting of the test material. Both devices are delicate instruments and need regular maintenance from skilled personnel. Also, often the pipette got clogged during or right in the beginning of the experiment. Then the measurement target was not what it was expected to be and the data gained was not suitable for modelling as it was discussed in Section 6.2.2. Since the tests were not performed in a clean room, there are many possible sources of the clogging particles. One source is the pipette tips used with the manual pipettor in filling or the micropipettes. The narrow nylon tips of the pipettes are put inside the micropipettes during filling and they may deliver impurities into the injection liquid. Another source is the plastic adapter used in connecting the micropipettes manufactured by WPI to the arm of the micromanipulator. When the micropipette is pushed through the adapter, some particles may detach from the inner parts of the connector and enter the micropipette. Furthermore, the electrode might bring some impurities to the micropipette. Also, the fluorescent dye used in the tests was rather old and it is said that old dyes may get clotty and thus cause clogging. This all can be summed up that the succeeding in the preparations is fatal for the success of the experiments and the staying clean of the micropipette should be assured in the preparation steps.

Since the data revealed that a clogged pipette does not obey the similar pipette resistance – injection pressure – injection volume relationship as the clean ones, in a ready injection guidance system, which adjusts the injection pressure using the pipette resistance measurement, the sudden ~10% increases should cause an error situation. Here, the operator should be informed that the pipette has gotten clogged and advised to try to clean it by using high pressures. If the pipette remains clogged, that is, the pipette resistance remains high after the cleaning trials, the operator should be advised to either

change the pipette or continue tests in manual mode since the pressure adjustment is no longer reliable.

The material and the quality of the electrodes used in the pipette resistance measurement were found to have a great impact on the measured resistance. Even though the electrode tests were only additional tests for the work, these findings seem to be really important and they should be taken into consideration when measuring the pipette resistance. The change in the offset changes also the amplitude of the measurement signal and thus changes also the resistance calculated using the amplitude. This has to be taken into account in the ready pressure adjustment system. Silver chloride and platinum are the most used electrode materials for this kind of measurements and thus there are not many materials to choose from. According to the tests made, the platinum electrodes could be more feasible for the pipette resistance measurement. The user interface of the injection guidance system should report the operator of the offset fluctuations and the need to change the electrode. Maybe even some kind of computational compensation of the variations in the offset is possible.

The future electrode tests should include at least five more 12 hours excitation tests with the both electrode materials to find out how repeatable the behaviour presented in this section is. Also, tests where for example two-hour excitation and two-hour rest are repeated would be important to study if the offset change is directly proportional to the total time of use or does the time of continuous excitation have some effect on the change as well. In addition, the effect of the measured resistance – that is – the pipette size on the wearing out rate should be studied. Anyhow, the electrodes are certainly a topic, which needs to get more attention in the future.

The connection between the pipette tip diameter and the pipette electrical resistance was also studied. The measured relationship between them was not similar to the assumption but the assumption contained some parameters, whose value was not known. Furthermore, the exact tip diameters of the pipettes could not be known or measured reliably. It is also more likely that the pipette electrical resistance is proportional to the pipette hydraulic resistance instead of the plain pipette tip diameter since the shape of the tip is also taken into consideration in the pipette hydraulic resistance.

It was found that the injection moment could be easily detected from the pipette resistance data. This observation itself does not provide any extra information since the injection moment can be found from the control data of the solenoid valve or recorded directly from the MART program but it helps to realize that the resistance data gathered during injections should not be used to detect clogging or to pressure adjustment since it is distorted. The actual reason of the peak is not clear, though.

7. CONCLUSION

This thesis work aimed at developing a method to estimate the injection volume in capillary pressure microinjection using measurements of the injection pressure and the pipette electrical resistance. The objective was to produce a mathematical model, with which the injection pressure could be controlled real-time to yield a desired constant injection volume with micropipettes with different tip diameters. This work was divided to Introduction, five chapters and Conclusion.

Chapter 2 introduced the capillary pressure microinjection technique to give the basic understanding of the method this thesis work is connected to and the usefulness of the objective of the work. The fundamentals of the capillary pressure microinjection as well as the most common applications of the technique with suspension and adherent cells were presented in the beginning. Next, the structure of the CPM system and the functions of its different parts were presented. This was followed by a discussion on the challenges in the CPM of adherent cells in detecting the contact between the pipette and the target cell and in measuring the injection volume. It was pointed out that while some solutions exist in the contact detection, there is no method to measure the injection volume online and therefore it is possible only to calibrate the system before experiments. The most commonly used calibration methods were discussed and their individual downsides as well as the cons of the whole calibration based determination of the injection volume were presented. Also, the basics of fluorescence measurements and their applications in the field of CPM were depicted since use of fluorescent dyes is an essential part of the experiments performed in this work. In the end, it was concluded that this work is concentrated on the CPM of adherent cells instead of suspension cells.

Chapter 3 discussed the impedance measurements of living cells and the potential of this method in the measurements needed for the injection volume estimation. First, the background of the technique was illustrated and then the electrical circuit models of the micropipette and the cell, which are the theoretical basis of interpreting the measurements, were presented. For this work, the electrical circuit model of the micropipette was the most important. After the models, a custom-made electric measurement circuitry for performing the impedance measurements in microinjections, the contact detection device, was presented. The structure, the operation principle and the purpose of use were introduced. In the end of the chapter, the connection between the pipette impedance and the pipette geometrical properties, which partially define the injection volume, was emphasized, and thus the significance of the impedance measurement of the pipette for this work was revealed. Therefore, the main result of the chapter was to show that the pipette electrical impedance is a useful parameter in the

injection volume estimation and it can be measured by using the CDD circuit, which thus should be a part of the test setup.

Chapter 4 presented the measurement setup for gathering data for the model of the injection volume and considered the potential error sources in it. In the beginning, the inputs and outputs of the model were justified. It was shown with some basic equations of liquid flow that the injection pressure and the pipette properties measured as the pipette electrical resistance define the injection volume. Thus, the measurement setup should consist of a microinjection system and the sensors for measuring the injection pressure and the pipette electrical resistance as well as a mean to estimate the injection volume. It was decided to use a fluorescent dye as the injection liquid to obtain the injection volume information in its intensity. The protocol was to calculate the intensity from the image data taken by a microscope camera during the microinjections and to measure the injection pressure with a pressure sensor and the pipette resistance with the CDD. Measurement data for modelling would be gathered from consecutive microinjections into liquid medium using several injection pressures and pipette sizes. All the parts of the test bench and the materials used in experiments were presented in their own sections. Then, the possible error sources were presented and their impact on the results was discussed. In the end of the section, the measurement algorithm was briefly discussed. The primary outcome of this chapter was the generation of the measurement setup for gathering information on the pipette resistance, the injection pressure and the injection volume during microinjection experiments.

Chapter 5 illustrated the nature of the measurement data gathered with the test bench and pointed out the need for automated data handling and organizing algorithm. Firstly, a data structure for the processed measurement data and the additional information on the tests and the testing materials was designed. The solution was a MATLAB structure array with separate fields for the data related to the injection pressure and the pressure measurement, the data related to the pipette resistance and its measurement, and the data related to the injection intensities and the measurement protocols for that. Also, the fields for the raw measurement data and the general information were included to the structure array. Secondly, an automated MATLAB algorithm for processing the data and organizing it to the structure array was generated as well. The result was an easy-to-use function with a simple user interface and minimum need of data pre-processing. The operation principle of the function is discussed and the processing of the resistance measurement data from the contact detection device, the pressure sensor unit output and the image data from the microscope camera are illustrated. Also, a brief insight into the visualization of the data was given in the end of the chapter.

Chapter 6 discussed the measurements done and the results gained. First, a more detailed, almost step-by-step, test procedure developed when making the measurements was given. Then, some important observations made during the experiments or data handling were illustrated. The most important of them was the finding that the general electrical model of the pipette presented in Chapter 3 cannot be applied on a clogged pipette, and thus the modelling of the injection volume using the electrical impedance

measurement also fails when the pipette gets clogged. However, it was proven that the pipette clogging can be detected pretty accurately. When 10 cases were analyzed, only one false positive and one case where the clogging was not detected were found. Next, the main results of the tests were discussed. The most significant of them was the injection pressure – pipette electrical resistance – injection intensity relationship, solving of which was the main objective of this thesis. Due to the various error sources encountered during the tests and the limited amount of data caused by that, the relationship gained was more of an indicative sketch than a ready model. The data was used to generate a second-order polynomial model but the result was not truly satisfying. However, the measurement data showed certain characteristics between the injection pressure and the injection volume and the pipette electrical resistance and the injection volume: it was illustrated that the relationship between the injection pressure and the injection volume was quite linear whereas the relationship between the pipette electrical resistance and the injection volume was steeply hyperbolic. This was an important finding. It stressed the significance of the measurement and the control of the injection volume since the data showed considerable differences between the injection volumes from different pipette sizes with the same pressures. Given that breaking of the pipette tip during microinjections is a relatively common problem and the tolerances of the micropipettes can be even up to 90%, adjusting injection pressure before the experiments based on the announced size is unviable. As the second result, the pipette resistance – pipette tip diameter relationship was depicted. Due to the uncertainty in the real pipette tip diameters, this relationship lacked reliability as well even though it showed some assumed behaviour. However, this relationship was of smaller importance since defining the pipette size itself is not essential for microinjections.

After the actual tests, some additional experiments were performed. First, the effect of moving the electrode during the experiment on the electrical resistance measurement was studied. Secondly, the influence of the electrode material was experimented. Two electrode materials, platinum and silver – silver chloride were compared. It was found out that both materials exhibited instability over time: in 12-hour tests where the electrical resistance of a micropipette was continuously measured, the resistance changed over time even though the micropipette remained unchanged. The change in the measured resistance seemed to be somehow connected with the change in offset of the measurement signal. Platinum seemed to be more durable electrode material compared with the Ag / AgCl electrodes and the changes were smaller in the test platinum was used. This finding emphasized the importance of the electrode material and condition on the measurement results and more research will be done in this area in the future.

Although a ready working model for the injection volume was not yielded in this work, a rough estimate of it was acquired. The relationships between the measured injection parameters could be estimated and thus the effect of increasing the injection pressure of the pipette resistance on the injection volume was approximated. This is a valuable new piece of information for the CPM technique. Other important contribution

of this thesis was to deepen the understanding of the microinjection process since the measurements performed in this work have not been reported to be done earlier. Thus, these experiments provide new information of the nature of CPM. Also, even though the CDD circuit has been in use in the MST-group for several years, a quantitative analysis of its reliability in detecting clogging or study on electrode materials have not been done. This thesis work offers also simple statistics for clogging detection and examination on electrode materials.

REFERENCES

1 Ammi, M., Ferreira, A. 2006. *Biological Cell Injection Visual and Haptic Interface*, Advanced Robotics 20 (3), pp. 283–304.

2 Axon Instruments Inc. 1993. *The Axon Guide for Electrophysiology & Biophysics Laboratory Techniques*.

3 Barnett, D.W. 1997. *Optimal Stimulus Desing for Multi-Frequency Cell Membrane Capacitance Estimation*, Proceedings of the 19th International Conference IEEE/EMBS, 1997 Chicago, IL. USA, pp. 2116–2119.

4 Brown, G. A. J. *The Microinjection Workshop*. [WWW]. [Cited 5.8.2009]. Available at: http://members.cox.net/microinjectionworkshop/.

5 Bruus, H. 2008. *Theoretical Microfluidics*, Oxford University Press, pp. 74–79.

6 Cho, S.-Y., Shim, J.-H. 2004. *A New Micro Biological Cell Injection System*, 2004 IEEE/RSJ International Conference on Intelligent Robots and Systems (IROS) 2, pp. 1642–1647.

7 Defilippi, P., Huez, G., Verhaegen-Lewalle, M., De Clercq, E., Imai, J., Torrencet, P. and Content, J. 1986. *Antiviral Activity of a Chemically Stabilized 2-5A Analog upon Microinjection into HeLa Cells*, FEBS Letters, Vol. 198, No. 2, pp. 326–332.

8 Eppendorf company web page. [WWW]. [Cited at 7.10.2009]. Available at: http://www.eppendorf.com/.

9 Eroglu, A., Lawitts, J. A., Toner, M. and Toth, T. L. 2003. *Quantitative Microinjection of Trehalose into Mouse Oocytes and Zygotes, and Its Effect on Development*, Cryobiology, Vol. 46, pp 121–134.

10 Feramisco, J., Perona, R. and Lacal, J. C. 1999. *Needle Microinjection: A Brief History*, Microinjection, Birkhäuser Verlag Basel, pp. 9–12.

11 Gawad, S., Schild, L., and Renaud, Ph. 2001. *Micromachined Impedance Spectroscopy Flow Cytometer for Cell Analysis and Particle Sizing*, Lab on a Chip, vol. 1, pp. 76–82.

12 Halttunen, J. 2009. *Anturifysiikka*, Tampere University of Technology lecture material, pp. 80–95.

13 Haugland, R.P. 2002. *Handbook of Fluorescent Probes and Research Products, Ninth Edition*, Molecular Probes, pp. 1–5.

14 Harvard Apparatus company web page. [WWW]. [Cited 7.10.2009]. Available at: http://www.harvardapparatus.com.

15 Hevonkorpi, V. 2005. *A Pressure System for Single Cell Injection and Aspiration*, Master of Science Thesis.

16 Hirvonen, J., Vilkko, M., Roinila, T. and Kallio, P. 2008. *Estimation of Electrical Cell–Capillary Admittance during Injection with Frequency Response Method*, Chung, M.J. et al. (eds.). IFAC 17th World Congress, Seoul, Korea.

17 Huang, H., Sun, D., Mills, J.K. and Cheng, S.H. 2008 *Automatic Suspended Cell Injection under Vision and Force Control Biomanipulation*, 2007 IEEE International Conference on Robotics and Biomimetics, ROBIO, art. no. 4522137, pp. 71–76.

18 Kallio, P. and Kuncova-Kallio, J. 2006. *Capillary Pressure Microinjection of Living Adherent Cells: Challenges in Automation*, Journal of Micromechatronics, Vol. 3, No. 3–4, pp.189–220.

19 Kallio P., Kuncova-Kallio, J., Savia, M. and Zhou, Q. 2005. *Introduction to Microsystem Technology*, Tampere University of Technology lecture material, pp.83–84.

20 Kallio, P., Ritala, T., Lukkari, M. and Kuikka, S. 2006. *Injection Guidance System for Cellular Microinjections*, IEEE / RAS-EMBS International Conference on Biomedical Robotics and Biomechatronics (BioRob), Pisa, Italy.

21 Kobayashi, N., Rivas-Carrillo, J.D., Soto-Gutierrez, A., Fukazawa, T., Chen, Y., Navarro-Alvarez, N. and Tanaka, N. 2005. *Gene Delivery to Embryonic Stem Cells*, Birth Defects Research Part C – Embryo Today: Reviews, Vol. 75 No. 1, pp. 10–18.

22 Kornreich, B. G. 2007. *The Patch Clamp Technique: Principles and Technical Considerations*, Journal of Veterinary Cardiology, vol. 9, issue 1, pp 25–37.

23 Kovanen, K., Lukkari, M., Purmonen, S., Ylikomi, T., Viitanen, J. and Kallio, P. 2007. *Electric Impedance Assisted Micropipette Aspiration*, The 29th Annual International Conference of the IEEE EMBS Engineering in Medicine and Biology Society in conjunction with the Biennial Conference of the French Society of Biological and Medical Engineering (SFGBM), Lyon, France.

24 Kovanen, K., Purmonen, S., Ylikomi, T. and Kallio, P. 2005. *Combined Cell Survival and Injection Success Rate in Microinjection of Living Adherent Cells*, CD Proceedings of the 3rd European Medical and Biological Engineering Conference, EMBEC'05, Prague, Czech Republic.

25 Kuncova, J. 2002. *Calibration of a Capillary Pressure Microinjection and Its Implementation within a Micromanipulator*, Master of Science Thesis.

26 Kuncova, J. and Kallio, P. 2004. *Novel Automatic Micromanipulator – a Tool for In-vitro Cell Toxicology Research*, International congress of toxicology, ICTX'04, Tampere, Finland, July 2004, published in Toxicology and Applied Pharmacology, Vol. 197, pp. 290.

27 Kushmerick, C. and von Gersdorff, H. 2003. *Exo-endocytosis at Mossy Fiber Terminals: Toward Capacitance Measurements in Cells with Arbitrary Geometry*, Proceedings of the National Academy of Sciences (PNAS), Vol. 100 No. 15 pp. 8618–8620.

28 Lappe-Siefke, C., Maas, C. and Kneussel, M. 2008. *Microinjection into Cultured Hippocampal Neurons: A Straightforward Approach for Controlled Cellular Delivery of Nucleic Acids, Peptides and Antibodies*, Journal of Neuroscience Methods, Vol. 175, pp. 88–95.

29 Lekkala, J. 2006. *Microsensors*, Tampere University of Technology lecture material.

30 Looi, J. and Haque, A. 2004. *Real Time Single Cell Health Monitoring by Impedance Measurement*, The Pennsylvania State University Graduate School.

31 Lu, Z., Chen, P.C.Y., Nam, J., Ge, R., Lin, W. 2007. *A Micromanipulation System with Dynamic Force-feedback for Automatic Batch Microinjection*, Journal of Micromechanics and Microengineering 17 (2), art. no. 018, pp. 314–321.

32 Luigs & Neumann company web page. [WWW]. [Cited 7.10.2009]. Available at: http://www.luigs-neumann.com/.

33 Lukkari, M. 2004. *Electrical Detection of a Contact between a Microinjection Pipette and Living Adherent Cells*, Master of Science Thesis.

34 Malmivuo, J. and Plonsey, R. 1995. *Bioelectromagnetism – Principles and Applications of Bioelectric and Biomagnetic Fields*, Oxford University Press, Ch. 4.5.

35 Matsuoka, H., Komazaki, T., Mukai, Y., Shibusawa, M., Akane, H., Chaki, A., Uetake, N. and Saito, M. 2005. *High Throughput Easy Microinjection with a Single-cell Manipulation Supporting Robot*, Journal of Biotechnology, Vol. 116, pp. 185–194.

36 Mattos, L., Grant, E., Thresher, R. 2006. *Semi-automated Blastocyst Microinjection*, Proceedings – IEEE International Conference on Robotics and Automation 2006, art. no. 1641964, pp. 1780–1785.

37 Minaschek, G., Bereiter-Hahn, J. and Berholdt, G. 1989. *Quantitation of the Volume of Liquid Injected into Cells by Means of Pressure*, Experimental Cell Research, Vol. 183, pp. 424–442.

38 Moe, A.E., Marx, S.R. Bhinderwala, I. and Wilson, D.M. 2004. *A Miniaturized Lock-in Amplifier Design Suitable for Impedance Measurements in Cells*, Sensors, Vol. 1, pp. 215–218.

39 Molleman, A. 2003. *Patch Clamping: An Introductory Guide to Patch Clamp Electrophysiology*, John Wiley & Sons, Ch. 2.3, pp. 18–42.

40 Morgan, H., Sun, T., Holmes, D., Gawad, S. and Green, N.G. 2007. *Single Cell Dielectric Spectroscopy*, Journal of Physics D: Applied Physics, Vol. 40, pp. 61–70.

41 Narishige company web page. [WWW]. [Cited 7.10.2009]. Available at: http://narishige-group.com/.

42 National Instruments, *PCI 6052E datasheet*. [WWW]. [Cited 26.6.2009]. Available at: http://www.ni.com/pdf/products/us/4daqsc199-201_ETCx3_212-213.pdf.

43 Neuman, M. R. 2000. *Biopotential Electrodes*, The Biomedical Engineering Handbook: Second Edition, Boca Raton: CRC Press LLC, Chapter 48.

44 O'Shaughnessy, T.J. and Kim, Y.I. 1995. *A Computer-based System for the Measurement of Membrane Capacitance to Monitor Exocytosis in Secretory Cells*, Journal of Neuroscience Methods, Vol. 57, pp. 1–8.

45 Pepperkok, R., Herr, S., Lorenz, P., Pyerin, W. and Ansorge, W. 1993. *System for Quantitation of Gene Expression in Single Cells by Computerized Microimaging: Applications to c-fos Expression after Microinjection of Anti-Casein Kinase II Antibody*, Experimental Cell Research, Vol. 204, pp. 278–285.

46 Pethig R. and Kell, D. B. 1987. *The Passive Electrical Properties of Biological Systems: Their Significance in Physiology, Biophysics and Biotechnology*, Physics in Medicine and Biology, Vol. 32, No 8, pp. 933–970.

47 Perona, R., Dolfi, F., Feramisco, J. and Lacal, J. C. 1999. *Microinjection of Macromolecules into Mammalian Cells in Culture*, Microinjection, Birkhäuser Verlag Basel, pp. 17–43.

48 Pillarisetti, A., Pekarev, M., Brooks, A.D., Desai, J.P. 2007. *Evaluating the Effect of Force Feedback in Cell Injection*, IEEE Transactions on Automation Science and Engineering 4 (3), art. no. 4266825, pp. 322–331.

49 Ritala, T. 2003. *Development of Real-Time Motion Control Software for a Micromanipulator*, Master of Science Thesis.

50 Rohlicek, V. and Schmid A. 1994. *Dual-frequency Method for Synchronous Measurement of Cell Capacitance, Membrane Conductance and Access Resistance on Single Cells*, Pflügers Archiv European Journal of Physiology, Vol. 428, No. 1, pp. 30–38.

51 Rohlicek, V. and Rech, F. 2002. *Improvement of the Accuracy by the Measurement of the Electrical Cell Membrane Parameters*, Physiological Research Journal, Vol. 51, pp. 169–177.

52 Scherp, P. and Hasenstei, K.H. 2003. *Microinjection – A Tool to Study Gravitropism*, Advances in Space Research, Vol. 31, No. 10, pp. 2221–2227.

53 SmarAct, *SmarAct SLC-1760 datasheet*. [WWW]. [Cited 12.10.2009]. Available at: http://www.smaract.de/index.php?show=111

54 Sun, Y., Wan, K.-T., Roberts, K.P., Bischof, J.C., Nelson, B.J. 2003. *Mechanical Property Characterization of Mouse Zona Pellucida*, IEEE Transactions on Nanobioscience 2 (4), pp. 279–286.

55 Thompson, R.E., Lindau, M. and Webb, W.W. 2001. *Robust, High-Resolution, Whole Cell Patch-Clamp Capacitance Measurements Using Square Wave Stimulation*, Biophysical Journal, Vol. 81, Issue 2, pp. 937–948.

56 Tiruppathi, C., Malik, A.B., Vecchio, P.J.D., Keese, C.R. and Giaever, I. 1992. *Electrical Method for Detection of Endothelial Cell Shape Change in Real Time: Assessment of Endothelial Barrier Function*, Proceedings of the National Academy of Sciences (PNAS), Vol. 89 No. 17 pp. 7919–7923.

57 Viigipuu, K. and Kallio, P. 2004. *Microinjection of Living Adherent Cells Using a Semi-automatic Microinjection System*, ATLA (Alternatives To Laboratory Animals) 32., Twenty-first Scandinavian Cell Toxicology Workshop, pp. 417–423, 2004

58 Viigipuu, K. and Kallio, P. 2003. *Proof of Successful Microinjection of Living Adherent Cells*, CD Proceedings of the World Congress on Medical Physics and Biomedical Engineering, WC2003, Sydney, Australia.

59 Wang, W., Liu, X., Gelinas, D., Ciruna, B. and Sun, Y. 2007. *A Fully Automated Robotic System for Microinjection of Zebrafish Embryos*, PLoS ONE, Vol. 2, Issue 9, pp. 1–7.

60 Word Precision Instruments company web page. [WWW]. [Cited 7.10.2009]. Available at: http://www.wpiinc.com/.

61 Yun, Y., Dong, Z., Shanov, V. N., and Schulz, M. J. 2007. *Electrochemical Impedance Measurement of Prostate Cancer Cells Using Carbon Nanotube Array Electrodes in a Microfluidic Channel*, Nanotechnology, Vol. 17, No. 46, pp. 7–14.

62 Youoku, S., Suto, Y., Ando, M. and Ito, A. 2007. *Automated Microinjection System for Adherent Cells*, Progress in Biomedical Optics and Imaging – Proceedings of SPIE 6633, art. no. 66330S.

63 Zhang, Y. and Yu L.-C. 2008. *Microinjection as a Tool of Mechanical Delivery*, Current Opinions in Biotechnology, Vol. 19, pp. 506–510.

64 Zhang, Y. and Yu, L.-C. 2008. *Single-cell Microinjection Technology in Cell Biology*, BioEssays, Vol. 30, No. 6, pp. 606–610.

APPENDIX A: PROGRAM USED FOR SELF-PULLED PIPETTES

The program used in pulling the pipettes used in the experiments with the Sutter P-2000 pipette puller is described here. Also, the meaning of the parameters and the procedure of pulling a micropipette are illustrated. Table A.1 presents the parameters of the program. The pipettes were pulled out of quartz glass tubings with the inner diameter of 0.9mm and the outer diameter of 1.2mm as discussed in Section 4.1.2. The program is taken from the appendix containing custom sample programs sent by Sutter Instruments. It is for making tips with ~12.5µm inner diameter from quartz glass tubings with 0.5mm I.D and 1.0mm O.D.

Table A.1: Program parameters used in pulling the 17µm and 27µm pipettes.

HEAT	FIL	VEL	DEL	PUL
700	4	55	130	55
700	4	40	130	40
850	4	45	128	0

Heat means the output power of the laser and its range is from 0 to 999.
Filament (FIL) determines the scanning patters of the laser beam that is used to supply heat to the glass and its range is from 0 to 15.
Velocity (VEL) specifies the velocity in which the glass carriages connected to the ends of the tubing should separate from each other before the hard pull is executed. Its range is from 0 to 255.
Delay (DEL) controls the delay between the deactivation of laser and the start of the hard pull. Its range is from 0 to 255.
Pull (PUL) determines the force of the hard pull. Its range is from 0 to 255.

The procedure of pulling a micropipette is called the pull cycle. It consists of the following steps:

1. Laser turns on and heats the tubing according to HEAT.
2. The glass heats up and a weak pull (gravity) draws the glass out until it reaches programmed VEL value
3. If DEL = 128 the laser turns off and the hard pull is activated according to PUL
   If DEL > 128 the laser turns off and the hard pull is activated according to PUL after (DEL – 128)ms
   If DEL < 128 the hard pull is activated according to PUL and the laser turns off after (128 – DEL)ms

If the glass is not separated after the third step, the pull cycle is repeated. If the program consists of more than one line (as in Table A.1), the parameters in the following line are used.